RADIOPAQUE IODINATED COMPOUND GRAFTED POLYMER: SYNTHESIS AND EVALUATION FOR EMBOLOTHERAPY

GOPIKA V. GOPAN

Ph.D. THESIS

2024

SREE CHITRA TIRUNAL INSTITUTE

FOR

MEDICAL SCIENCES AND TECHNOLOGY, TRIVANDRUM

Thiruvananthapuram

RADIOPAQUE IODINATED COMPOUND GRAFTED POLYMER: SYNTHESIS AND EVALUATION FOR EMBOLOTHERAPY

A THESIS PRESENTED BY

GOPIKA V. GOPAN

TO

SREE CHITRA TIRUNAL INSTITUTE
FOR MEDICAL SCIENCES AND TECHNOLOGY
TRIVANDRUM
INDIA

IN PARTIAL FULFILMENT OF THE REQUIREMENTS
FOR THE AWARD OF

DOCTOR OF PHILOSOPHY

2024

DECLARATION

I, Gopika V. Gopan, hereby certify that I had personally carried out the work depicted in the thesis entitled "**Radiopaque iodinated compound grafted polymer: synthesis and evaluation for embolotherapy**", except the animal works and *in vitro* nidus model for precipitation study. No part of the thesis has been submitted for the award of any other degree or diploma prior to this date.

Gopika V. Gopan
Reg. No. 2018/PhD/01

21.06.2024
Trivandrum

Tele : 0471-2340801

Fax : 0471-2341814 / 2340819

श्री चित्रा तिरुनाल आयुर्विज्ञान तथा प्रौद्योगिकी संस्थान
बायो मेडिकल टैक्नोलॉजी विंग
पूजापुरा, तिरुवनन्तपुरम-695 012, इन्डिया

SREE CHITRA TIRUNAL INSTITUTE FOR MEDICAL SCIENCES AND TECHNOLOGY
BIO MEDICAL TECHNOLOGY WING
POOJAPPURA, THIRUVANANTHAPURAM-695 012, INDIA
(An Institute of National Importance under Govt. of India)

Dr. Roy Joseph PhD
Ref: Scientist G (Sr. Gr.)
Division of Polymeric Medical Devices
Department of Medical Devices and Engineering
BMT Wing, SCTIMST, Trivandrum

21.06.2024
Date:……

CERTIFICATE

This is to certify that Ms. **Gopika V. Gopan,** Division of Polymeric Medical Devices, Biomedical Technology Wing has fulfilled the requirements prescribed for the Ph.D. degree of the Sree Chitra Tirunal Institute for Medical Sciences and Technology, Trivandrum.

The thesis entitled "***Radiopaque iodinated compound grafted polymer: synthesis and evaluation for embolotherapy***" was carried out under my direct supervision. No part of the thesis was submitted for the award of any degree or diploma prior to this date. All animal experiments were carried out with clearance from the Institutional Animal Ethics Committee (IAEC)/Committee for the Purpose of Control and Supervision of Experiments on Animals (CPCSEA).

Roy Joseph

Dr. Roy Joseph
Scientist G, Division of Polymeric Medical Devices
Biomedical Technology Wing,
Sree Chitra Tirunal Institute for Medical Sciences
and Technology, Poojapura, Trivandrum - 695012

The Thesis Entitled

RADIOPAQUE IODINATED COMPOUND GRAFTED POLYMER: SYNTHESIS AND EVALUATION FOR EMBOLOTHERAPY

Submitted by

Gopika V. Gopan

For the award of

Doctor of Philosophy

of

SREE CHITRA TIRUNAL INSTITUTE
FOR MEDICAL SCIENCES AND TECHNOLOGY
TRIVANDRUM

is evaluated and approved by

(Research Guide)

Dr. Roy Joseph
Scientist G, Division of Polymeric Medical Devices
Biomedical Technology Wing,
Sree Chitra Tirunal Institute for Medical Sciences
and Technology, Poojapura, Trivandrum - 695012

Examiner
Professor Santanu Dhara
IIT Kharagpur, West Bengal

ACKNOWLEDGEMENTS

I would like to acknowledge and sincerely thank all the people who have helped me to make this thesis possible.

First of all I would like to express my sincere gratitude to my supervisor, Dr. Roy Joseph, for his continuous support, encouragement and valuable guidance during the entire course of the work. I woukd like to acknowledge my thanks to doctoral advisory committee members, Dr. Ramesh P., Dr. Umashankar P. R and Dr. Jayadevan E. R. for their time and valuable suggestions.

I owe my sincere gratitude to Dr.Sanjay Behari, Director; Dr. Asha Kishore, former Director; Dr. Harikrishna Varma, Head, BMT Wing for all the facilities provided during the course of my work. I extended my thanks to the Registrar, Deputy Registrar and all the staff in the academic section for their academic assistance.

I would like to thank Dr. Renjith S., Dr. Radhakumary C., Mr. Hari, Mr. Wiili Paul, Ms. Nimi and Dr. Sasikala, Central Analytical Facility, for FTIR, TGA, DSC and rheology data. I thank Mr. Chandrakanth, Ms. Thara, Dr. Soumini, Ms Viji and Mr. Harish Raj, CSIR-NIIST, for NMR, EDX and Mass spectroscopic analysis.I thank Er. Arvind Kumar Prajapati and Mr. Rahul, Division of Artificial internal Organ, for in vitro testing model development. I thank Dr. Anilkumar P.R, Dr. Naresh and Mr. Vinod, Tissue Culture lab for in vitro cytotoxicity data. I thank Dr. P. V. Mohanan, Dr. Remya N. S and all the staff of Toxicology division for all the support given for toxicological analysis. I thank Dr. Umashankar P. R., Dr. Sachin J. Shenoy and all the staff in In vivo models and testing; Dr. Jayadevan, Imaging Sciences and Intervention Radiology Dept. for animal studies and radiology images. I am grateful to Dr. Sabareeswaran and all thee staff of Histopathology, for all the histopathological analysis. I am thankful to Dr. AnughyaBhatt and all the staff in Thrombosis Research Unit; Dr. Naresh and Mr. Senthil in Tissue culture lab and Dr. Sabareeswaran and Mr. Viswanatham Naikin Histopathology for the facilities and guidance for RT-PCR analysis.

I express my sincere gratitude to Ms. Kezia Susan, Ms. Aleesha Vahab, Ms. Reshmi G. and Ms. Eliza Divya Srishti Minz for helping me in the various stages of the study. I am also indebted to all other labmates for their help and the environment provided for the smooth running of my work.

I greatly acknowledge Technical Research Centre for Biomedical Devices scheme of Department of Science and Technology, Govt. of India for the financial support.

Lastly I would like to thank all my family members for their love, support and encouragement.

Gopika V. Gopan

TABLE OF CONTENTS

LIST OF FIGURES

LIST OF SCHEMES

LIST OF TABLES

ABBREVIATIONS

AVM	Arteriovenous malformation
EV	Ethylene vinyl alcohol
DMSO	Dimethyl sulfoxide
BHP	4,4-bis(4-hydroxyphenyl)pentanoic acid
IBHP	4,4-bis(4-hydroxy-3,5-diiodophenyl)pentanoic acid
IBHOH	4,4-bis(4-hydroxy-3,5-diiodophenyl)pentanol
HR	(4-(5-bromo-2-(4-hydroxy-3, 5-diiodophenyl) pentan-2-yl)-2, 6-diiodophenol
FTIR	Fourier transform infrared spectroscopy
ATR	Attenuated total reflection
NMR	Nuclear magnetic resonance
TGA	Thermogravimetric analysis
MTT	(3-(4,5-dimethylthiazol-2-yl)-2,5-diphenyltetrazoliumbromide)
EV27-g-IBHP	4,4-bis(4-hydroxy-3,5-diiodophenyl)pentanoic acid grafted ethylene vinyl alcohol
EV27-g-HR	(4-(5-bromo-2-(4-hydroxy-3, 5-diiodophenyl) pentan-2-yl)-2, 6-diiodophenol grafted ethylene vinyl alcohol
EDS	Energy dispersive spectroscopy
XRD	X-ray diffraction analysis
RT-PCR	Real time polymerase chain reaction
HU	Hounsfield unit
THF	Tetrahydrofuran
DMF	Dimethylformamide

DCC	Dicyclohexylcarbodiimide
DMAP	Dimethylaminopyridine
DCU	Dicyclohexyl urea
LES	Liquid embolic system
LEA	Liquid embolic agent
PTFE	Polytetrafluoroethylene
DS	Degree of substitution
LCMS	Liquid chromatography mass spectrometry
CT	Computed tomography
EtO	Ethylene oxide
UHMWPE	Ultra-high molecular weight polyethylene
PBS	Phosphate buffered saline
LEM	Liquid embolic material
EDTA	Ethylenediaminetetraacetic acid
HPLC	High performance liquid chromatography
FFPE	Formalin fixed paraffin embedded
H&E	Hematoxylin and eosin
MMP-9	Matrix metallopeptidase-9
TGF	Transforming growth factor
IL-6	Interleukin-6
TNF	Tumor necrosis factor
VEGF	Vascular Endothelial Growth Factor
IL-10	Interleukin-10

PECAM	Platelet endothelial cell adhesion molecule
GAPDH	Glyceraldehyde 3-phosphate dehydrogenase
RNA	Ribonucleic acid
cDNA	Complementary deoxyribonucleic acid
RT	Reverse transcriptase
dNTP	Deoxynucleoside triphosphates
MeOH	Methanol
Tg	Glass transition tempearature
PHIL	Precipitating hydrophobic injectable liquid
RM	Rete mirabile
IEL	Internal elastic lamina

SYNOPSIS

The therapeutic introduction of various substances into circulation to occlude blood vessels is called embolization. It is a minimally invasive technique and the substances used for embolization are called embolic agents. An ideal embolic agent should be biocompatible, radiopaque, sterile, and achieve the desired level of occlusion. The selection of an embolic agent depends on the vascular territory to be embolized, the desired clinical outcome, the degree of occlusion, the permanence of occlusion, the inherent properties, and the behavior of the selected agent. Liquid embolic agents (LEA) are specially used for a disease condition known as arteriovenous malformation (AVM) due to their ease of flow through complex vascular structures. LEAs are of two types: polymerizing LEA and precipitating LEA. Cyanoacrylate-based glue is an example of polymerizing LEA and it consists of n-butyl cyanoacrylate (NBCA), ethiodized oil, and tantalum powder which are mixed immediately before use. On contact with blood, NBCAs undergo polymerization and occlude the blood vessels. The role of the ethiodized oil and tantalum are to act as a polymerization retardant and radiopacity agent respectively. Examples of precipitating LEAs are Onyx®, Squid^{Tm}, and PHIL™. They occlude the blood vessels by precipitation of the polymer and the solvent subsequently diffuses away through the bloodstream. Onyx® and Squid^{Tm} have similar material composition consisting of ethylene vinyl alcohol (EV) copolymer, tantalum particles and dimethyl sulfoxide (DMSO). The tantalum particles provide radiopacity in both the embolic systems.

These metal particles added for radiopacity are heavy and sediment on storage. This creates non-uniformity in the liquid embolic system and requires an additional step of shaking before use. The shaking provides the system a certain level of uniformity through the re-suspension of the metal particles in the polymer solution. Moreover, the metal particles create problems during imaging due to beam hardening. Thus, the development of an alternative system to avoid these problems would be attractive. A better approach would be to covalently bond a radiopaque element such as iodine to a biocompatible polymer, dissolve the resultant polymer in a biocompatible solvent, and use this clear injectable solution for embolization. PHIL™ is an example of this type of LEA which is made by dissolving triiodophenol-modified copolymers of poly(lactide-co-glycolide) (PLGA) and poly(2-hydroxyethyl methacrylate) (pHEMA) in DMSO. Here the triiodophenol part provides radiopacity and the homogenous distribution of radiopaque moiety is ensured via covalent bonding. In this context, it is hypothesized that polymeric liquid embolic agents with adequate radiopacity can be formulated by functionalizing compounds with three or more iodine atoms per molecule and by grafting these iodocompounds onto non-radiopaque polymers. An increase in opacity is also observed when there is an increase in the number of iodine atoms.

Modifying ethylene vinyl alcohol (EV) copolymers to impart radiopacity is advantageous as these have been previously used for embolization. Imparting radiopacity is possible by the covalent linking of iodinated organic compounds onto the hydroxyl functionality of EV copolymer. Iodine content in these polymer chains can be increased by increasing the grafting efficiency. The radiopaque polymer prepared in this

way may be formulated into an injectable liquid by dissolving in a biologically safe solvent like DMSO. The system can be designed and formulated to possess appropriate viscosity, biocompatibility, radiopacity, biostability, good flow behavior, and the instant ability to precipitate on contact with a biological fluid. So, the main objective of this work was to impart radiopacity to EV, characterize the material for its physicochemical and biological properties, both *in vitro* and *in vivo*, and finally evaluate its suitability for embolization.

The primary step was to impart radiopacity. Three tetraiodo compounds with different functionalities were synthesized and characterized to ascertain their suitability. 4,4-bis(4-hydroxy-3,5-diiodophenyl)pentanoic acid (IBHP), 4,4-bis(4-hydroxy-3,5-diiodophenyl)pentanol (IBHOH), and (4-(5-bromo-2-(4-hydroxy-3,5-diiodophenyl)pentan-2-yl)-2,6-diiodophenol (HR) having carboxyl, hydroxyl and haloalkane functionalities, respectively were the three synthesized compounds. Two series of iodinated radiopaque EV copolymers were then prepared by grafting onto EV and the two liquid embolic systems were formulated by subsequently dissolving them in DMSO. The most promising system was then evaluated for the treatment of arteriovenous malformation by embolizing the rete mirabile of swine for a period of 3 months.

The first chapter of the thesis gives an introduction to embolization, its importance in treating the disease arteriovenous malformation (AVM) and describes the overall contents of the thesis. Chapter 2 gives a review of the literature and state-of-the-art

research on embolic agents. Details of all the materials, synthetic procedures used for the preparation of iodocompounds, polymer modifications, physicochemical characterization techniques and biological evaluations carried out are described in detail in chapter 3. Chapter 4, subdivided into five sessions contains the results and discussions of the complete data generated. The first part of this chapter describes the characterization of iodocompounds by spectroscopic techniques like FTIR, NMR, and mass spectroscopy. The radiopacity of these iodocompounds was also measured with the aid of a CT scanner. The second session describes the preparation and characterization of the radiopaque EV copolymer. Iodocompounds having carboxyl (IBHP) and haloalkane functionality (HR) were covalently linked to different grades of EV copolymer through ester and ether linkages, respectively. These materials were characterized by spectroscopic techniques (FTIR and NMR), Energy-Dispersive X-ray analysis, X-ray diffraction, and thermal methods such as thermogravimetric analysis and differential scanning calorimetry. Cytotoxicity of the modified polymers and selected iodocompounds were evaluated by *in vitro* cell cytotoxicity tests using L929 cells and EA.hy926 endothelial cells.

The third session of the chapter deals with the formulation of LEAs. The essential characteristics of the liquid embolic agents including viscosity, precipitation behavior, radiopacity, and flow behaviors were evaluated. A model *in vitro* test system, representing nidus, was designed and fabricated to evaluate the precipitation of the LEA, and the results obtained were discussed. The fourth session describes the safety evaluation studies carried out for the selected system. These include *in vitro*

hemocompatibility and degradation studies, storage stability studies, acute systemic toxicity studies, and local systemic effects after muscular implantation of the material in a rabbit model. Tissue responses were tested by histological and RT-PCR analysis. The material was further analyzed for its *in vivo* functional performance in swine rete mirabile which is a popular animal model for AVM studies. The details of the functional evaluation carried out were described in the fifth section. The liquid embolic system was successfully implanted in swine for 3 months and its interaction with the tissues was studied by histological analysis.

Chapter 5 summarizes the results and conclusions drawn from the present study.

1. INTRODUCTION

The vascular system, also called the circulatory system, is made up of the vessels that carry blood and lymph fluid through the body. The diseases which affect vascular system are known as vascular diseases. There are different types of vascular diseases, out of which arteriovenous fistula (AVF) is a life threatening one. It is an abnormal connection between artery and vein. If the fistula happened in the brain, it is called arteriovenous malformation (AVM). A minimally invasive procedure to reduce the risk of arteriovenous malformation is embolization (Figure 1).

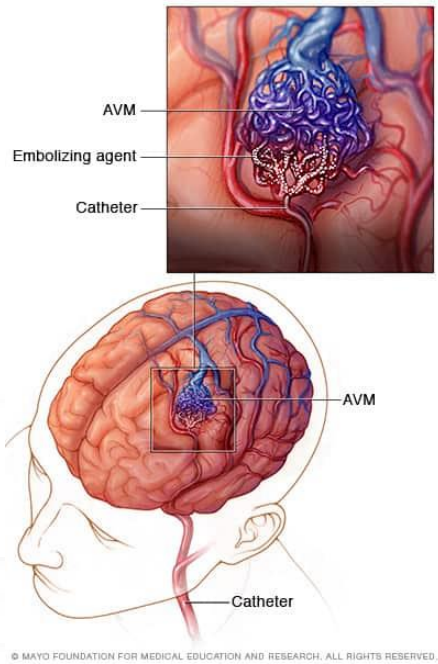

Figure 1. Embolization procedure in Arteriovenous malformation.
(Taken from: https://www.mayoclinic.org/-/media/kcms/gbs/patient-consumer/images/2014/03/20/15/17/mcdc7_endovascular_embolization.jpg)

Embolization is the therapeutic introduction of substances into the circulation to occlude vessels, either to arrest or prevent hemorrhage, or to devitalize a structure, tumor, or organ by occluding its blood supply (Stedman, 1920).

Embolization has three distinctive goals: an adjective goal, a curative goal, and a palliative goal. In adjective goal, embolization is done as a preoperative procedure that helps to cut the blood supply that feeds the tumor during the surgical removal of the tumor. In curative goals, embolization is used as a treatment for aneurysms, arteriovenous malformations (AVMs), arteriovenous fistula and traumatic bleeding. In palliative goal, it relieves the symptoms of large AVMs. The agents used for embolization are known as embolic agents. Modern embolic agents are either temporary or permanent. Among them, permanent agents are more commonly used and include liquid agents, particulates, coils, etc. Liquid agents are particularly used for arteriovenous malformation and permit deeper penetration and homogenous filling of the vascular area.

The significant characteristics of a liquid embolic agent are its radiopacity and precipitation behavior in biological fluids. Radiopacity is imparted to the agent for its easy deployment in the destination site. There are literature reports on the insolubility and sudden precipitation of ethylene vinyl alcohol (EV) copolymer in aqueous medium. This behavior suggests it may be a suitable candidate for the preparation of liquid embolic agents. Radiopacity can be imparted to this polymer by blending or incorporating heavy elements such as tantalum, bismuth, or barium salts (Davy and

Causton, 1982; Thanoo and Jayakrishnan, 1990) or by attaching iodine in the polymer chain either by grafting iodine-containing organic molecules (Jayakrishnan et al., 1990; James et al., 2006; Shiralizadeh et al., 2016) or by polymerization of iodinated monomers (Jayakrishnan et al., 1992; Galperin et al., 2007). The incorporation of heavy elements into the polymers, especially as powders, causes non-uniformity and sedimentation of the heavy elements when the embolic agents are supplied in liquid form. So, covalent linkage with iodine is a highly desirable method. Iodine is a suitable candidate for biomedical imaging due to its safety, low cost, largest mass attenuation coefficient, excellent radiopacity, non-toxicity, and excellent radiopacity in non-ionic environments.

The work described in this thesis is based on the hypothesis that polymeric liquid embolic agents with adequate radiopacity can be formulated by synthesizing compounds with three or more iodine atoms per molecule and by grafting these iodocompounds onto non-radiopaque polymers. In this way, polymers with inherent radiopacity can be produced. Radiopacity can be introduced into the EV copolymer by the chemical grafting of iodinated organic compounds with the hydroxyl functionality of EV. It would be possible to introduce more iodine content by increasing the grafting efficiency of iodinated organic moiety into the polymer. Since the liquid embolic agents are particularly meant for treating arteriovenous malformation, the radiopaque EV copolymer is expected to be soluble in a biologically safe solvent (like DMSO), low in viscosity, biocompatible, highly radiopaque, precipitate immediately on contact with blood, bio-stable and exhibit suitable flow characteristics.

As the first step to reach this goal, a parent organic compound having more than three sterically free sites for iodination and a suitable functionality (carboxyl) for grafting in the polymer was identified. This compound was 4,4-bis(4-hydroxyphenyl)pentanoic acid (BHP) (Figure 2). It was iodinated using sodium iodide/sodium hypochlorite to make 4,4-bis(4-hydroxy-3,5-diiodophenyl)pentanoic acid (IBHP) (Figure 3). IBHP was then grafted onto EV through an esterification reaction (EV-g-IBHP). There are literature reports that suggest ether linkages are more stable than ester linkages. So, another iodocompound was synthesized by modifying IBHP so that the modified iodocompound could be grafted onto EV through an ether linkage. For this, the carboxyl functionality in IBHP was converted to a haloalkane functionality. In this process an intermediate radiopaque compound, 4,4-bis(4-hydroxy-3,5-diiodophenyl)pentanol (IBHOH), having hydroxyl functionality was prepared (Figure 4). The hydroxyl functionality of IBHOH was converted to haloalkane functionality and prepared (4-(5-bromo-2-(4-hydroxy-3, 5-diiodophenyl) pentan-2-yl)-2, 6-diiodophenol (HR) (Figure 5). All the above materials were characterized by appropriate physicochemical techniques. The iodocompound HR was chemically grafted with EV through ether linkage to make the radiopaque EV copolymer (EV-g-HR). The iodine content and grafting efficiency of both EV-g-IBHP and EV-g-HR were estimated using ^{1}H NMR spectroscopy and it was found that the iodine content was less for EV-g-HR.

Separate liquid embolic formulations were prepared by dissolving EV-g-IBHP and EV-g-HR in DMSO and their suitability as liquid embolic agents were evaluated. EV-g-IBHP was found to be a better system and it was successfully implanted in the rete

mirabile of swine for a period of 3 months. The material was retrieved and the tissue response of implanted material was analyzed by histopathology and RT-PCR. Through this work, some promising radiopaque compounds could be synthesized that could have the potential for embolization in interventional radiology.

This thesis elucidates the contents in the following manner. Chapter 2 discusses the current literature on radiopaque polymers, materials used for endovascular embolization, specifically liquid embolic agents. Chapter 3 describes the details of all the materials, synthetic procedures, physicochemical characterization techniques, *in vitro* and *in vivo* biological studies and preclinical evaluation procedures used for the present study. Chapter 4 presents the properties and critical evaluation of the iodocompounds and iodocompound-grafted EVOH copolymers. It discusses the effectiveness of each system as a liquid embolic agent and also evaluates the biocompatibility of the EV-g-IBHP. Chapter 5 summarizes the important results of the study and concludes the importance of the findings for the medical field.

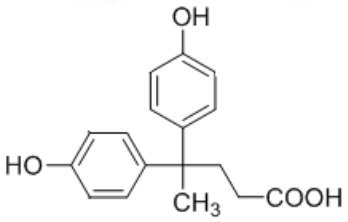

Figure 2. 4,4-bis(4-hydroxyphenyl)pentanoic acid (BHP)

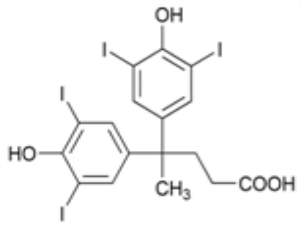

Figure 3. 4,4-bis(4-hydroxy-3,5-diiodophenyl)pentanoic acid (IBHP)

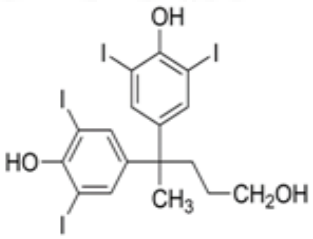

Figure 4. 4,4-bis(4-hydroxy-3,5-diiodophenyl)pentanol (IBHOH)

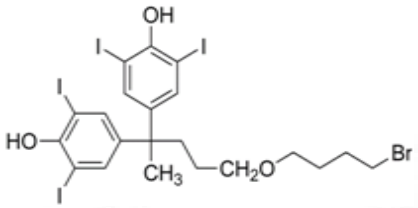

Figure 5. (4-(5-bromo-2-(4-hydroxy-3, 5-diiodophenyl) pentan-2-yl)-2, 6-diiodophenol (HR)

2. LITERATURE REVIEW

2.1 Arteriovenous malformation

In our circulatory system, arteries carry oxygenated blood away from the heart and veins carry oxygen-depleted blood from various body parts to the heart. The arteries and veins are connected by very small blood vessels called capillaries. Here the oxygen and nutrients are exchanged for carbon dioxide and waste. But in arteriovenous malformation (AVM), there is an abnormal tangle of these blood vessels which disrupts normal blood flow and oxygen circulation (Figure 6). The malformed blood vessels have a higher rate of bleeding than normal blood vessels.

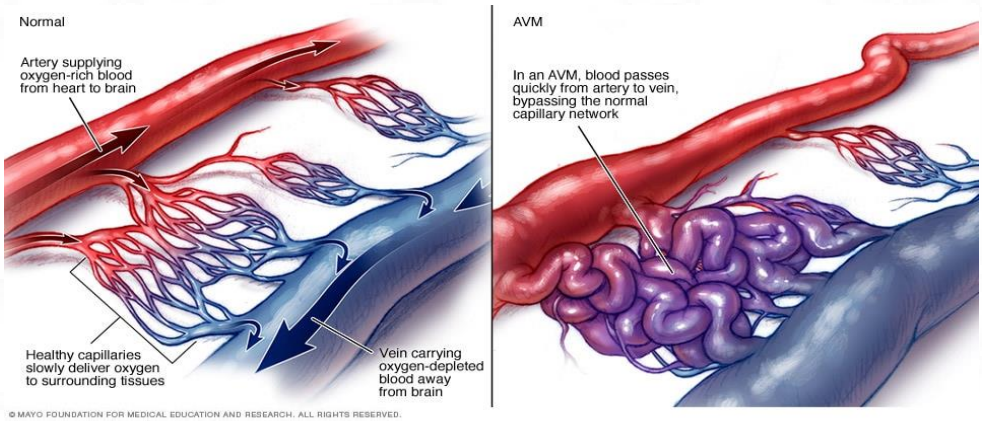

Figure 6. Normal and malformed capillary (taken from https://www.mayoclinic.org/-/media/kcms/gbs/patient-consumer/images/2013/08/26/10/15/ds01126_im03707_bn7_avm_blood_vesselsthu_jpg.jpg)

According to the American stroke association (accessed on January 24, 2022), brain AVM occurs in less than 1% of the population and it is very common in males than females. AVM is not hereditary, usually, it is inborn. It does not spread to other parts of

the body. The AVM that occurs in the coverings of the brain is called dural AVM which can occur following an injury.

The brain AVM can occur anywhere within the brain or on its covering. This includes the four major lobes, the back part of the brain, the brain stem, and the ventricles. AVMs grow and change over time. AVMs are often organized using a scale called the Schöbinger staging system (Johns Hopkins medicine, accessed January 24, 2022). Not all AVMs go through every stage.

Stage I (quiescence): The AVM is "quiet." The skin on top of the AVM may be warm and pink or red.

Stage II (expansion): The AVM gets larger. A pulse can be felt or heard in the AVM.

Stage III (destruction): The AVM causes pain, bleeding, or ulcers.

Stage IV (decompensation): Heart failure occurs.

The symptoms of AVM vary according to its location. According to the American stroke association (accessed January 24, 2022):

- More than 50% of patients with AVM have cerebral bleeding
- 20-25% has focal or generalized seizures
- Patients may have localized pain
- 15% have difficulty with movement, speech, and vision

The abnormal and weakened blood vessels in AVM are the main reason for the bleeding. The chance of bleeding is only 1-3% per year. The chance for repeated bleeding is higher after the first bleed. The risk of death related to cerebral bleed is 10-15%. The chance for permanent brain damage after bleeding is 20-30%. During bleeding the blood leaks into the brain and the normal brain tissue is damaged. This results in loss of normal function of the brain which may be temporary or permanent.

2.1.1. Types of AVM

There are different types of brain AVMs.

- True arteriovenous malformation: This is the most common AVM. It consists of a tangle of abnormal vessels in capillaries.
- Occult/cryptic AVM/ cavernous malformations: Here the active diversion of blood doesn't occur. This causes bleeding and often produces seizures.
- Venous malformation: Here abnormality happened only to the veins.
- Hemangioma: Here abnormal blood vessels are found at the surface of the brain and on the skin or facial structures.
- Dural fistula: Abnormal connection between blood vessels in the dura mater (covering of the brain) is called a dural fistula. It is again of three types:
    - Dural carotid-cavernous sinus fistula: These occur behind the eye. Symptoms are eye swelling, decreased vision, redness, and congestion of the eye. They often can hear a "swishing" noise.

- Transverse-Sigmoid sinus dural fistula: These occur behind the ear. Symptoms are local pain behind the ear, headaches, and neck pain. They hear a continuous noise (bruit) that occurs with each heartbeat.
- Sagittal sinus and scalp dural fistula: These occur toward the top of the head. Symptoms are headaches, and pain near the top of the head; they hear noise (bruit) and have prominent blood vessels on the scalp and above the ear.

2.1.2. The grading system for AVM

Spetzler et al. (1986) proposed a grading system for AVM by considering three variables: 1) Size of AVM, 2) Pattern of venous drainage, and 3) neurological eloquence of the brain regions adjacent to AVM.

AVM may be of size small (< 3 cm), medium (3-6 cm), or large (> 6 cm). The lowest grade of AVM is Grade I, which is small, located in a non-eloquent region, and has superficial drainage. Complete removal of such AVM has minor technical difficulties and has very little risk. The highest grade in this sequence is Grade V, which is larger than 6 cm, located within or immediately adjacent to the eloquent brain and a portion of the drainage would empty into the deep venous system. It has a significant risk in the surgery.

2.1.3. Diagnostic methods for AVM

2.1.3.1. Cerebral angiography

It is also known as arteriography. It is the most detailed test to diagnose AVM. The location and characteristics of the feeding arteries and draining vein can be easily identified using this test. Here, a catheter is inserted into the artery in the groin and threads into the brain. A contrast agent is injected which highlights the structure of blood vessels on X-rays (Figure 7 (A)). Cloft et al. (1999) studied the risk of cerebral angiography in patients with arteriovenous malformation and found that the risk of permanent neurological complications associated with cerebral angiography is very low i.e., around 0.07%.

2.1.3.2. Computed tomography

In computed tomography (CT), X-rays are used to create a detailed cross-sectional image (Figure 7 (B)) of the brain and show bleeding in the brain, if any. Here also dye is injected into the vein to view the feeding artery and draining vein. That is called computed tomography angiography.

2.1.3.3. Magnetic resonance imaging

Here powerful magnets and radio waves are used to get images of the brain. Magnetic resonance imaging (MRI) is more sensitive than CT and can pick small changes in the tissue. So, an AVM can easily identify in MRI (Figure 7 (C)).

2.1.3.4. Magnetic resonance angiography

It looks specifically at the blood vessel. Unlike a traditional angiogram, MRA is a less invasive and less painful test. In some cases, a contrast agent is added to the bloodstream to make the blood vessel easier to see. Figure 7 (D) represents a magnetic resonance angiogram of AVM.

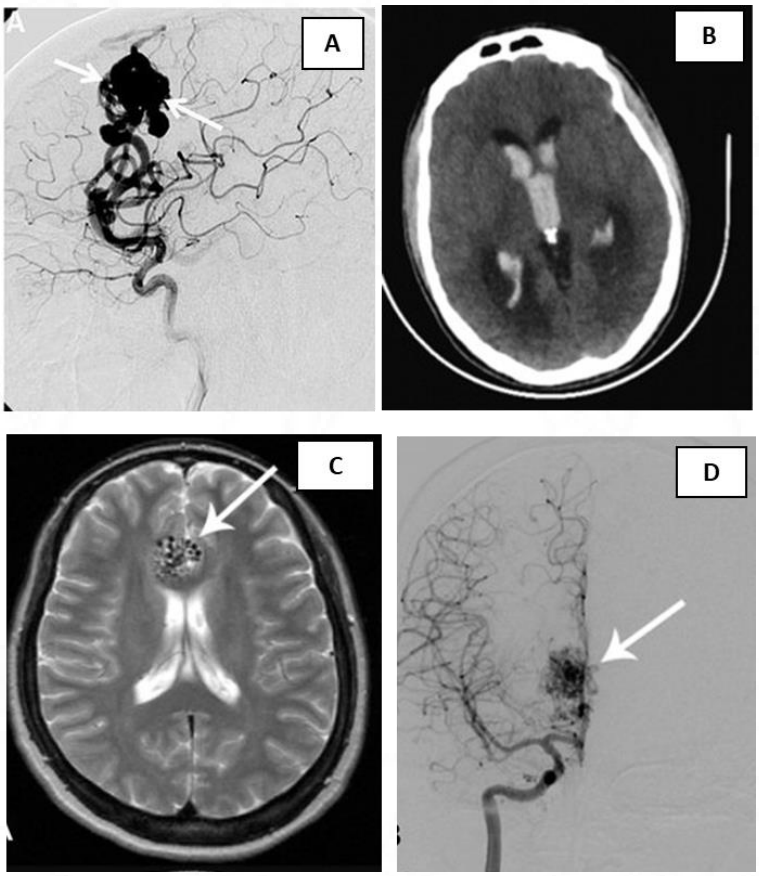

Figure 7 (A). Angiography image of arteriovenous malformation (Sackey et al., 2017); (B) AVM rupture (intraventricular haemorrhage) in CT (Barreau et al., 2014); (C) Magnetic resonance image of AVM; (D) Magnetic resonance angiogram of AVM (Karakida et al., 2013).

2.1.4. Treatment options for AVM

The treatment method for AVM depends on the age and health of a person and the size and location of the abnormal blood vessel.

2.1.4.1. Medical therapy

A person with AVM must be avoiding hard work that causes an increase in blood pressure and should undergo a regular check-up. For persons without any symptoms, conservative medical management is indicated.

2.1.4.2. Stereotactic radiosurgery

Stereotactic radiosurgery (SRS) is used for treating small AVMs found in an area difficult to reach. Here, through an angiogram, the exact location of AVM would be found. Then high-energy beams would be focused to produce direct damage to the diseased vessels. SRS preserves healthy tissue surrounding the target area. Here anesthesia is not given to the patient and no incisions are made. After 2 or 3 years of the treatment, the AVM will close completely in 80% of patients and no hospital stay is needed.

SRS has many disadvantages also. It can only be done for small AVMs. In 3-5% of patients, long term side effects may occur. Until the AVM is completely closed off there is a chance of bleeding every year. Radiosurgery is suitable for smaller AVM ($< 10\ cm^3$) because more radiation can be delivered safely (Flickinger et al., 1996).

2.1.4.3. Surgery

Surgery is recommended for AVM if it is bleeding or in an area that can be easily operated on. A portion of the skull is removed first and closed-off arteries that feed AVM are then seals of the AVM with special clips and carefully remove from the surrounding brain tissue (Figure 8).

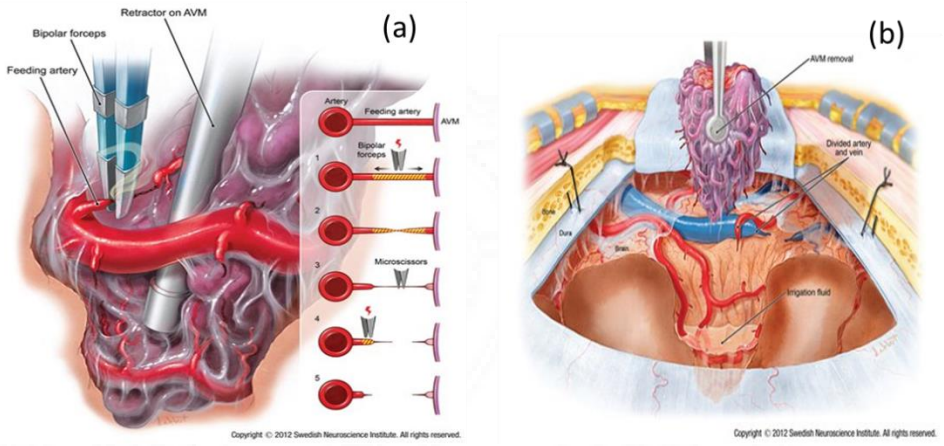

Figure 8. Surgical procedure for treating AVM: (a) Closing off arteries that feed AVM; (b) Removal of AVM (https://seattleneurosciences.com/conditions/arteriovenous-malformation-avm/)

Since complete removal of AVM takes place here it gives complete protection against bleeding. Unlike other methods here only one surgical procedure is required.

The disadvantages of surgical procedures are that it is possible only if the AVM is located in an area that is easily accessible to the surgeon. A longer hospital stay is required and there is a chance of infection, stroke or permanent deficit. The requirement of blood transfusion is also there in the case of surgical procedures.

2.1.4.4. Endovascular embolization

Embolization is also known as embolotherapy or endovascular therapy. This technique has been used to treat AVM since the early 1980s. In this procedure, a catheter is inserted into a leg artery and threads through blood vessels to the brain under fluoroscopy. The catheter is positioned in one of the feeding arteries to AVM and injects some particles or liquid called the embolizing agent to block the artery. It is a less invasive method than surgery. Usually, it is done alone but frequently it is done prior to

other surgical treatments to reduce the size of AVM for a safer procedure. If it is prior to done before surgery it reduces the blood flow through the AVM which helps the surgeon to remove the AVM safely. It is also used to reduce the risk of stroke-like symptoms in some large AVM by redirecting blood back to normal brain tissue. Since it doesn't involve an open procedure, a short hospital stay is enough and it can yearly be repeated and staged. The chance of cure with embolization alone is 70-80% in small AVM and 20-40% in large AVM.

Willinsky et al. (2001) reviewed the experience using embolization in the treatment of small AVMs (< 3 cm) and he concluded that embolization is an effective treatment of small AVMs when the angioarchitecture is favorable. Pierot et al. (2013) evaluated the safety and efficacy of the combined treatment of brain AVMs with the use of Onyx embolization followed by radiosurgery. The AVM sizes considered here were < 3 cm in 7 patients and ≥ 3 cm in 13 patients. The conclusion made by him was that the safety and efficacy of combined treatment by Onyx embolization followed by radiosurgery are satisfactory with a low rate of clinical complications (5%) and 58.8% rate of complete obliteration.

2.2 Embolic agents for endovascular embolization

The different embolic agents available have different properties and are selected on the basis of application. Embolic agents are classified into temporary and permanent based on the length of time needed for vascular occlusion. For instance, in an injury a temporary agent is ideal but for arteriovenous fistulae or tumors permanent agent is

preferable. The selection of embolic agents also depends on the desired level of occlusion and can be used for distal or proximal occlusion. The level of occlusion depends on the pathologic process that requires embolotherapy. Examples of common embolic agents are autologous clots, gelatin sponges, polyvinyl alcohol (PVA) particles, and coils.

2.2.1. Temporary embolic agents

The temporary embolic agents produce recanalization of the embolized vessels within hours to weeks. Examples are autologous clots, gelatin sponges, oxidized cellulose, and microfibrillar collagen.

2.2.1.1. Autologous clot

Occlusion with autologous clots is temporary in nature. In this procedure, the blood is drawn from the patient and allowed to clot by adding thrombin. It is then injected into the patient. The advantage of this embolic agent is its low cost and low toxicity. This was subsequently replaced by a gelatin sponge. Akpinar & Yilmaz (2016) treated post-traumatic high-flow priapism using autologous blood clot embolization successfully. Due to the recanalization on the 7^{th} day, a second embolization was performed and complete thrombus formation was observed on follow-up.

2.2.1.2. Gelatin sponge

This is available in various thicknesses and is also a temporary embolic agent (Figure 9). Here small stripes of gel foam are tightly rolled down and injected through a catheter. The slurry can also be prepared using stripes of gel foam. This is then connected with a

3-way stopcock to another syringe that is filled with the contrast agent and then injected. However, there is a chance of infection in using gel foam due to the air bubbles trapped inside it (Vaidya et al., 2008).

Figure 9. Gelatin sponge (taken from: https://www.merit.com/wp-content/uploads/2021/08/EMBO_withcubes_png.png)

Oxidized cellulose and microfibrillar collagen are rarely used due to the difficulty in preparation and administration. Gelfoam is used in patients with postpartum hemorrhage or in patients with traumatic pelvic fracture when there are multiple smaller bleeding sites from different internal iliac artery branches (Lopera, 2010; Kirby et al., 2009).

2.2.2. Permanent embolic agents

Embolic agents that produce permanent occlusion are called permanent embolic agents. They are classified as non-absorbable microparticles (PVA, tris-acryl gelatin microspheres), mechanical agents (coils, detachable plugs), and liquid embolic agents (NBCA, ethylene vinyl alcohol, ethanol, etc.).

2.2.2.1. Nonabsorbable microparticles

PVA particles: PVA particles are available in various diameters ranging from 45 to 1200 µm (Figure 10). They are irregular in shape and can be loaded into the smallest vessel into which they fit. Sharma et al. (2010) developed PVA hydrogel microspheres

with ethoidized oil as a radiopaque agent and were used to visualize the distribution of embolic material during an embolization procedure. However, the PVA particles manifest disadvantages including inflammatory reaction, vessel fibrosis (Vaidya et al., 2008), aggregation, and blockage of the catheter.

Figure 10. PVA particles (taken from: https://mydevicemd.com/assets/uploads/device/1624907710390G09665_1479397366843.jpg)

Tris-acryl gelatin microspheres: These are spherical acrylic copolymer beads crosslinked with gelatin and are available in sizes of 40-1200 µm (Figure 11). Unlike PVA, the hydrophilic nature of microspheres prevents aggregation. The disadvantage of these microspheres is that they require periodic shaking to keep the particles in suspension and moreover gelatin may be allergic to some people.

Figure 11. Gelatin microspheres (taken from: https://www.merit.com/wp-content/uploads/2019/01/EmboSphere-Micro-Group.png).

2.2.2.2. Mechanical embolic agents

Coils: Mechanical embolic agents include coils made up of stainless steel or platinum (Figure 12). When selecting a suitable coil, it should be 20-30 % larger than the target vessel because under-sized coils result in non-targeted vessel embolization. The coils are available in different shapes including straight, helical, spiral, and complex 3D. Steel coils are cheap and have high radial force. Platinum coils are expensive but they are more malleable and radiopaque. The available dimensions of coils are 1-30 cm in length and 460 - 890 micrometers (0.018 - 0.035 inches) in diameter. Coils are coated with polyester fibers, nylon fibers, or silk fibers to induce thrombogenic behavior. The coils are delivered to the site by pushing using coil pushers. Pushable, injectable, and detachable coils that are cheap and can quickly deploy are commonly used. However, they cannot be quickly retrieved once extruded from the catheter tip. Detachable coils that provide accurate placement of embolic agents (Osuga et al., 2006) during high vascular flow also manifested longer procedure time and higher costs.

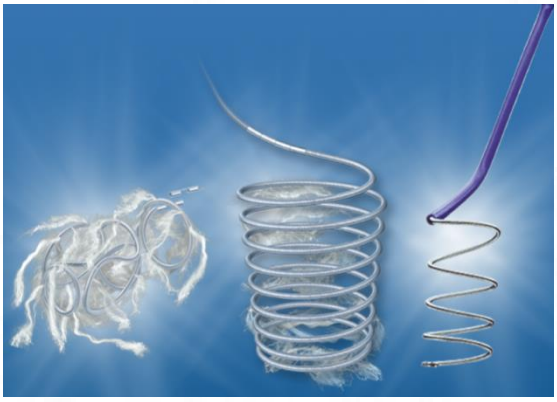

Figure 12. Embolization coils (taken from: https://www.bostonscientific.com/content/dam/bostonscientific/pi/portfolio-group/embolization/interlock/interlock-video-thumb-960x960.png).

In addition, hydrogel coils made up of platinum coated with an expandable polymer that can swell when exposed to physiological conditions and liquid coils have also been investigated. Kurata et al. (2005) reported the application of platinum liquid coil (Figure 13) as an embolic material for arteriovenous malformation. Liquid coils are non-toxic and bio inert material and has good radiopacity.

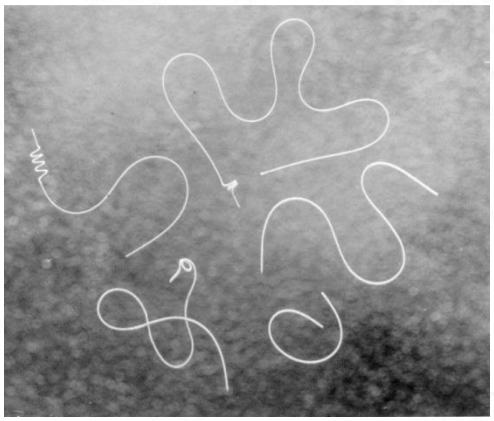

Figure 13. Platinum liquid coil, both helical and straight forms (Kurata et al., 2005).

Detachable plugs: One example of a detachable plug is an amplatzer vascular plug (AVP) (Figure 14) composed of self-expanding nitinol mesh that can reposition for correct deployment. They have the size ranging from 4-16 mm. The deployment of AVP is through sheaths ranging from 3-8 French. They are expensive but the procedure is completed within a short time. This method is not useful in patients with severe coagulopathy because its success depends on the patients' ability to form a thrombus that takes around 15 minutes (Wang et al., 2012).

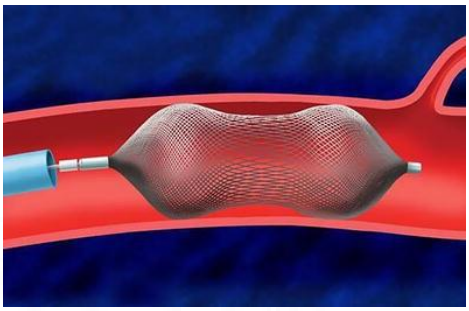

Figure 14. Amplatzer vascular plug (taken from https://media.springernature.com/lw685/springer-static/image/art%3A10.1007%2Fs10140-007-0696-8/MediaObjects/10140_2007_696_Fig1_HTML.jpg).

2.2.2.3. Liquid embolic agents

Liquid embolic agents are classified into polymerizing, precipitating, and phase-transitioning types. In the polymerizing system, there is a carrier solution having monomers that polymerize upon contact with suitable initiators. These polymerizing systems must be premixed with an initiator to provide effective embolization and avoid microcatheter entrapment. A dual lumen microcatheter can also be used, which has a rapid rate of reaction to prevent washout of embolic material.

In a precipitating system, a polymer is dissolved in a biocompatible carrier solvent. Upon contact with aqueous condition, precipitation occurs and subsequently the carrier solvent diffuses into the aqueous medium. It has the advantage of forming precipitate only on contact with physiological fluid and can avoid problems associated with microcatheter blockage. However, if the precipitation is not fast, the blood flow causes washout of the material.

Some polymers also undergo sol-gel phase transition in response to external stimuli such as pH, temperature, ion concentrations or electric fields.

2.2.2.3.1. Polymerizing formulations

Cyanoacrylate glues: Liquid alkyl-2-cyanoacrylate monomers called cyanoacrylate glues form flexible polymers with strong adhesive bonds on contact with soft tissues in an ionic medium. In the monomeric form, they are non-viscous and radiolucent. When they are combined as a two-component embolic agent with tantalum powder or ethiodized oil (Figure 15), the added agent prolongs the polymerization time and opacifies the liquid agent. The rate of polymerization and physical properties of the polymer varies with the aliphatic side chain. The Food and Drug Administration (FDA) has approved the use of n-butyl-2-cyanoacrylate (n-BCA) for embolization of cerebral AVMs due to their super selective catheter delivery in a flow-directed fashion (Mattamal, 2008).

Figure 15. n-BCA liquid embolic agent (taken from: https://www.jnjmedtech.com/sites/default/files/styles/crop_presets/public/2022-05/196727-211123_Trufill_n-BCA-Content_Card_Module_02.jpg?itok=Jr609bpS).

However, these isobutyl derivatives are not favorable because the N-butyl version causes sarcomas (Lord et al., 2020). Polymer retardants such as glacial acetic acid and

lipiodol (lipiodol imparts radiopacity to the system) can be added to control the rate of polymerization. Since the glue is adhesive in nature, the microcatheter must be immediately withdrawn post-delivery of the glue to prevent entrapment of the microcatheter at the site of administration (Hill et al., 2018). To reduce the adhesion towards cyanoacrylate glue, microcatheters with a hydrophilic coating have been developed (Mathis et al., 1997). An example of this type of microcatheter is the Apollo microcatheter. N-BCA which is widely used in the clinic due to its low cost though there are risks of microcatheter blocking and entrapment.

Instylla hydrogel embolic system: It is a two-component Polyethylene glycol (PEG)-based system that polymerizes on mixing with an initiator. The two components are injected from separate syringes and allowed to flow down a dual-lumen arrangement. The liquid has low viscosity which undergoes rapid gelation to form an embolic gel. For radiopacity, the material must be mixed with contrast agents prior to delivery. In high flow rate tests of 150 ml/min, successful polymerization of the gel was observed. The *in vitro* and *in vivo* testing of the liquid embolic system is currently under progress (Ganguli et al., 2021).

PPODA-QT: It is a polymerizing system composed of poly (propylene glycol) diacrylate (PPODA) and pentaerythritol tetrakis(3-mercapto propionate) (QT) and the gelling is based on Michael type addition reaction (Scheme 1). A catalytic amount of hydroxide is incorporated into it, which deprotonates the QT thiol group which then undergoes nucleophilic attack on the acrylate group of PPODA. This gelation depends

on the pH of the medium and can be controlled by changing the pH. The injection takes around 10 minutes. It is used for the treatment of cerebral aneurysms. Huckleberry et al. (2021) tested the rabbit elastase aneurysm model to evaluate the tissue response following PPODA-QT embolization.

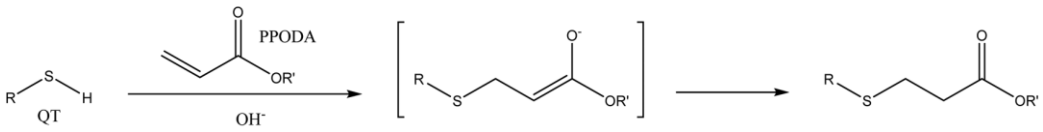

Scheme 1. Michael type addition- Nucleophilic thiol group of QT adds to acrylate of PPODA under basic conditions (Lord et al., 2020).

2.2.2.3.2. Precipitating formulations

Ethylene vinyl alcohol copolymer (Onyx®): Onyx®, sold by Medtronic Inc., consists of ethylene vinyl alcohol copolymer dissolved in DMSO (Figure 16).

Figure 16. Different grades of Onyx® liquid embolic agent (taken from https://encrypted-tbn0.gstatic.com/images?q=tbn:ANd9GcRiscSEbmMdDC8AxtdbZe04YTu02Ia4Uod5tw&usqp=CAU).

It contains tantalum powder for radiopacity. Before delivery, the Onyx® vial must be shaken for 20 min to ensure uniform mixing of the tantalum particles present in it as metal particles are susceptible to sedimentation (Onyx® manual). On delivery, the polymer precipitates in blood by the diffusion of DMSO, and the tantalum powder gets entrapped in the precipitate. Onyx® is available in a wide range of viscosities (18 mPas, 34 mPas & 500 mPas). Depending on the size of the vessel and blood flow rate, different

formulations are applied. Onyx® 18 is a low viscosity grade and it can penetrate deep into the nidus (Siekmann, 2005). The high viscosity grade (Onyx® 500) is suitable for the embolization of aneurysms (Ashour et al., 2014). Compared to n-BCA glue, Onyx® does not initiate any inflammatory responses but the solvent DMSO causes a decrease in the diameter of the blood vessel which in turn decreases the blood flow (Chaloupka et al., 1994). This vasospasm can be prevented by a slow injection rate (Chaloupka et al., 1999 and the optimized injection rate of 0.16 mL/min is being followed. The recommended microcatheters for the delivery of DMSO based liquid embolic agents are Rebar™ (Medtronic Inc.), Progreat® (Terumo) and Apollo™ (Medtronic Inc.). Onyx® reduces the risk of microcatheter entrapment and blockage due to its non-adhesive nature (Taki et al., 1990; Terada et al., 1991).

Onyx® displays artifacts under X-ray imaging as a result of beam hardening and scattering of X-ray due to the presence of tantalum metal particles (Jia et al., 2015) (Figure 17). This in turn hinders further monitoring and diagnosis of the disease. This led to the development of a new "L" range of Onyx® having less tantalum particles (Ev3).

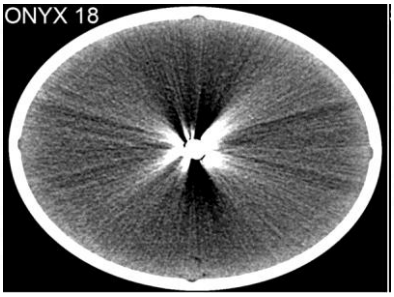

Figure 17. Artifacts in CT due to Onyx 18 (Pop et al., 2019).

Squid™/ SquidPeri™: It is similar to Onyx®, and is composed of EVA copolymer in DMSO with micronized tantalum powder. Squid™ and SquidPeri™ are used for neuro and peripheral applications, respectively. The tantalum powder grain size is smaller than the one present in Onyx®, which slows down the rate of sedimentation (Mason et al., 2018). The available formulations of Squid™ are Squid™12, Squid™12LD, Squid™18 and Squid™18LD which have viscosities of 12 mPas and 18 mPas (Figure 18). Squid™12 is suitable for the treatment of AVM due to their deeper penetration into vasculature and the higher viscosity grade Squid™18 is suitable for the treatment of endoleaks. The LD versions have 30% less tantalum which causes a reduction in the imaging artifact.

Figure 18. Different grades of Squid™ liquid embolic system (taken from https://www.debene.com/productos/balt/media/docs/balt__squid__brochure.pdf).

Precipitating Hydrophobic Injectable Liquid (PHIL™): It is designed for embolization of the peripheral and neurovasculature that include AVM and hypervascular tumors (Helmy et al., 2017; Lamin et al., 2017; Sirakov et al., 2019). The carrier solvent utilized is DMSO and the polymeric material precipitates out on contact with an aqueous environment to form a solid embolus. The polymer used here is a non-adhesive, 2,4,6-triidophenol-lactide-lactide-co-glycolic acrylate and hydroxyl ethyl-

methacrylate (HEMA) (2:1 monomer ratio) copolymer. The radiopacifying agent, iodine is covalently linked to the polymer, so no premixing is needed to achieve homogeneous suspension. In this case, the streak artifacts obtained in imaging are less than those observed in Onyx® (Kocer et al., 2016). PHIL™ is available in the market in preloaded syringes to reduce the overall procedural time (Figure 19). Different viscosity ranges of PHIL™ are available in the market. Available concentrations are 25, 30, and 35 wt.% having viscosities of 16, 36, and 72 mPas. PHIL™ precipitates with a greater volume per ml than Onyx® (Vollherbst et al., 2017). So, the amount of liquid embolic formulation needed is much less which reduces the overall cost. Additionally, there have been no microcatheter blockages reported for PHIL™ and the histological analysis of the material in the tissue revealed that it elicited a greater inflammatory reaction in the surrounding tissue (Kocer et al., 2016).

Figure 19. PHIL™ liquid embolic agent (taken from https://www.whichmedicaldevice.com/uploads/products/large/PHIL.jpg).

Iodinated Polyvinyl Alcohol (I- PVAL): Dudeck et al. (2006) reported that iodinated PVAL can be used as a liquid embolic agent and evaluated it in porcine models of wide-necked aneurysms. The carrier solvent used is N-methyl pyrrolidone which has recently been commercialized by Antia Therapeutics AG as Easyx™. Here the iodine-containing moieties have been covalently linked to the polymer through ether linkages (Antia

Therapeutics 2011). Easyx™ can be used for the embolization of hypervascular lesions including tumors and AVM. The inherent opacity imparted by iodine atoms allows clear visualization by computed tomography without the shading and beam hardening artifacts observed in the case of Onyx® (Kulcsa´r et al., 2017). The literature indicates that the Easyx™ embolization is effective with homogeneous visibility under CT (Kulcsa´r et al., 2017; Antia Therapeutics, 2011; Agusti et al., 2015). Currently, Leati et al. (2023) used Easyx™ in type II endoleak treatment with trans lumbar approach. They experienced the efficacy of Easyx™ for this particular treatment but they also suggested the evaluation in more extensive studies.

Eudragit-E® (poly(MM-co-BM-co-DMAEMA)): Eudragit® is a copolymer of methyl methacrylate, butyl methacrylate and dimethyl aminoethyl methacrylate. Carrier solvent is a mixture of 50:50 ethanol and iopamidol contrast agent (Tamura et al., 2015). To prevent premature precipitation and occlusion of the lumen the microcatheter has to be initially flushed with ethanol. However, Arakawa et al. (2007) reported that after injection of this embolic agent there was a tissue reaction (inflammation and thrombosis along with endothelial damage) similar tothat obtained using n-BCA. This could be due to the toxicity of the carrier solvent, ethanol, which is a sclerosant. The opacity in the system is provided by iopamidol which is transient and this finally diffuses out of the precipitated polymer. Tamura et al. (2015) reported their experience in using this material for treating 22 human brain AVM. They get 27.3 % of complete obliteration with embolization alone. They reported the satisfactory result for the safety and effectiveness of Eudragit E® embolization.

2.2.2.3.3. Phase transitioning type embolics

GPX: This liquid embolic agent consists of polyelectrolyte complexes that are stabilized in aqueous solutions of high ionic strength. It is based on liquid glue secreted by sandcastle worms and composed of protamine sulfate and sodium inositol hexaphosphate (Stewart et al., 2017). The formulation is made radiopaque by the addition of tantalum powder and the stabilized solution is delivered through a microcatheter. At the injection site, the polyelectrolyte complexes become destabilized due to the reduction of the ionic and physiological strength as a result of dilution in the blood. This rapid gelation of the complexes is formed in seconds and the embolic mass obtained is non-cytotoxic, non-hemolytic, non-inflammatory, and non-adhesive. Embolization in rabbit renal arteries revealed higher levels of vascular penetration and complete occlusion of the kidney (Jonson, 2018).

Calcium Alginate: Becker et al. (2007) reported calcium alginate as a liquid embolic agent in a side-wall aneurysm swine animal model. Evaluations done for 30 and 90 days showed that the presence of alginate allowed tissue overgrowth of the aneurysm opening with moderate fibrous tissue formation. In a study by Barnett et al. (2009), it was reported that the co-delivery of alginate and iohexol contrast agent in one stream and calcium ions in the other, with mixing at the exit point of catheter resulted in a string-like gel (embogel^{TM}). However, this procedure requires special microcatheters that lead to an increase in the overall cost in the development of alginate-based systems. Alternative methods are being explored for the modification of properties by mixing with other components. Huang et al. (2016) reported a liquid embolic system by mixing

alginate, calcium, poloxamer 407, hydroxyl methyl cellulose, and iodixanol. It demonstrated the ability to switch between flowing sol to gel at body temperatures and proved feasible delivery and embolization in rabbit renal arteries.

Temperature-sensitive hydrogel systems: This system is based on the phase transition of polymeric material from sol to gel with an increase in temperature. Cappello et al. (1998) developed a phase-transitioning injectable material using Silk Elastin Protein Polymer (SELP). The feasibility of embolization in a rabbit model was demonstrated by Poursaid et al. (2015) and it was found that selective occlusion of lobar hepatic arterial branches was possible by this system. Poly (N-isopropylacrylamide-co-butyl methacrylate), a temperature-sensitive nanogel-forming material, was used as a liquid embolic agent (Zhao et al., 2013). This was an aqueous-based system that requires no organic solvent and forms a non-adhesive hydrogel that does not stick to the catheter. It has no intrinsic opacity and has to be mixed with iohexol to impart radiopacity. A rapid delivery (>0.1mL/s) is essential to ensure its distribution to more peripheral vessels prior to gelation.

Another system that has similar properties to the above-mentioned system is based on chitosan and β-glycerophosphate. This system was evaluated in a rabbit renal artery model by Wang et al. and in swine rete mirabile by Ning et al. in 2011 and 2015, respectively.

PuraMatrix™: It is a 16 amino acid-containing peptide comprised of arginine, aspartate, and alanine repeating units. The formulation consists of 2.5 wt. % peptide in

aqueous media mixed with an iodinated contrast agent (Baba et al., 2018). The peptide sequence has an alternating hydrophobic part that promotes β-strand formation and self-assembled into a nano fiber-based hydrogel material (Cormier et al., 2013). Pathological analysis after embolization reveals that it reaches distal locations and imparts hardly any inflammation on the vessel and surrounding tissues.

Shear Thinning Biomaterial: This material has rheological properties wherein the viscosity drops when sheared by injection through a narrow lumen of a microcatheter and is currently under investigation as a liquid embolic material. On exiting the catheter, the shear stress is removed, and the material returns to a gel state to form an embolus. Avery et al. (2016) developed a nanocomposite hydrogel containing gelatin and silicate nanoplatelets, to function as an embolic agent for endovascular embolization procedures (Figure 20). These in *situ* gelling hydrogels represent safe, feasible, and economical methods for endovascular embolization.

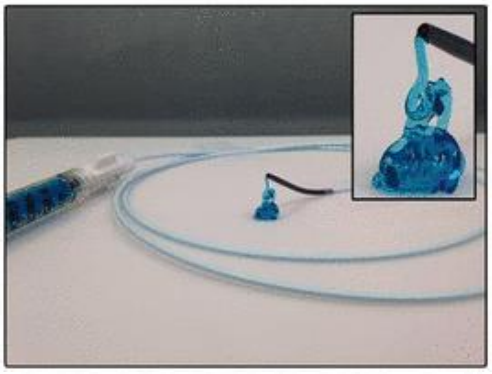

Figure 20. Shear thinning biomaterial (Avery et al., 2016).

There are numerous liquid embolic materials that are currently under development, but a number of prerequisites must be fulfilled to obtain a desirable system. These include

reduced artifact on imaging, suitable gelation triggers to avoid catheter blockage, and suitable viscosity for the occlusion of desired location.

2.3 Embolization using liquid embolic agents

Liquid embolic agents that use DMSO as a solvent are extensively used for embolization because they can be easily filled in large areas. Vollherbst et al. (2017) compared the efficacy of the commercially available liquid embolic agent Onyx® and a novel precipitating hydrophobic injectable liquid (PHIL^{TM}) in an *in vitro* AVM model. The shorter pause time and lower volume results obtained using PHIL^{TM} result in a higher embolization success compared to Onyx® for the same extent of embolization. This is due to the homogeneity of the radiopacifier in PHIL^{TM} (covalently linked organo-iodo compound) when compared to Onyx® (tantalum powder) liquid embolic agent. Vollherbst et al. (2018 (a)) also evaluated the successful embolization of PHIL^{TM} liquid embolic agent in porcine rete mirabile. Sixteen embolization procedures were done using PHIL^{TM} (n=8) and control Onyx® (n=8) and the results revealed that there were no significant differences observed in embolization characteristics or extent using either PHIL® or Onyx®. Both the evaluated embolic agents reveal moderate disintegration and mild inflammation of embolized blood vessels. They then further evaluated the feasibility of PHIL^{TM} for transarterial embolization. Lamin et al. (2017) also evaluated the efficacy of PHIL^{TM} liquid embolic agent for endovascular treatment of cranial dural arteriovenous fistulas by treating 26 patients manifesting this condition. They concluded that the use of iodine as a radiopacifier produces fewer artifacts on CT compared with

tantalum-based embolic materials. A preliminary study using PHIL™ and Onyx® was carried out to evaluate brain arteriovenous malformation. Kocer et al. (2016) reported that the smallest vessel containing PHIL™ was 2.9 µm in comparison to 5 µm with Onyx® which highlights the good penetration behavior of PHIL™ liquid embolic agent compared to the Onyx®.

The composition of an embolic agent significantly influences the performance of endovascular embolization. Vollherbst et al. (2018 (b)) investigated the effects of a new version of PHIL™ that was endowed with extra low viscosity in an *in vivo* embolization model. They observed a higher embolization extent for low-viscosity PHIL™ when compared to its higher-viscosity counterpart. The distal penetration of this system is very effective and has advantages that include adequate visibility, a low amount of reflex, and good flow control. Ayx et al. (2017) determined the success of Onyx® LEA for bronchial artery embolization in patients with acute hemoptysis. It had a good clinical outcome and presented a lower number of recurrences. Kannath et al. (2017) studied percutaneous direct puncture embolization as an additional treatment option for patients with scalps with AVMs using the SQUID™ liquid embolic agent. In their opinion, this should be considered as the primary treatment option for patients unwilling to undergo surgery. Sirrakov et al. (2019) reported their initial experience with Menox 18™ (EVOH copolymer-based LEA) in the endovascular treatment of cerebral arteriovenous malformations. They suggested that the Menox™ embolization system offers similar technical and clinical results in comparison with other LEAs.

Izaaryene et al. (2016) assessed the distal dispersion, adhesion strength to the catheter, vascular toxicity, and the ability to exclude embolized vessels using Purefill® (α-hexil cyanoacrylate), an embolic material, in pig rete mirabile. Purefill® had a reduced angle and distance of displacement compared to other glues and displayed limited adhesive strength. They compared the results with n-BCA (Histoacryl®) and a mixture of n-BCA and methacryloxysulfolane and found that the embolic efficacies obtained were similar in all three cases.

Lee et al. (1989) evaluated the effectiveness of three embolic agents including liquid suspensions (microfibrillar collagen hemostat (MCH), glutaraldehyde crosslinked collagen (GAX), and fibrin sealant (Tisseel) in pig rete. The results obtained suggested that the MCH with ethanol system showed ease of handling and effective small vessel occlusion. Liquid embolic agents can also be used for preoperative embolization. Ko et al. (2003) reported a preoperative portal vein embolization in patients with hepatocellular carcinoma using ethanol as solvent. They used Embol-78 (obtained by the hydrolysis of polyvinyl acetate) dissolved in a mixture of ethanol and non-ionic water as an embolic agent. Agusti et al. (2015) developed radiopaque iodinated ether of polyvinyl alcohol and tested for embolization in an aneurysm model. He argued that the system resists hydrolysis and is bio stable in nature. Additionally, he suggested N-methyl pyrrolidone as a solvent for embolization in addition to dimethyl sulfoxide.

Mottu et al. (2002) synthesized cellulose acetate iodobenzoate mixed ester-based embolic liquids for the treatment of cerebral aneurysms and arteriovenous malformation.

A 32% solution of radiopaque polymer in diglyme or dimethyl isosorbide (DMI) was used and the efficacy of embolization was tested in sheep aorta. The viscosity possessed by the 32% system in DMSO or diglyme was 240 and 415 cSt, respectively, at 25 ˚C. However, the 32% solution in DMI showed a higher viscosity (2400 cSt at 25 ˚C). In the previously conducted *in vitro* study they used a macrocatheter for the injection of the high-viscosity sample. A hard and coherent mass of precipitate was obtained from this concentration highlighting the importance of higher polymer concentration in embolization.

Corkill et al. (2007) analyzed the endovascular treatment results using the Onyx® liquid embolic system for spinal intramedullary arteriovenous malformation in 17 patients and concluded that the system served as a promising treatment method for spinal vascular malformations. Li et al. (2020) evaluated the efficacy of a new liquid embolic agent, Fe_3O_4-EVOH, for endovascular arteriovenous malformation embolization in an *in vivo* swine rete mirabile model and found that it is an effective endovascular occlusion material, and displayed advantageous characteristics of stability and biocompatibility.

Jayaraman et al. (2008) examined the overall neurologic complication rate in patients undergoing AVM embolization and analyzed the factors that determine increased risk. They classified the complications as none, non-neurologic (mild), transient neurologic deficit, permanent non-disabling, and permanent disabling deficits. The permanent complications were further classified into ischemic and hemorrhagic. On careful analysis of all the results obtained, he concluded that embolization of brain AVM can be

performed with a high degree of technical success and a remarkably low rate of permanent neurologic complications.

To ensure effective and safe embolization procedures prior knowledge of special properties of the agent is necessary. Vollherbst et al. (2021) described the properties and indications of currently available liquid embolic agents: Cyanoacrylates (glue) and copolymers (Onyx®, Squid^{Tm}, and PHIL^{TM}) as well as their subtypes. Even though cyanoacrylates are considered an old LEA, they still find application in specific situations like the occlusion of macro shunts in the pressure cooker technique. Onyx®, the first copolymer-based embolic agent suffers from drawbacks that include temporary loss of visibility during longer injection and artifacts in cross-sectional imaging. Squid^{TM} and PHIL^{TM} however, overcome these limitations and enhance the success rate of endovascular embolization. These new liquid embolic agents have lower viscosities, more stable visibility, and lower degree of imaging artifacts. According to Vollherbst et al. (2021), all the commercially available liquid embolic agents have potential advantages and disadvantages and the most appropriate embolic agent should be selected based on material characteristics and the specific anatomical characteristics of the target.

2.4 In vivo models for AVM

Medical researchers have tried to build *in vitro* or *in vivo* experimental models for brain AVM. Massoud et al. (1994, 1996, 2000) reported that the pig's rete mirabile could serve as an experimental AVM model. An *in vivo* experimental model in sheep was performed by Qian et al. (1999). Schumacher & Schellhammer (1999) performed a

bilateral high-flow fistula in dogs. Pietila et al. (2000) performed an arteriovenous fistula by interposing the middle cerebral artery and the dorsal sagittal sinus in dogs. Herman et al. (1995) performed the occlusion of the draining vein of the transverse sinus in a rat model. Tu et al. (2010) investigated the morphological characteristics of the animal AVM model (Sprague-Dawley rats) and compared it to human AVMs. The morphological similarities obtained in the above studies include heterogeneously thickened walls, splitting of the elastic lamina, thickened endothelial layers, endothelial cushions, lack of tight junctions, loss of endothelial continuity, endothelial-subendothelial adherent junctions and luminally directed filopodia. These findings support the use of animal models for human AVM studies.

Computer and biomathematical models were also designed for research purposes (Young et al., 2007). Jain et al. (2019) constructed a theoretical electrical circuit AVM model with a nidus described by a stochastic block model of 57 nodes and an average of 1000 plexiform and fistulous vessels. This model served as a useful tool for theoretical investigations of AVM therapies and their hemodynamic sequelae. In addition, the first DSA based AVM model was developed by Zhang et al. (2020).

2.5 Histological characteristics of brain AVM

The histological analysis of brain AVM (BAVM) tissues showed higher angiogenic proliferation with evidence of increased endothelial turnover (Moftakhar et al., 2009). The growth, remodeling, and rupture of brain AVM depend on vasculogenesis and flow through the nidal vessel (Rangel-Castilla et al., 2014). So, the animal model having

histological features similar to human brain AVM could be useful for the evaluation of new non-invasive therapies (Moftakhar et al., 2009). The first swine model for AVM was described by Massoud et al. (1994, 2000) and it was further adapted by Wakhloo et al. (2005). Papagiannaki et al. (2017) evaluated the histopathological changes induced by common carotid artery (CCA) and external carotid artery (ECA) occlusion. They concluded that the CCA-ECA occlusion showed angiogenesis triggering of the rete mirabile.

The difference in pathology possessed by high-risk arteriovenous malformations has still not been explored. Hermanto et al. (2016) reviewed hematoxylin-eosin specimens from 54 surgically treated BAVMs. They found significant differences in the degree of venous enlargement and intimal hyperplasia. The high-risk profiles of BAVMs patients were well reflected in the nidus pathology obtained.

Sadato et al. (2000) studied the effects of a mixture of low concentrations of n-Butylcyanoacrylate and Ethiodol on tissue in a rabbit model. In the acute stage, the histopathological findings included acute necrotizing vasculitis, loss of endothelium, and intact or destroyed media. In the chronic stage, chronic granulomatous vasculitis and fibrosis of the embolized vessels was revealed. The histological examination of the renal arteries immediately after embolization reveals stripping of the endothelium and morphologically intact internal elastic lamina and smooth muscle layer.

In order to understand the role of presurgical embolotherapy in the treatment of intracranial AVM, Schweitzer et al. (1993) carried out a detailed pathological analysis of

specimens treated with various embolic materials. He observed that Avitene™ (an absorbable microfibrillar collagen hemostat) produced the mildest tissue response but resulted in early endothelialization and recanalization. Cyanoacrylates lasted for a longer duration but demonstrated more acute and chronic inflammation and vessel wall changes. Polyvinyl alcohol foam/ ethanol mixture was associated with intermediate properties. This immunohistochemical study confirms the endothelial proliferation over embolization material.

The histopathological changes associated with brain arteriovenous malformation after embolization using Onyx® or N-butyl cyanoacrylate were investigated by Natarajan et al. (2009). The smallest vessel occluded was 5 microns and 20 microns by Onyx® and n-BCA, respectively. There was vascular, perivascular inflammation (in 90%) and angio-necrosis of the embolized vessels (in 59.1% for Onyx® and 40% for n-BCA) noted in the specimens treated with both Onyx® and n-BCA. However, chronic foreign body giant cells (in 54.5%) and recanalization (in 18.2%) were observed only for specimens treated with Onyx®.

Recently Jarvelin et al. (2020) investigated tissue samples from surgically treated BAVMs using standard histological and immunohistochemical staining. On analysis, they found microhemorrhages from nidal vessels and these were associated with the presence of immature, pathological nidal vessels, perivascular inflammation (with the adhesion of neutrophils), and neutrophil infiltration.

2.6 Radiopaque polymers

Polymers present a wide range of applications in the medical field ranging from disposable devices to permanent implants. They are generally radiolucent and are not visible under fluoroscopic imaging owing to their low electron density and low specific gravity. Several strategies are described in the literature to impart radiopacity in polymers by incorporating heavy elements such as derivatives of Lead (ZPb=82) and Bismuth (ZBi=83) or inorganic salts such as Barium sulfate (ZBa=56) into polymeric systems (Jayakrishnan et al., 1990; Thanoo et al., 1991 (a) and (b)). The drawback of this approach is the nonhomogeneity of the resultant polymeric system which may negatively affect the properties of the end product. This problem can be overcome by the production of single-phase radiopaque polymer salt complexes by the incorporation of a radiopaque heavy metal salt. Currently, iodination of the polymer is found to be a more attractive approach.

X-ray absorption depends on the fourth power of atomic numbers (eq. 1) (Kramers, 1923).

$$\mu = K\lambda^3 Z^4 + 0.2 \qquad \text{(eq. 1)}$$

Where λ is the wavelength of the X-ray beam, K is a constant, and 0.2 is the average scattering coefficient which is independent of λ. So, the elements having higher atomic number (Z) exhibit better radiopacity.

2.6.1. Types of radiopaque polymer systems

Radiopaque polymer systems are classified into heterogeneous mixtures with inorganic salt ($BaSO_4$), blends with organo-radiopaque derivatives, polymerization products of radiopaque monomers, and radiopaque polymer-salt complexes, and homogeneous systems.

The heterogeneous mixtures are prepared by incorporating the radiopacifying agent with polymer. These additives leach out with time and are used only for temporary radiopacity. Polymer-salt complexes are produced by the incorporation of radiopaque heavy metal salt into polymer ligands through chelation. This is a homogeneous system and can be used for permanent radiopacity. In polymerization products of radiopaque monomers, the monomer unit is produced by the electrovalent or covalent interaction of radiopacifying elements or compounds. The electrovalent bond is susceptible to hydrolysis so permanent radiopacity cannot be achieved. The covalently bound systems have a higher cost which limits their usage so research is ongoing for producing more viable materials.

2.6.1.1. Heterogeneous systems

For dental and medical applications gold gauze, lead foil, and fine wires inserted in poly (methyl methacrylate) (PMMA) and its derivatives (Smid et al., 1987). Finely divided metals provide homogeneity but when mixed with polymers the transparency of the materials would be lost. The heterogeneity of the mixture adversely affects the material

properties and enhances penetration of moisture and other liquids causing leaching of additives, bacteria penetration, loss of optical transparency, and mechanical cracks.

2.6.1.2. Homogeneous systems

High boiling aliphatic and aromatic halides (1, 1, 2, 2-tetrabromoethane, 1, 2-dibromoethane, iodobenzene) can be dissolved in PMMA and its derivatives. But these also tend to leach out with time (Combe et al., 1971; Davy et al., 1982). The problem of leaching can be resolved by dissolving the metal salts in polymers containing cation-chelating moieties. Literature suggests that carbonyl and phosphate-containing monomers and polymers solubilize a variety of heavy metal salts (Combe, 1972) (Cabasso et al., 1989). Triphenyl bismuth forms miscible and optically transparent blends of high radiopacity with a broad range of polymeric materials such as polystyrenes, polyalkenes, polyacrylates, poly (vinyl chloride) and epoxy resins (Delaviz et al., 1990 (a)) (Chatterjee et al., 1995).

2.6.1.3. Polymers with chemically bound radiopacifier

Davy and Causton (1982) reported a material having radiopacity equivalent to aluminium by copolymerization of methyl methacrylate (MMA) and 35 wt% of 2,3-dibromopropyl methacrylate. Horak et al. (1987) developed spherical radiopaque hydrogel particles for endovascular occlusion by the hydroxyl acylation of low cross-linked pHEMA beads with a nontoxic radiopaque compound based on triiodo benzoic acid. The monomer styryldiphenyl bismuth produces polymers with covalently bound triphenyl bismuth (Delaviz et al., 1990 (b)). Apart from Bismuth compounds, tin and

lead have also been reported but their higher toxicity makes them less attractive as radiopacifiers.

2.6.2. Applications of radiopaque polymers

2.6.2.1. Medical applications

Radiopaque polymers find applications in medical devices such as implants, catheters, sutures, and medical adhesives. In dentistry, they are used as fillings and as restorative materials (Moszner and Salz, 2001; He et al., 2012). They have been used in the monitoring of fallopian tube blockage and for the identification of changes in kidneys and other body functions (Shah, 2000). All the above applications mainly employ iodinated organic compounds containing monomers or polymers.

Iodinated methacrylate-based polymers were reported by Moszner et al. (1995), Dawlee et al. (2009) and Wang et al. (2010). Functionalized 1,3,5-triiodo benzene covalently linked to polyethyleneglycol-amine finds application as a contrast agent for X-ray radiology (Hainfeld, 2021). Wang et al. (2010) synthesized iodine-containing methacrylate-based polymer through RAFT polymerization and the material has the potential to be used for biomedicine and therapeutics. James et al. (2006), Kiran et al. (2009), Dawlee and Jayabalan (2011), Qu et al.(2011) and Kiran et al. (2012) synthesized radiopaque iodinated polyurethanes for various medical applications. 4-iodo-phenylalanine (4-iodobenzyl bromide) linked polylactic acid has been tested for biomedical imaging (Lex et al., 2020). Polyester prepared by the poly condensation of 2,2-bis(iodomethyl)-1,3-propanediol and the corresponding diacids are used as contrast

agents for implants (Houston et al., 2017). 2,3,5-triiodobenzoyl chloride grafted polyvinyl alcohol nanoparticle has been utilized for spectral photon-counting computed tomography (Balegamire et al., 2020). Radiopaque polymeric nanoparticles prepared by the emulsion polymerization of the monomer 2-methacryloyloxyethyl (2,3,5-triiodobenzoate) have found applications in X-ray imaging (Galperin et al., 2007). 2,3,4-triiodobenzoic acid linked cellulose and partially substituted cellulose acetate have been used for embolization of cerebral aneurysms and arteriovenous malformations (Mottu et al., 2002). Shiralizadeh et al. (2016) synthesized a copolymer of methyl methacrylate and acrylic acid which was made radiopaque using 4-iodophenyl isocyanate and 3,4,5-triiodophenyl isocyanate. Further, 4-iodo benzyl and 2,3,5-triiodo benzyl group grafted polyvinyl alcohol (through ether linkage) was found to be suitable as a radiopaque polymer for vascular embolization (Agusti et al., 2015).

2.6.2.2. Other applications

Radiopaque polymers find application in the plastic wrapping of toys and can be detected if a child accidentally swallows them (Silberman, 1988). It can also be used for coding purposes, the detection of mechanical deficiencies such as cracks and crazes, and in explosives.

2.6.2.3. Applications in embolization

In embolization procedures, a variety of radiopacifiers have been used to introduce radiopacity. These include barium sulfate, tantalum, and organoiodine compounds. These embolization procedures are guided by ultrasound and X-ray imaging. Compared

to ultrasound-guided procedures, X-rays have higher frequencies and can provide more detailed and clearer images. X-ray fluoroscopy helps in interventional procedures like guidance of catheters for embolization and the X-ray angiogram in turn helps to map the vasculature. Recently, computed tomography that provides three-dimensional images has also been used for noninvasive imaging. A contrast agent having different radiopacity than the surrounding tissue is used to enhance the images of X-ray. For effective imaging of a contrast agent, it should be taken with a peak voltage higher than the K-edge of the agent. K-absorption edge (K-edge) is the increase in photoelectric absorption of X-ray photons observed at an energy level just beyond the binding energy of the K-shell electrons of the absorbing atom. K-shell binding energy is specific to each element. As atomic number increases K-shell binding energy increases, therefore greater the photon energy at which k-edge occurs. For example, iodine (Z=53) has a k-edge value 33.2 keV (Roberts and Williams 2020). X-ray attenuation is quantified by Hounsfield unit (HU) (eq.2)

$$\mathrm{HU} = \frac{1000 \times (\mu - \mu_{\mathrm{water}})}{\mu_{\mathrm{water}} - \mu_{\mathrm{air}}} \qquad \text{(eq.2)}$$

μ is the linear attenuation coefficient. The Hounsfield scale is standardized by HU_{water}= 0 and HU_{air}= -1000 (Chhour et al., 2017; Lusic and Grinstaff, 2013).

A major limitation of the currently used radiopaque liquid embolic agents are the sedimentation of tantalum powder that causes premature catheter blockage. The presence of metallic tantalum powder in the vascular channels can cause arcing and excessive fume generation and it also cause significant artifacts in the follow up CT and

MRI scans. Since metallic particles are used in the current system, a 20 min. long shaking is needed for making a uniform suspension prior to embolization procedure. This is time consuming. An experienced person can only use the current system. It is very expensive too. In this work, an attempt was made to develop an alternative system which is a non-adhesive precipitating polymer free of metal particles that can be freely injected into the blood stream. To develop such a system, a series of radiopaque compounds were synthesized and grafted onto a precipitating polymer, ethylene vinyl alcohol copolymer (EV). The radiopaque compounds, and grafted polymer were characterized for their physicochemical and biological properties. Liquid embolic formulations were developed and characterized for its suitability for clinical applications.

2.7 Market survey of liquid embolic agent

According to Global Market Research (accessed on October 20, 2023), the global liquid embolic agent market is expected to rise at a considerable rate during the period 2022-2031. The market growth is anticipated to continue due to the adoption of newer strategies by key players. Factors driving this growth could include advancements in medical technology, increased prevalence of vascular disorders, and expanding applications of liquid embolic agents in minimally invasive procedures. Additionally, as healthcare systems continue to prioritize less invasive treatment options, the demand for liquid embolic agents may further escalate. The market's growth trajectory underscores

the importance of continued innovation and development in this sector, potentially leading to improved patient outcomes and expanded therapeutic options for clinicians.

The latest research revealed that the Global Liquid Embolic Agents market size was USD 332.05 million in 2023 and is expected to expand at a CAGR of 9.3 % during the forecast period which reaches USD 565.55 million by 2030. (Ref.: *Liquid Embolic Agent Market Size, Share, Trends & Forecast (verifiedmarketresearch.com)*).

The largest manufacturers of Liquid Embolic Agents are MicroVention, Terumo, Medtronic, Meril Life, etc. Most of the Liquid Embolic agent companies are from the United States and Europe. More than 90 % of the market share was contributed by the top two companies. The leading regions of the liquid embolic agent market are North America (US, Canada, Mexico), Europe (Germany, UK, France, Italy, Russia, Turkey, etc.), Asia-Pacific (China, Japan, Korea, India, Australia, Indonesia, Thailand, Philippines, Malaysia, and Vietnam), South America (Brazil, Argentina, and Colombia), Middle East and Africa (Saudi Arabia, UAE, Egypt, Nigeria and South Africa). The North American liquid embolic market was dominated by the US with a market share of 79.9 % in 2021. In the European market, Germany is expected to dominate with a share of 23.7 %. In East Asia, South Korea held nearly 7.6 % share in 2020.

3. MATERIALS AND METHODS

3.1 Materials

The materials used for the work, purity, sources, and other details are listed in Table 1.

Table 1. List of chemicals used for the work

Sl. No.	Name of the chemical	Purity	Source	Grade / Remarks, if any
1	1,4-dibromo butane	98 %	M/s. Merck Ltd., Mumbai, India	For synthesis, Assay (GC, area %)
2	4,4-bis(4-hydroxy phenyl) pentanoic acid	95 %	Sigma Aldrich, India	-
3	Borane-THF complex solution	1 M in THF	Sigma Aldrich, MO, USA	
4	Chloroform	99.5 %	M/s. Spectrochem Pvt. Ltd, Mumbai, India	
5	Dicyclohexyl carbodiimide	99 %	Sigma Aldrich, MO, USA	
6	Dimethyl Amino Pyridine	99 %	M/s. Merck Ltd., Mumbai, India	Reagent plus
7	Dimethyl formamide	99 %	M/s. Spectrochem Pvt. Ltd, Mumbai, India	Puriss for synthesis
8	Dimethyl sulfoxide	0.025 % H_2O	M/s. Merck Ltd., Mumbai, India	Dried (max.0.025 % H_2O) SeccoSolv®
9	Dimethyl sulfoxide	99.5 %	M/s. Merck Ltd., Mumbai, India	
10	Ethylene vinyl alcohol copolymer	Ethylene content – 27 mol %, 32 mol % & 38 mol %	Sigma Aldrich, MO, USA	
11	HCl	37 %	M/s. Merck Ltd., Mumbai, India	Emsure, For analysis
12	Methanol	99.9 %	M/s. Merck Ltd., Mumbai, India	-

13	Potassium carbonate	99 %	S.D Fine chemicals Ltd., Mumbai	Anhydrous, extrapure
14	Sodium chloride	99.8 %	Sigma Aldrich, MO, USA	
15	Sodium hydroxide	99 %	M/s. Merck Ltd., Mumbai, India	Emsure, Pellets for Analysis.
16	Sodium hypochlorite	4.8-8 % (w/v)	M/s. Merck Ltd., Mumbai, India	Emplura, About 4 % w/v available chlorine
17	Sodium iodide	98.5 %	M/s. Merck Ltd., Mumbai, India	
18	Sodium sulphate (Anhydrous)	99.5 %	M/s. Merck Ltd., Mumbai, India	G.R. grade
19	Sodium thiosulfate pentahydrate	98.5 %	M/s. Merck Ltd., Mumbai, India	Emplura
20	Tetrahydro furan specially dried	99.5 %	M/s. Merck Ltd., Mumbai, India	G.R.

3.2 Methods

3.2.1. Raw materials and their characterization

The major raw materials used for the study are 4,4-bis(4-hydroxyphenyl) pentanoic acid (BHP) and ethylene vinyl alcohol copolymer (EV).

3.2.1.1. 4, 4-bis(4-hydroxydophenyl) pentanoic acid

BHP was characterized by the following techniques.

FTIR spectroscopy: IR spectrum of BHP was obtained in a Nicolet 5700 model FTIR spectrometer with an ATR accessory. A small amount of pure compound was ground to a fine powder, placed on the diamond crystal of the ATR equipment and scanned in the range of 4000-400 cm^{-1} at a resolution of 4 cm^{-1}.

^{1}H NMR spectroscopy: The different types of protons in BHP were determined by ^{1}H NMR spectroscopy. ^{1}H NMR spectrum was recorded on a 500 MHz instrument (Bruker AV 500) using DMSO-d^6 as the solvent.

UV-Visible spectroscopy: For UV measurements 1×10^{-6} M solution of BHP was prepared in methanol and the spectrum was recorded using a UV 1800 spectrophotometer (Shimadzu) at a wavelength range of 200-800 nm. The corresponding pure solvent absorbance was subtracted from the spectrum.

Mass spectroscopy: In mass spectroscopy, powdered samples are ionized by spraying, which results in some molecules breaking into charged fragments. These ions are then separated according to their mass-to-charge ratio, typically by accelerating them and subjecting them to an electric or magnetic field: ions of the same mass-to-charge ratio will undergo the same amount of deflection. Here the mass spectrum of BHP was recorded on M/s. Thermofischer Scientific Exactive LCMS instrument (Germany).

Thermogravimetric analysis: The temperature-dependent decomposition of BHP was found from the Simultaneous Differential thermal analyzer - Thermogravimetric analyzer (DTA-TGA) (SDT Q 600) in a nitrogen atmosphere from room temperature to 1000 ˚C at a heating rate of 10 ˚C min^{-1}.

3.2.1.2. Poly (vinyl alcohol-co-ethylene)

Poly (vinyl alcohol-co-ethylene) is also referred in the literature as ethylene vinyl alcohol copolymer (EV). All the grades of EV were characterized by the following techniques.

FTIR spectroscopy: For FTIR characterization, EV pellets were powdered using a pulverizer and this powder was used for the characterization. The method used was same as that described in section 3.2.1.1.

^{1}H NMR spectroscopy: ^{1}H NMR characterization of EV was determined as the same method explained in section 3.2.1.1.

Thermogravimetric analysis: TGA analysis of EV was determined in powder form using the same method in 3.2.1.1.

Differential scanning calorimetry: The heat flow associated with phase transitions or reactions, i.e., melting and glass transition was recorded using a differential scanning calorimeter (DSC) (Q20 model, TA instruments) under a nitrogen atmosphere.

X-ray powder diffraction: The crystallinity of EV was identified using X-ray crystallography technique. The powdered samples were analyzed by X-ray diffractometer, Rigaku DmaxC model with CuKα radiation (λ = 1.5418 Å). The scanning was done in θ–2θ mode in the range of 10–50˚ with a fixed incident angle of 1˚.

All other materials listed in section 3.1 were used as such without doing any characterization techniques.

3.2.2. Synthesis of radiopaque iodocompounds

3.2.2.1. 4, 4-bis(4-hydroxy-3,5 diiodophenyl) pentanoic acid

The tetra iodocompound, 4, 4-bis(4-hydroxy-3,5 diiodophenyl) pentanoic acid (IBHP) was synthesized from 4,4-bis (4-hydroxyphenyl) pentanoic acid (BHP) by adopting a procedure similar to that reported by Kiran et al. (2009) (Scheme 2). For this, 2g BHP was dissolved in 50 ml of methanol. Two equivalents of sodium hydroxide (NaOH) (0.13g) and 6 equivalents of sodium iodide (6.3g) were then added and the solution was cooled to 0°C (by the frequent addition of ice). Aqueous sodium hypochlorite (NaOCl) (3.104g, 6 equiv.) was then added drop wise for 75 min at 0-3°C.As each drop hit the solution, a red color appeared and faded almost instantly, resulting in a yellow-colored solution. After the complete addition of hypochlorite, 2 drops of 3 M HCl were added, stirred for 1 h at 0-2°C, and was precipitated by adding 10% sodium thiosulfate and 10% HCl. The precipitate was filtered, washed with water, and dried in a hot air oven. The yield of the product obtained was 75%.

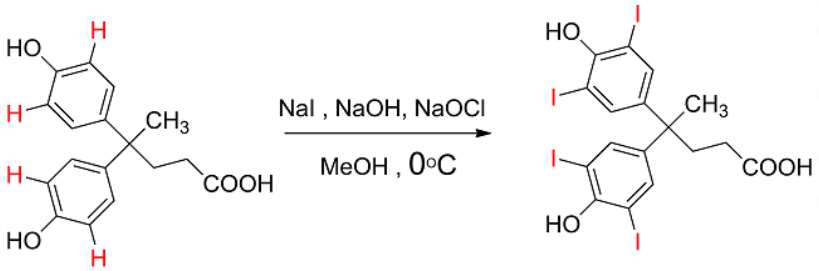

Scheme 2. Iodination of 4,4-bis (4-hydroxyphenyl) pentanoic acid

3.2.2.2. 4,4-bis (4-hydroxy 3,5-diiodo phenyl) pentanol

4,4-bis (4-hydroxy 3,5-diiodo phenyl) pentanol (IBHOH) was synthesized by the reduction of the carboxyl group of IBHP using borane-THF complex (Scheme 3). About 2g 4,4-bis (4-hydroxy 3,5-diiodo phenyl) pentanoic acid was dissolved in 7.3mL THF, cooled to 0ºC, and then treated with 7.9 mL of 1M borane solution in THF. The resulting mixture was then stirred at 25ºC for 5hrs. The mixture was subsequently cooled to 0ºC and 20mL of 3N NaOH was added to destroy the excess hydride and to hydrolyze the amine-borane complex obtained. This procedure required 12 h at 25ºC. The two phases obtained were then separated. The aqueous phase was saturated with K_2CO_3, and extracted with five 30 mL portions of ether. The other THF phase was separated and the combined organic extracts were dried over anhydrous sodium sulfate stripping off the solvents on a rotary evaporator (Yoon et al., 1973). The yield obtained was 89%.

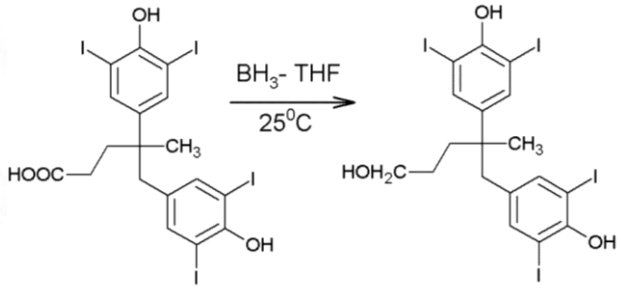

Scheme 3. Conversion of 4, 4-bis(4-hydroxy-3,5 diiodophenyl) pentanoic acid to 4, 4-bis (4-hydroxy 3,5-diiodo phenyl) pentanol.

3.2.2.3. (4-(5-bromo-2-(4-hydroxy-3, 5-diiodophenyl) pentan-2-yl)-2, 6-diiodophenol

For synthesizing (4-(5-bromo-2-(4-hydroxy-3, 5-diiodophenyl) pentan-2-yl)-2, 6-diiodophenol (HR), the approach adopted was haloalkylation of the hydroxyl group of IBHOH using dibromobutane and potassium carbonate (K_2CO_3) (Scheme 4). Initially, IBHOH (2 g) and K_2CO_3 (2 equiv.) were taken in a 250 ml two-neck round bottom flask containing 30-40 ml dry DMF. After stirring the mixture for 30 min at room temperature 2 equiv. of dibromobutane was added drop wise. The reaction mixture was then stirred at 90°C for 24 h. After 24 h, the reaction mixture was cooled and poured into water, and extracted three times with chloroform. The combined organic layer was washed with brine (NaCl solution), water and dried over anhydrous sodium sulfate. The solvent was evaporated under reduced pressure (Nagarimadugu et al., 2008). The yield of the product obtained was 89%.

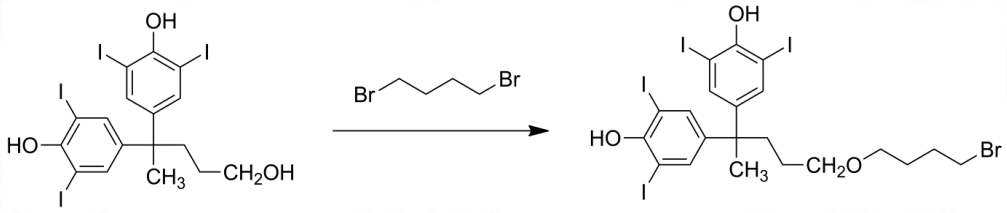

Scheme 4. Conversion of 4,4-bis (4-hydroxy 3,5-diiodo phenyl) pentanol to (4-(5-bromo-2-(4-hydroxy-3,5-diiodophenyl) pentan-2-yl)-2,6-diiodophenol.

3.2.3. Characterization of radiopaque iodocompounds

Radiopaque iodocompounds were characterized by the following methods.

FTIR spectroscopy: The influence of iodine in the stretching and bending vibrations of the parent compound and conversion of different functional groups in different

iodocompounds were characterized by FTIR spectroscopy as the same method described in 3.2.1.1.

^{1}H NMR spectroscopy: Tetraiodination and different types of protons present in different iodocompounds were characterized by ^{1}H NMR spectroscopy. The method used is as same as in section 3.2.1.1.

^{13}C NMR spectroscopy: Different types of carbon atoms in HR were determined by ^{13}C NMR spectroscopy using 500 MHz Bruker AV 500 instrument using $CDCl_3$ as solvent. The scan range used was 0-200 ppm.

UV-visible spectroscopy: UV-Visible spectroscopy determined the influence of iodine in the absorption wavelength. The method used for the determination was described in section 3.2.1.1.

Mass spectroscopy: The increase/decrease in molecular weight after iodination and functional group substitution were determined by mass spectroscopic analysis as described in 3.2.1.1.

Energy Dispersive X-ray analysis: The presence of iodine in IBHP was determined by EDX analysis. It was taken in an ESEM; Quanta 200, The Netherlands.

Radiopacity measurement: For radiopacity measurements, individual solutions of iodocompounds were prepared by dissolving them in DMSO and put in a CT scanner (Philips Brilliance 16-Slice). The attenuation of X-rays by the material was recorded. The values were reported in Hounsfield units (HU). Scan parameters used were 140 kV

and 470 mA. The specimens were kept in longitudinal positions (head-to-foot) to obtain direct cross-sectional images.

3.2.4. Synthesis of radiopaque poly (vinyl alcohol-co-ethylene)

3.2.4.1. Grafting of HR onto EV

HR was grafted onto EV (EV-g-HR) through an ether linkage by Williamson ether synthesis (Scheme 5). At first, EV (1 g) was dissolved in 50 ml DMSO at 90°C by stirring under nitrogen gas flow (Figure 21). This is then cooled to 50°C, ground and dried sodium hydroxide powder (10 mmol, 2eq.) was added, followed by HR (5 mmol, 1eq.). The reaction was carried out at different periods such as 5 h, 8 h h, 48 h and 120 h and different reactions were set up for different time periods. After the corresponding period, the mixture was cooled to room temperature and 50 ml cold water was added under stirring to precipitate the polymer. After filtration the precipitated solid was recovered and washed with water and chloroform and further dried in a hot air oven (Agusti et al., 2015). The weight of material obtained was 1.2 g.

Figure 21. Reaction setup used for the synthesis of EV-g-HR.

Two available grades of EV (27 mol% and 38 mol %) were used to synthesize HR grafted EV (ie. EV27-g-HR and EV38-g-HR), using various ratios of EV to HR such as 1:5, 1:8 and 1:10. Similar procedures were used for all syntheses.

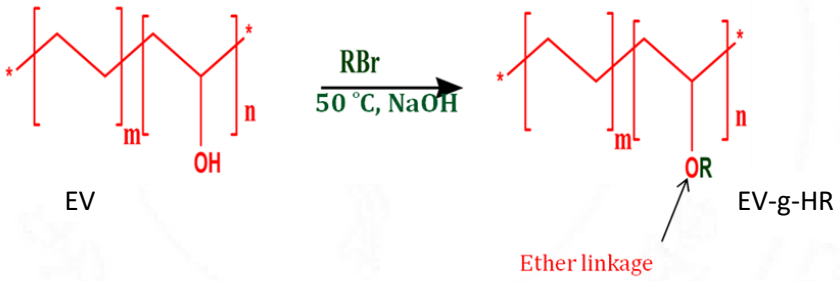

Scheme 5. The scheme of synthesis of EV-g-HR

3.2.4.2. Grafting of IBHP onto EV

IBHP was grafted onto EV (EV-g-IBHP) through an ester linkage by Steglisch esterification reaction (Scheme 6). 1g EV was dissolved in 100 ml DMSO at 70˚C in a 250 ml round bottom flask. After cooling to room temperature, IBHP (10 mmol, 1 eq) was added to the mixture by stirring. To this mixture, DCC (11 mmol, 1.1 eq) and

DMAP (10 mmol, 1 eq) were added and stirred magnetically at room temperature (James et al., 2006). Reactions were set at different periods: 24 h, 48 h, 72 h, 96 h, 120 h and 144 h. After the corresponding period, the precipitated dicyclohexylurea (DCU) was removed by filtration and the reaction mixture poured into water to precipitate the IBHP grafted EV (EV-g-IBHP). The precipitate was purified by washing with water and methanol to remove the untreated reagents and dried at 60 ˚C. The yield obtained was 4.46 g. The reaction set-up used was shown in Figure 22.

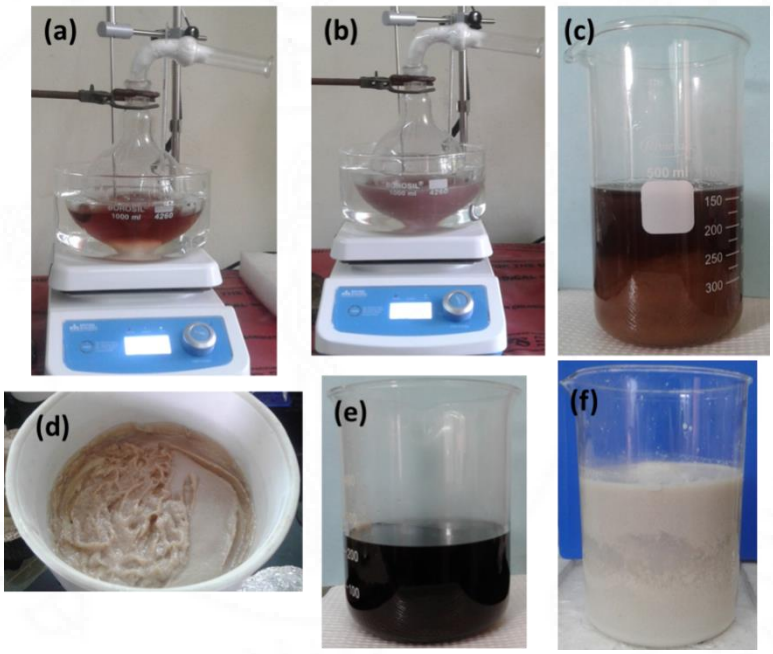

Figure 22. Different stages of EV-g-IBHP synthesis (a) Reaction at beginning (b) Reaction after 5 days (c) DCU precipitated out in reaction mixture after 5 days (d) DCU filtered out (e) Reaction mixture after filtration of DCU (f) Precipitation of grafted polymer when the reaction mixture added to distilled water

3 different grades of EV (27 mol%, 32 mol%, and 38 mol% ethylene content) were used to synthesize EV-g-IBHP (ie. EV27-g-IBHP, EV32-g-IBHP, EV38-g-IBHP) , using various ratios of EV to IBHP such as 1:3, 1:5, 1:8 and 1:10. All these syntheses were done following similar procedures and different trials were done to find out the optimum

system with augmented radiopacity and polymeric properties. The Iodine contents (%) of the respective systems were evaluated.

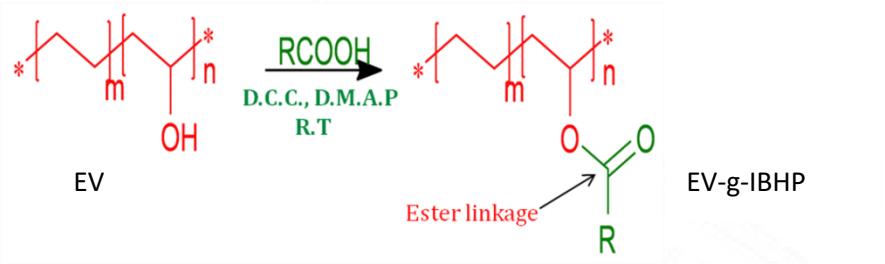

Scheme 6. The scheme of grafting of IBHP onto EV

3.2.5. Characterization of radiopaque ethylene vinyl alcohol

The grafted polymer systems were characterized by the following methods.

FTIR spectroscopy: Grafting of iodocompounds through ester and ether linkages and the presence of iodocompounds in the polymer chain were analyzed by FTIR spectroscopy using the same method explained in section 3.2.1.1. The radiopaque polymer was obtained in a powder form so it was used as such for FTIR analysis.

^{1}H NMR spectroscopy: Different types of protons in the radiopaque polymer were determined by ^{1}H NMR spectroscopy analysis. ^{1}H NMR spectrum was also analyzed for degree of substitution (DS) and % iodine content in the polymer backbone. The DS and iodine content were calculated by comparing the intensity of methine proton attached to OH group (Ia) and the intensity of methine proton attached to bulky iodocompound (Ib) using the equations (3) and (4) (Agusti et al., 2015; Farrokhi et al., 2019).

$$Degree\ of\ substitution = \frac{Ib}{Ib+Ia} \times 100 \qquad (3)$$

$$\%\ iodine = \frac{DS \times M_{iodine} \times n}{(M_{nongrafted} \times (1-DS)) + (M_{grafted} \times DS)} \times 100 \qquad (4)$$

Where DS is the degree of substitution (in numerals), M_{iodine} is the atomic mass of iodine atom (= 127 g mol^{-1}), n is the number of iodine atoms per iodinated compound (= 4), $M_{nongrafted}$ is the molar mass of non-grafted repeat unit and $M_{grafted}$ is the molar mass of grafted repeat unit.

Thermogravimetric analysis: Change in thermal stability after grafting was identified using TGA analysis as the same method described in 3.2.1.1.

Differential scanning calorimetry: The change in melting and glass transition temperature after grafting was recorded in DSC analysis using the method explained in 3.2.1.2.

X-ray powder diffraction: The change in crystallinity, if any, after grafting was analyzed by XRD. The parameters set for the measurement was similar to described in section 3.2.1.2.

EDX analysis: Presence of iodine in the polymer chain and the atomic and weight % of iodine in different grades of polymer after grafting was identified by EDX analysis. The method is similar to as explained in 3.2.3.

3.2.6. Formulation of Liquid embolic system

Liquid embolic systems (LEA) were formulated by dissolving the different iodocompound grafted EV grades in DMSO.

3.2.6.1. LES from EV-g-HR

Different concentrations of EV27-g-HR and EV38-g-HR LEAs were prepared with different grafting times (24 h, 48 h and 72 h) by dissolving the dried powder in biological grade dried dimethyl sulfoxide (DMSO) at 50˚C and stirring at 600 rpm for 8h for complete dissolution. After complete dissolution, it was filtered through a 0.22 µm, hydrophilic, PTFE syringe filter and stored in a closed container. The formulations prepared from EV-g-HR were tabulated in Table 2.

Table 2. EV-g-HR liquid embolic formulations prepared for various studies.

Formulation code	Grafting time (h)	Concentration (%, w/v)
EV27-g-HR-24h-10%	24	10
EV27-g-HR-48h-5%	48	5
EV27-g-HR-48h-10%	48	10
EV27-g-HR-48h-15%	48	15
EV27-g-HR-48h-20%	48	20
EV27-g-HR-72h-10%	72	10

3.2.6.2. LES from EV-g-IBHP

Different concentrations of EV27-g-IBHP, EV32-g-IBHP and EV38-g-IBHP were prepared for different grafting times (24 h, 48 h, 72 h, 96 h, 120 h and 144 h) by accurately weighing and dissolving the radiopaque polymers in DMSO. Dried powder of grafted polymer was weighed in a sample vial and biological grade dried DMSO (containing 0.025 % water) was added and the vial kept airtight away from light for 6 h. It was then subsequently mixed in a lab dancer to obtain a homogeneous solution of liquid embolic material. The liquid embolic agent was then filtered using a 0.22 µ,

hydrophilic, PTFE syringe filter to further sterilizes the LEA and transferred to an airtight container. The details of the formulations made were tabulated in Table 3.

Table 3. EV-g-IBHP liquid embolic formulations prepared for various studies

Formulation code	Grafting time (h)	Concentrations (%, w/v)
EV27-g-IBHP-24h-10%	24	10
EV27-g-IBHP-48h-10%	48	10
EV27-g-IBHP-72h-10%	72	10
EV27-g-IBHP-96h-10%	96	10
EV27-g-IBHP-120h-5%	120	5
EV27-g-IBHP-120h-10%	120	10
EV27-g-IBHP-120h-20%	120	20
EV27-g-IBHP-120h-30%	120	30
EV27-g-IBHP-120h-35%	120	35
EV27-g-IBHP-120h-35.5%	120	35.5
EV27-g-IBHP-144h-10%	144	10

3.2.7. Characterizations of LES

3.2.7.1. Viscosity analysis

The viscosity of the samples were measured by Anton Paar, Rolling-ball micro viscometer (Lovis 2000 M/ME), at 25^0C, 37^0C and 40^0C. The instrument was set for an auto-angle measurement at different temperatures and the capillary used for the measurement is 1.8 mm. The shear rate of the sample was set by adjusting the shear angle. The shear rate increased with the increase of the shear angle.

3.2.7.2. Precipitation behavior

Solutions of grafted polymers were made in DMSO, taken in a syringe and slowly injected into saline (0.9% sodium chloride solution). Once the release of DMSO from

the precipitate was complete, the precipitate was taken out from the saline and checked for its firmness by pressing with han.

3.2.7.3. Flow behavior

The flow behavior of the solution was analyzed by a modular compact parallel plate rheometer (Anton-Paar, MCR 302 SN83147616). The liquid samples were added to the disk at a gap height of 5mm. The gap height set for the measurement was 0.5 mm and the shear rate was stepped from 0.1 s^{-1} to 500 s^{-1}. The viscosities of the sample with respect to different shear rates were measured at three different temperatures; 25, 37 and 40˚C.

3.2.7.4. Radiopacity measurements

The radiopacity of prepared LEAs were measured in the same CT scanner explained in section 3.2.3. The parameters set for the measurement and the measuring units were same as described above.

3.2.7.5. In vitro precipitation behavior and visibility under fluoroscope

The precipitation behavior of EV27-g-IBHP-120h-35.5% was assessed in an in-house developed artificial nidus model (Figure 23). The nidus was continuously pumped with saline throughout the experiment using a flow pump (Cole-Parmer; Masterflex L/S pump; Model no. 7550-30). A catheter was inserted into the artificial nidus via Y-connector until the tip reached the proximal end of the artificial nidus. In the beginning, the microcatheter was filled with DMSO and subsequently the syringe containing LEA was delivered through the catheter for embolization. The entire nidus setup (Figure 24)

was placed under a fluoroscopy machine (GE; Innova 3131 Biplane) and embolization of the nidus was studied under fluoroscopic conditions. The injection of the embolic agent continued until the LEA was completely precipitated and filled the artificial nidus.

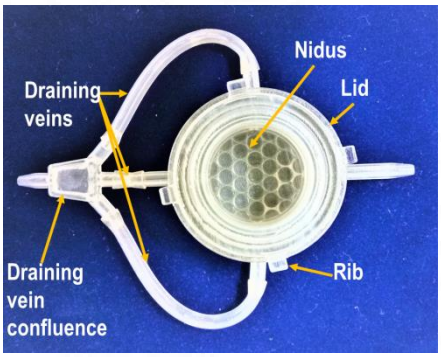

Figure 23. Artificial nidus

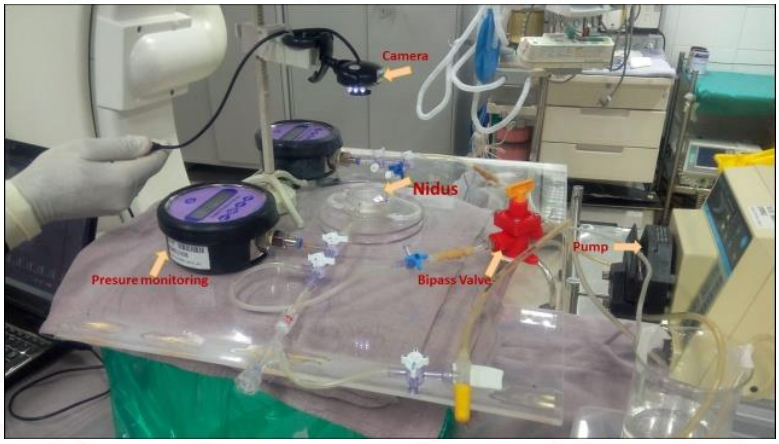

Figure 24. Nidus system arrangement for precipitation of LEA

3.2.8. Biological Safety Evaluation of LEA

3.2.8.1. In vitro cell culture cytotoxicity

The in vitro cell culture cytotoxicity of the iodinated polymer was determined by the method described in the ISO 10993-5 standard. The cell lines selected for the studies are L929 (mouse fibroblast cell line) and EA.hy926 (Endothelial cell, Procured from ATCC,

CRL-2922). For this, the LEA was slowly added to water taken in a beaker. The beaker was kept on a magnetic stirrer. Due to high speed stirring, the polymer was precipitated as powder. The powder was filtered, dried and was sterilized by EtO.

Test on extract: The extract of the above material was prepared by incubating 0.2g of powder in 1mL physiological saline at 37±1°C for 24±2h and 72±2h. The extract was filtered using a 0.22µm syringe filter. The filtered extract was mixed with MEM2X (1 part of extract and 1 part of MEM 2X (double concentrated medium) medium to get 50% extract and further diluted with culture medium to 25% and 12.5%. Physiological saline without test material processed in conditions similar to test material extract was considered as reagent control. Ultra-high molecular weight polyethylene and dilute phenol were used as negative and positive control, respectively. The cells were incubated with extracts of the test sample and controls at 37± 1°C for 24 to 26h, The incubated cells were then examined microscopically and cellular responses were scored as 0, 1, 2, 3 and 4 based on the Table 4.

Table 4. Cellular response grade for toxicity determination

Grade	Reactivity	Conditions of all cultures
0	None	Discrete intra-cytoplasmatic granules, no cell lysis, no reduction of cell growth
1	Slight	Not more than 20 % of the cells are round, loosely attached, and without intra cytoplasmatic granules, or show changes in morphology; occasional lysed cells are present, and only slight growth inhibition is observable
2	Mild	Not more than 50 % of the cells are round, devoid of intra cytoplasmatic granules, no extensive cell lysis, and not more than 50 % growth inhibition observable
3	Moderate	Not more than 70 % of the cell layers contain rounded cells or are lysed; cell layers are not completely destroyed but more than 50 % growth inhibition is observable
4	Severe	Nearly complete or complete destruction of the cell layers

MTT assay: It is a qualitative test that measures the metabolic activity of cells to reduce yellow-colored tetrazolium salt 3-(4,5-Dimethylthiazol-2-yl)-2,5- diphenyltetrazolium bromide to purple-colored formazan. An extract of 0.2 g test material was prepared in 1 ml physiological saline at 37±1°C for 24±2h and 72±2h. The extract was mixed with MEM2X medium to get 50% extract. This was diluted with culture medium to get 25%, 12.5% and 6.25% solutions of extract. Physiological saline without test material was considered as a reagent control. Cells cultured in a normal medium were considered as cell control. About 100 µL of test samples, negative control, positive control, reagent control and cell control were placed on the subconfluent monolayer of L929 cells. After incubation at 37 ±1°C for 24 ± 2h, the extract and control medium were replaced by 50 µL MTT solution, wrapped with aluminium foil and incubated at 37± 2°C for 2 h. After discarding the MTT solution, 100 µL of IPA was added to the wells and the color formation was quantified by spectrophotometer at 570 nm. The results obtained were compared with the cell control.

Direct contact assay: Circular discs of 1 cm diameter were used for the direct contact analysis. The test was performed according to the standard ISO10993-5. Ultra-high molecular weight polyethylene (UHMWPE) and stabilized PVC disc were taken as negative and positive controls, respectively. The culture medium from the L929/EA.hy926 monolayer cell was replaced by a fresh medium. Test samples, negative control and positive control in triplicate were placed on the cells. After incubation at 37±

1°C for 24 to 26h, the cell monolayer was examined microscopically to assess the obtained response around the test samples. The reactivity was graded as 0, 1, 2, 3and 4 based on the zone of lysis, vacuolization, detachment and membrane disintegration as per table 5.

Table 5. Grading system used to assess reactivity.

Grade	Reactivity	Description of reactivity zone
0	None	No detectable zone around or under the specimen
1	Slight	Some malformed or degenerated cells under the specimen
2	Mild	Zone limited to the area under the specimen
3	Moderate	Zone extending specimen size up to 1 cm
4	Severe	Zone extending farther than 1 cm beyond the specimen

Alamar blue assay: The cell viability was quantitatively determined by Alamar blue assay. For that, EA.hy926 cell lines were seeded in a 12-well plate at a rate of 25,000 cells per well. After it became sub-confluent, sterile test samples (EV27-g-IBHP-120h-35.5% in pellet form), negative control (ultra-high molecular weight polyethylene), and positive control (stabilized PVC disc) were placed on the cells and incubated at 37±1°C for 24 to 26 h. Then the medium was replaced by 2% (v/v in serum-free medium) Alamar blue reagent for 4 h. After the incubation, aliquots (100 µL) of spent Alamar blue reagent were taken into a fresh 96-well plate and the absorbance was measured at 570 nm with path length correction at 600 nm in a plate reader (BioTek, USA). The cell viability (%) was determined according to equation (5).

$$\%\ Cell\ viability = \frac{(O_2 \times A_1) - (O_1 \times A_2)}{(O_2 \times P_1) - (O_1 \times P_2)} \times 100 \qquad (5)$$

Where O_1 is the molar extinction coefficient of oxidized Alamar blue at 570 nm = 80,586; O_2 is the molar extinction coefficient of oxidized Alamar blue at 600 nm = 117,216; A_1 is the absorbance of test wells at 570 nm; A_2 is the absorbance of test wells at 600 nm; P_1 is the absorbance of positive growth control well (cell control) at 570 nm; P_2 is the absorbance of cell control at 600 nm.

3.2.8.2. In vitro hemocompatibility

Since the radiopaque polymer is expected to be in direct contact with blood, the hemolytic potential of EV27-g-IBHP-120h-35.5% was assessed as per the standard protocol (ISO 10993-4). Tests were performed with the approval of the Institutional ethics committee (Approval number: SCT/IEC/594/April 2014). Blood from the human volunteer was collected in an anti-coagulant, citrate-phosphate-dextrose solution with adenine (CPD-A). The precipitated form of LEM was immersed in PBS. PBS was aspirated out and 2.5 ml of blood was added. 0.5 ml blood was taken immediately for initial analysis and the remaining 2 mL blood was incubated with the samples for 30 min under agitation at 70±5 rpm using an Environ shaker at 35±2˚C. Empty polystyrene plates exposed to blood were taken as reference. The blood samples were centrifuged at 4000 rpm for 15 min to aspirate platelet-poor plasma. The total hemoglobin (Hb) in the whole blood samples was measured using an automatic hematology analyzer (Sysmex-K 4500). The free hemoglobin released into the plasma after exposure and was measured using a diode array spectrophotometer. The percentage hemolysis was calculated using the equation (6).

$$\% \text{ hemolysis} = \frac{\text{Free Hb}}{\text{Total Hb} \times 1000} \times 100 \qquad (6)$$

3.2.8.3. *In vitro* bacterial reverse mutation assay: Ames test

This biological assay is used to assess the mutagenic potential of chemical compounds. Here several strains of the salmonella typhimurium bacterium that carry mutations in genes involved in histidine synthesis is used for the test. The test method used here was according to ISO 10993-3, ISO 10993-12 and OECD 471. The strains of salmonella typhimurium isolated for the study are TA98, TA100, TA1535, TA1537, TA102. Since the test material was precipitated in the medium, the test material was prepared by the following method. The DMSO extract (extraction condition: 37 ℃ ± 1 ℃, 100 rpm for 72 ± 2 h) of 1 ml of test sample (EV27-g-IBHP-120h-35.5% precipitated in water, washed and then dried) at a concentration of 0.2 g/mL was exposed to 100 µL PBS at 37 ℃ for 30 min. and allowed to precipitate. The precipitate was spun down and the clear supernatant was used for the Ames test. The test and control suspensions were prepared by mixing fresh culture of salmonella strains, His/Bio solution, sodium phosphate buffer (absence of S9 mix) or S9 (presence of S9 mix), 50 µL test material (prepared by the above method)/ positive control (listed in table 6)/ negative control (DMSO) and make upto 1 ml with autoclaved distilled water. The suspensions were incubated at 37 °C for 20 min. and then spread onto minimal glucose agar plate and covered with sterile aluminium foil to protect from photoreactive substances. The plates were incubated at 37 °C for 48 h. After 48 h spontaneous revertant colonies were appeared. They are clearly

visible with unaided eyes and the number of colonies in each plate were counted and compared with the historical data of lab.

Table 6. Positive controls used for Ames test

Tester strains	Chemical	Dose (µg/plate)
Without metabolic activation		
TA98	2-nitrofluorene	10
TA100	Sodium azide	1
TA1535	Sodium azide	1
TA1537	9-aminoacridine	50
TA102	Mitomycin C	0.5
With metabolic activation		
S. typhimurium TA98, TA100, TA1535, TA1537, TA102	2-aminoanthracene	5

3.2.8.4. Acute systemic toxicity evaluation

According to ISO 10993-11, acute systemic toxicity is defined as the adverse effect occurring at any time within 72 h after single, multiple or continuous exposures of a test sample for 24 h. The routes of administration chosen were intravenous and intraperitoneal. Intravenous route is appropriate for devices with direct contact with blood and if particulates are present intraperitoneal routes are preferred. Since this material precipitates on contact with body fluid, intraperitoneal routes were also taken into consideration. Both polar (physiological saline) and non-polar (cotton seed oil) extraction media were chosen for the study.

3.2.8.4.1. Acute intraperitoneal application of cotton seed oil extract of grafted polymer in albino mice

The test evaluated mice's systemic response after intraperitoneal injection of cotton seed oil extract of the test material. The procedure adopted for the test was according to the standard ISO 10993-11: 2017.

The test material (EV27-g-IBHP-120h-35.5%) in powder form was sterilized by EtO. 10 adult Albino mice, either sex, having body weight ranges of 17-23 g (5 tests and 5 controls) were selected for the test. Cotton seed oil extract and control materials were prepared according to the table 7. The cotton seed oil extract of the test material and the control (pure cotton seed oil) were injected intraperitoneally (Figure 25) at a dose of 50 mL/Kg and the animals were observed immediately and at 4 h, 24 h, 48 h, and 72 h for evidence of abnormalities including clinical signs, loss in body weight or death.

Table 7. Criteria for preparing cotton seed oil extract of the material

	Test	Control
Surface area/ Weight of sample	4g	-
Extraction temperature	37 °C ± 1 °C	37 °C ± 1 °C
Extraction media	Cotton seed oil	Cotton seed oil
Volume of media	20 mL	20 mL
Period of extraction	72 h ± 2 h	72 h ± 2 h
No. of replicates	Nil	Nil
Speed of agitation	50 rpm	50 rpm

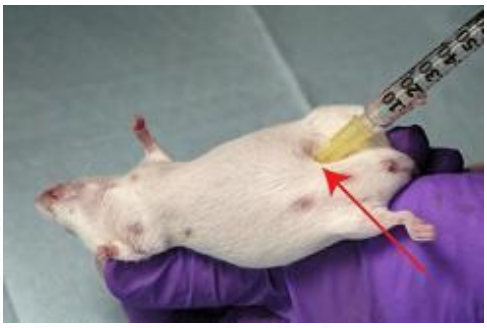

Figure 25. Intra peritoneal injection into mouse (taken from https://theodora.com/rodent_laboratory/injections.html)

3.2.8.4.2. Acute intravenous application of physiological saline extract of grafted polymer in albino mice

The test evaluated the systemic response of mice following intravenous injection of physiological saline extract of the test material (EV27-g-IBHP-120h-35.5% powder form).

EtO sterilized samples were used for the study. 10 Albino mice having a body weight range of 17-23 g were selected for the test. 5 mice were selected for the test and another 5 as control. The extracts of test and control material were prepared according to the table 8. The physiological saline extract of test material and control (pure physiological saline) were injected intravenously (Figure 26) (dose: 50 ml/Kg)and the animals were observed immediately and at 4 hrs, 24 hrs, 48 hrs and 72 hrs for evidence of abnormalities including clinical signs, loss in body weight or death.

Table 8. Criteria for preparing physiological saline extract of the material

	Test	Control
Surface area/ Weight of sample	4g	-
Extraction temperature	37 °C ± 1 °C	37 °C ± 1 °C
Extraction media	Physiological saline	Physiological saline
Volume of media	20 mL	20 mL
Period of extraction	72 h ± 2 h	72 h ± 2 h
No. of replicates	Nil	Nil
Speed of agitation	50 rpm	50 rpm
pH of extract	6.5	7.5

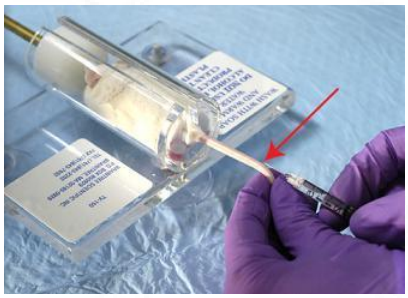

Figure 26. Intravenous injections into mouse (taken from https://theodora.com/rodent_laboratory/injections.html)

3.2.8.5. *In vivo* toxicokinetic study

The study was designed to evaluate the toxicokinetic response of test material, EV27-g-IBHP-120h-35.5%, following intraperitoneal injection in rabbits. The test was carried out with the approval of the Institutional Ethics Committee (IAEC approval number: SCT/IAEC-382/November/2020/107).

Three healthy adult rabbits not less than 2000g from the in-house facility (Division of Laboratory Animal Sciences, BMT Wing, SCTIMST) were selected for the study. The details of the animals are given in table 9.

Table 9. Details of animals used for toxicokinetic study

Test animal	Newzealand white rabbits		
No. of animals	3		
Source of animal supply	Division of Laboratory Animal Sciences, BMT Wing, SCTIMST		
Animal ID/sex	361♂	332♀	315♀
Body weight of animals	3160 g	3645 g	3025 g

The test material was precipitated in distilled water under stirring and the powder obtained was dried and suspended in physiological saline and three rabbits were injected intraperitoneally at a dose of 50 mg/Kg body weight. Blood samples were collected before injection and at 1h, 3 h, 6 h, 24 h, 48 h, 72 h, and 7 days after injection. Around 2 ml of blood was collected each time in EDTA tubes to prevent coagulation.

The collected blood was centrifuged for 15 min. at 4500 rpm, plasma was then separated and the plasma was treated with twice the volume of acetonitrile to precipitate proteins. After mixing well it was kept in the refrigerator for 15 min. Then it was centrifuged at 1700 rpm for 15 min. The supernatant was gently collected and filtered through a 0.45 µ, PTFE syringe filter. The filtrate was kept at 4˚C until further use.

To investigate the direct effect of the polymer sample on blood, it was spiked with the polymer material (50 mg in 1 ml blood) for 6 hr. The same procedure explained above was repeated for the collection of plasma for the analysis. The blood collected before injection of the material and the blood spiked with the material were taken as control.

The samples were analyzed for nanodrop micro UV-Visible spectrophotometric analysis and HPLC analysis. For UV analysis a 1:1 mixture of sample solution/distilled water was prepared. 2 µL sample solution was added to the pedestal of the spectrophotometer

and a simple read was taken from 190-850 nm. A 1:1 mixture of acetonitrile/distilled water was taken as blank.

For HPLC analysis, samples were loaded to the equipment and the peaks were detected by UV detector by setting a wavelength of 280 nm. Chromatographic separations were performed on a C18 column. 20 µL of the samples were injected and the run time was set as 10 min. The mobile phase used was a 1:1 acetonitrile/distilled water mixture.

3.2.8.6. Muscular implantation of LEA in rabbit model

The study was designed to evaluate and differentiate the responses of muscle tissue following implantation of the test material (EV27-g-IBHP-120h-35.5%) against a commercial control (Onyx® LEA). This study was approved by Institutional Ethics committee and the approval number was SCT/IAEC-417/July/2021/110. The weights of the rabbits selected for the study were not less than 2 Kg. They were anesthetized using Ketamine (80 mg/Kg) + Xylaxin (5 mg/Kg). The outer hair of the rabbits was removed from one side of the spine and lightly swabbed with povidone-iodine and alcohol. An incision of around 5 cm was made in the outer skin layer and the fascias (connective tissue) were removed and exposed to the muscle layer. Then 0.3 mL of previously shaken (shaking time: 20 min) control material (Onyx® 18, Ref: 105-7100-060, eV3, Micro Therapeutics, USA)) was injected intramuscularly (paravertebral muscle) in 5 sites on the right side of the spine about 25 mm apart from each other. Similarly, the test material was injected into the left side as such without any shaking. It was observed that both test and control material precipitated on contact with body fluid. The incision was

then closed using sterile sutures. The overall procedure was shown in Figure 27 and the study was conducted on 6 rabbits (3 for a 1-week study and 3 for a 12-weeks study).

After corresponding study periods, Rabbits were sacrificed by giving an excess dose of anesthesia and the implants with surrounding tissues were collected and analyzed by a High-frequency mobile X-ray machine (MARS 15, Allengers) at 58 kV to identify the exact location of each implantation site. After X-ray analysis, each implantation site was cut into pieces and put in formalin for histopathological studies and further RT-PCR analysis.

3.2.8.6.1. Histological assessment of LEA implanted muscular tissue of rabbit

The sections of the implant site perpendicular to the implant were taken for histopathological evaluations. The tissue sections were fixed in 10% phosphate-buffered formalin. The samples were then trimmed for adequate size and orientation. For dehydration, the specimens were treated with ethanol, cleared with xylene and infiltration was further done in paraffin. Tissue samples were properly positioned inside a metal base mold. This FFPE tissue blocks were cut into 5 µm size in a rotary microtome and stained with hematoxylin-eosin (H&E). The tissue sections were mounted on a cover slip, examined using light microscopy and the observations graded according to the parameters tabulated in table 10.

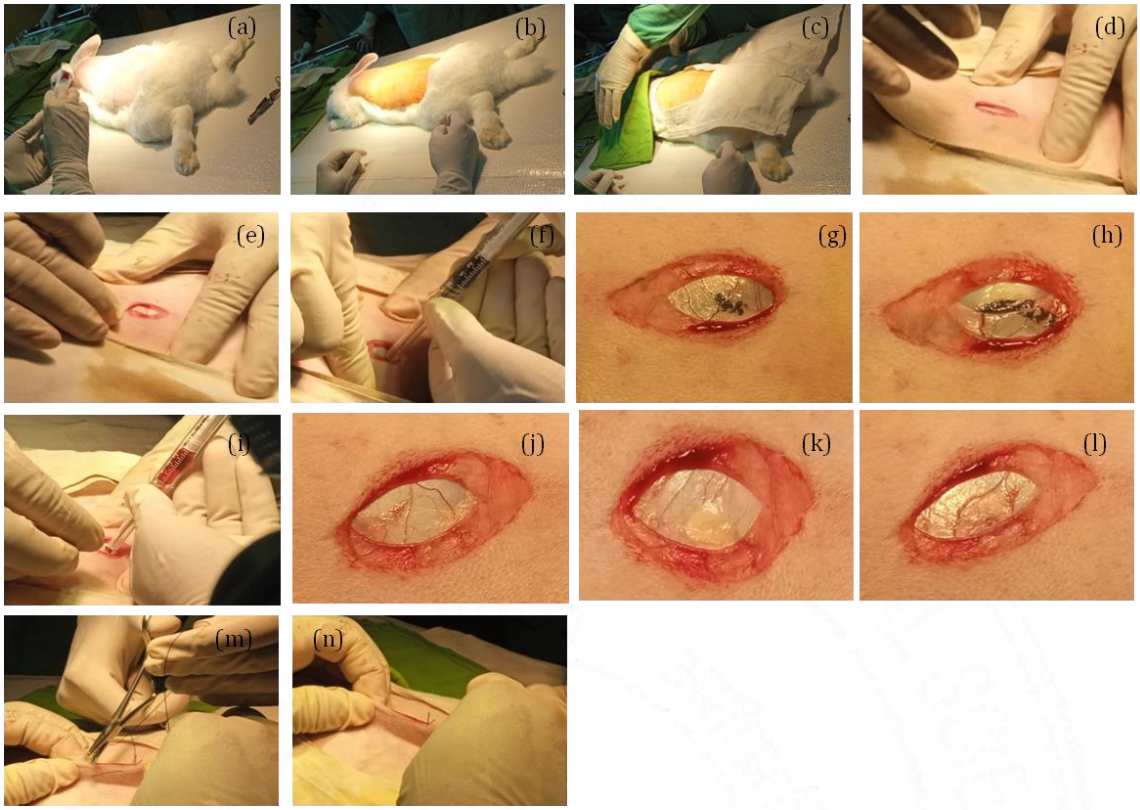

Figure 27. Muscular implantation of test & control LEA: (a) Removing outer hair from one side of spine, (b) Skin swabbed with povidone-iodine, (c) Covering all other parts with cloth except the implantation site, (d) Incision made in the outer layer of skin, (e) Stretch the skin to focus the implantation site, (f) Injection of control material (Onyx®) on the left side, (g)-(h) Control material precipitated in the implantation site, (i) Injection of test material on right side, (j)-(l) Precipitated test material in the implantation site, (m)-(n) Closing the incision was using sterile sutures.

After grading all the parameters, a group total of 4 sections of n=3 was calculated separately for each period. Then from the mean group average, the overall score was determined and the test material was classified as non–irritant for scores 0-2.9; slight irritant for 3-8.9; moderate irritant for 9-15, and severe irritant for >15.

Table 10. Grading parameters for different inflammatory components

Grades	0	1	2	3	4
Inflammatory cells (polymorphonuclear cells, lymphocytes, plasma cells, and macrophages)	0 cells	1-5 cells	6-10 cells	Heavy infiltration	Packed cells
Giant cells	0 cells	1-2 cells	3-5 cells	Heavy infiltration	Packed cells
Neovascularization	No capillaries	1-3 capillaries	4-7 capillaries	Broad blood vessels	Extensive vascularization
Fibrosis	Absent	<5µm	6-15 µm	16-30 µm	>30 µm
Necrosis (determined by cell debris and inflammation)	Not present	Minimally present	Mild degree	Moderate degree	Severe degree
Fatty infiltrate (determined by the amount of fat tissues)	Not present	Minimally present	Mild degree	Moderate degree	Severe degree
Tissue ingrowth (determined by the amount of tissue ingrowth in the case of porous and/or degradable materials	Not present	Minimally present	Mild degree	Moderate degree	Severe degree

†All are graded at magnification 400X

3.2.8.6.2. Genomic study of LEA implanted rabbit muscular tissue

The effect of implantation of test and control material on the production of pleotropic cytokines: Matrix metallopeptidase-9 (MMP-9) and Transforming growth factor (TGF); pro-inflammatory cytokines: Interleukin-6 (IL-6) and Tumor necrosis factor (TNF); Angiogenic cytokines: Vascular Endothelial Growth Factor (VEGF) and anti-inflammatory cytokine: Interleukin-10(IL-10) was investigated by Reverse Transcription Polymerase Chain Reaction (RT-PCR). GAPDH was used as the housekeeping gene. For that >50 micron-sized sections were cut from formalin-fixed-paraffin embedded (FFPE) tissue blocks using a microtome and collected in a 2 ml microcentrifuge tube. The RNA was isolated from the tissue sections according to the following procedure.

RNA extraction from Formalin-fixed paraffin embedded (FFPE) tissue: RNA was isolated from Formalin Fixed Paraffin Embedded (FFPE) rete tissue samples using

Reliaprep FFPE Total RNA Miniprep system, Promega. For deparaffinization of the tissue sample, 500 µL of mineral oil was added to the sections. Tissue sections with mineral oil were incubated at 80˚C for 1 min and vortexed for adequate mixing. Sample lysis was done by adding 100 µL of lysis buffer and centrifugating at 10,000 x g for 15 seconds at room temperature. This separates two phases; lower blue (aqueous) phase and an upper (oil) phase. 10 µL of proteinase K was added directly to the lower blue phase and mixed by pipetting. After thorough mixing, the samples were incubated at 56˚C for 15 min and 80˚C for 1 hour. After 1 h the samples were removed from 80˚C and placed in ice for a minute and at room temperature for 2 min. 30 µL of freshly prepared DNase treatment mix (13 µL, 0.09 M $MnCl_2$; 7 µL DNase buffer and 10 µL DNase I enzyme) was added directly to the lower blue phase of the sample and mixed by pipetting. Samples were again incubated for 15 min at room temperature.

For nucleic acid binding, 325 µL of BL buffer and 200 µL of 100% IPA were added to the samples. Once vortexed, the samples were centrifuged at 10,000 x g for 15 s at room temperature leading to the formation of two phases: a lower blue phase and an upper oil phase. The entire lower blue phase of the sample was transferred to the binding column/collection tube assembly and the column subsequently capped and the oil phase discarded. After centrifuging the assembly at 10,000 x g for 30 s at room temperature we discard the flow through and reinsert the binding column into the collection tube. Then column washing and elution were done using 1X wash solution at 10,000 x g for 30 s at room temperature. After drying the column, it was transferred to a clean elution tube. 40 µL of nuclease-free water was added to the column and centrifuged at 16,000 x g for 1

min at room temperature. The binding column was discarded and the elution tube was capped tightly. After isolating the RNA, the yield and purity of RNA were determined by a Nanodrop 2000/2000 c spectrophotometer (M/s. Thermofisher Scientific, Waltham, Massachusetts, U.S.). It was then immediately converted to cDNA.

cDNA synthesis: Aliquotes of 1 to 3 µg of RNA were used for first-strand cDNA synthesis using an RT core kit (Eurogentec, Belgium). RT reaction mix in the following composition (table 11) was used for the synthesis.

Table 11. Composition of RT reaction mix

Component	**Volume (µL) For 1 rean.**	**Final concentration**
10X reaction buffer	1	1X
25 mM $MgCl_2$	2	5 mM
2.5 mM dNTP	2	500 µM
Random nonamer	0.5	2.5 µM
RNase inhibitor	0.2	0.4 U/ µL
Euroscript RT	0.25	1.25 U/ µL

All the components (prepare as a bulk) were mixed and 5.95 µL of the reaction mix was added to each reaction vial. This reaction setup was done on ice. The template (1-3 µL) and the corresponding volume of water were then added to the vial and mixed by inversion. The real-time thermocycler (Mycycler^{TM} thermal cycler, Bio-Rad) program consisted of an initial step of 10 min at 25˚C followed by a reverse transcriptase step of 30 min at 48˚C and inactivation of the RT enzyme for 5 min at 95˚C.

RT-PCR: Real-time PCR was performed in a 20 µL reaction volume containing 10 µL of Takyon SYBR Green PCR master mix (Eurogentec, Europe), 5 µL of cDNA

template, and 1.5 µL (300 nM con) of primer using the iQ5 real-time PCR Detection System (Bio-Rad). The amplification program consisted of Takyon activation at 95˚C for 3 min. followed by 40 cycles of denaturation at 95˚C for 10 s and annealing/extension at 55-60˚C for 50s. The fold change was calculated by the relative quantification method ($2^{-\Delta\Delta Ct}$) and normalized to the housekeeping gene GAPDH. The primer sequences selected are listed in Table 12.

Table 12. Primer sequences selected for RT-PCR study of rabbit.

Primer	Sequence (5'→3')
IL-6 F	GCC-GGC-GGT-GAA-TAA-TGA-GA
IL-6 R	TCG-TCA-CTC-CTG-AAC-TTG-GC
VEGF F	AAA-ACA-CAG-ACT-CGC-GTT-GC
VEGF R	CCT-CGG-CTT-GTC-ACA-TCT-GC
GAPDH F	TCG-GAG-TGA-ACG-GAT-TTG-GC
GAPDH R	TGC-CGT-GGG-TGG-AAT-CAT-AC
TGF F	CTG-GAA-CGG-GCT-CAA-CAT-CT
TGF R	TCC-TGG-AAA-AGG-ACC-AAC-AGT
TNF F	AGC-CCA-CGT-AGT-AGC-AAA-CC
TNF R	GTT-GTC-CGT-GAG-CTT-CAT-GC
MMP-9 F	TCC-AGT-ACC-GAG-AGA-AAG-CC
MMP-9 R	GCA-GTG-CAG-GAT-GTC-AAA-GC
IL-10 F	CTG-CGA-CAA-TGT-CAC-CGA-TT
IL-10 R	TGT-CAA-ACT-CAC-TCA-TGG-CT

3.2.9. In vitro degradation

Degradation of implant materials in the biological environment is one of the major factors that need to be addressed in the case of biomedical devices. A degradation study of the iodinated polymer was conducted by making a pellet of 0.2 g of the polymer sample (EV27-g-IBHP-120h-35.5%). The initial dry weight (W_0) of the pellets was recorded before they were immersed in PBS solution (pH 7.4) and kept in a shaking incubator at 37˚C and 60 rpm (physiological conditions). The periods selected for the

analysis were 1 day, 7 days, 14 days, 30 days, 90 days, 180 days, 270 days and 360 days. Triplets for each sample evaluated were taken for each period for statistical analysis. After every 2 days, the medium was replaced by fresh medium. After each interval, the samples were taken out, washed with distilled water, dried at room temperature and weighed until constant weights (W_t) were obtained. For estimating the degradation, the percentage weight remaining was calculated using equation 7.

$$\%\ \text{weight remaining} = 100 - \left(\frac{W_0 - W_t}{W_0}\right) \times 100 \qquad (7)$$

Where W_0 is the initial dry weight of the sample and W_t is the dry weight of the sample after each time period.

3.2.10. Storage stability of LEA

For storage stability studies, the formulation EV27-g-IBHP-120h-35.5% was selected. Parameters such as viscosity, precipitation behavior and FTIR spectrum of the precipitated sample were analyzed. For this study 2 ml solution of LEA was sealed in an air-tight opaque glass bottle and kept at two different temperature conditions: room temperature and 37˚C. The periods selected for the study were 1 week, 1 month, 3 months, 6 months, 9 months and 12 months. Separate, triplet sample vials were kept for different time periods. After each period the samples were taken out and the viscosity, precipitation behavior, and FTIR spectrum were evaluated and compared with the initial one.

3.2.11. Preclinical Functional Evaluation of LEA

3.2.11.1. Implantation of LEA in swine rete mirabile

Eleven Ankamali swine (Figure 28 A), from either sex, weighing 35-60 kg from the in-house facility were used for this study. All animals were subject to institutional animal care and all procedures were approved by the Institutional Ethics Committee (approval No: ACAE16SR.Y19).

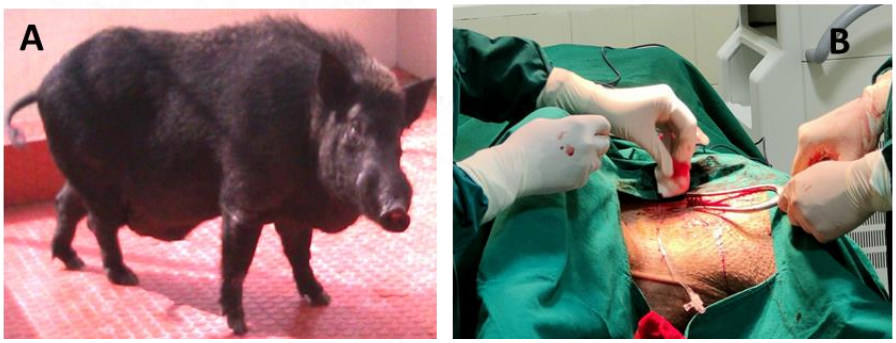

Figure 28. (A) Ankamali swine, (B) Implantation procedure of LEA in swine.

Animals were anesthetized with Atropine at 0.25 mg/kg, xylazine at 1.5 mg/kg and Ketamine at 15 mg/kg body weight intramuscularly. Anesthesia was maintained with 1.8% isofluorane after endotracheal intubation. The animals were controlled on dorsal recumbence and a neck cutdown was performed on the ventral neck under strict asepsis conditions. After reflecting the sternohyoideus muscle and sternomastoideus muscles with retractors the left carotid artery of the swine was exposed and a 6-french sheath was placed following the modified Sedlinger technique under general anesthesia. The animal was heparinized with Heparin at 300 IU/kg body weight intravenously. A 6-Fr introducing catheter was positioned in the common carotid artery, and the internal carotid artery was selectively catheterized coaxially with a 4-Fr catheter (Figure 28 B).

The test/control embolic agents (0.6 ml) (Figure 29) were injected directly through the catheter to obliterate the lumen of the ascending pharyngeal artery supplying the Rete Mirabile. Nine RMs were embolized with EV27-g-IBHP-120h-35.5% embolic agent and two with Onyx® control material. Control material was used after 20 min. shaking in a vortex mixer but the test material was used as such since it is a homogeneous solution.

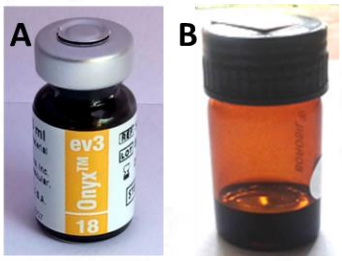

Figure 29. (A) Control material (B) Test material

The ability of the device to embolize the Rete Mirabile, catheter entrapment and catheter blockage was assessed. After the procedure, the catheters were withdrawn and the sheath removed. The arteriotomy site was reconstructed by a figure of eight sutures with 6/0 proline sutures and the neck incision was routinely closed. The animals were monitored closely by veterinary staff daily. The wound was dressed daily and sutures were removed on the 10^{th} postoperative day. The animals were administered 500 mg streptopenicillin, 0.5 mg per kg body meloxicam and multivitamin injections intramuscularly for 5 days. The angiographic assessment was done before and after embolization to assess the obliteration in a fully integrated biplane angiographic X-ray system (GE Innova 3131, Avante Health Solutions).

After 90 days the animals were sacrificed with an excess dose of thiopentone sodium at 100 mg/kg body weight, pancuronium bromide at 0.8 mg/kg body weight and potassium

Chloride at 7.5% (35 ml). Prior to sacrifice, an angiographic assessment was done to assess the presence of an embolization cast and to further check for recanalization. A detailed histological evaluation of the interface was also carried out.

3.2.11.2. MicroCT analysis

After preclinical evaluation in swine, the explanted whole rete, embolized with test material and control was fixed in 10% neutral buffered formalin. X-ray imaging was then performed using microCT (μCT 40, SCANCO Medical AG, Switzerland) at a resolution of 1μm (45kV and 177 μA). The samples were scanned for a full 360˚ rotation and the images were reconstructed with a cone beam conventional back-projection algorithm with a 20 μm voxel size.

3.2.11.3. Histological assessment of LEA implanted swine rete

Prior to analysis, photographs of the rete were taken to determine the presence of embolic material. The rete tissues were fixed in 10% phosphate buffered formalin. After fixation, tissue samples were properly trimmed to obtain adequate size and orientation. The specimens were dehydrated in ethanol, cleared in xylene and finally infiltrated in paraffin. After infiltrated by paraffin, tissue samples were removed from the cassettes and positioned inside a metal base mold. These paraffin blocks were cut to 5 μm size using a rotary microtome and further stained with hematoxylin-eosin (H&E). All sections were examined by light microscopy after staining. The heart, liver, kidney, and spleen were grossly examined to study the effect of embolization on the end organ.

4. RESULTS AND DISCUSSION

4.1 Characterization of radiopaque organic compounds

The radiopaque element selected in this study to synthesize radiopaque organic compounds was iodine. It was chosen because iodine is atomically dense and does not permit penetration by X-rays. Iodine possesses radiopacity, nontoxicity, high stability in non-ionic environments, and a large mass attenuation coefficient. In addition, it was available at low cost. The parent compound selected for iodination was 4, 4-bis(4-hydroxyphenyl) pentanoic acid (BHP) since it had four sterically free sites for iodination. The ortho-para directing effect of the hydroxyl group also favors iodination in the four ortho positions of two hydroxyl groups.

4.1.1. 4,4-bis (4-hydroxy-3,5 diiodophenyl) pentanoic acid (IBHP)

4.1.1.1. Spectral and thermal characterizations of IBHP

Figure 30. A) 4,4-bis (4-hydroxyphenyl) pentanoic acid; B) 4, 4-bis(4-hydroxy-3,5 diiodophenyl) pentanoic acid

The tetra iodocompound, 4,4-bis(4-hydroxy-3,5 diiodophenyl) pentanoic acid (IBHP) was synthesized by iodinating 4, 4-bis(4-hydroxyphenyl) pentanoic acid. The iodination was done by adopting a similar procedure reported by Kiran et al. (2009). The tetra iodination was possible by using 6 equiv of sodium iodide and sodium hypochlorite. It took place by the in situ oxidation of sodium iodide in methanol in the presence of sodium hypochlorite. The yield obtained for 2g of reactant was around 6 g which is the expected yield for tetra iodination. After iodination, the color of BHP changed to light brown (Figure 30) which is common in the case of iodocompounds. To confirm the formation of IBHP, characterization techniques such as ^{1}HNMR spectroscopy, FTIR spectroscopy, UV-Visible spectroscopy, EDX spectroscopy, and mass spectroscopy were used.

The different types of protons in BHP and IBHP were evaluated using ^{1}HNMR spectroscopy (500 MHz, dimethyl sulphoxide (DMSO)-d6). The ortho-para directing nature of the hydroxyl group redirected the iodine molecule to the ortho position since the para position was already occupied. In addition, the steric hindrance caused by the bulky iodine atom limited further iodination. The NMR spectrum of BHP showed the following chemical shifts: δ = 12 ppm (–COOH), δ = 9.18 ppm (-C_6H_5OH), near δ = 2 ppm (-CH_2), δ = 6.65 and 6.9 ppm (-C_6H_5) (Figure 31).

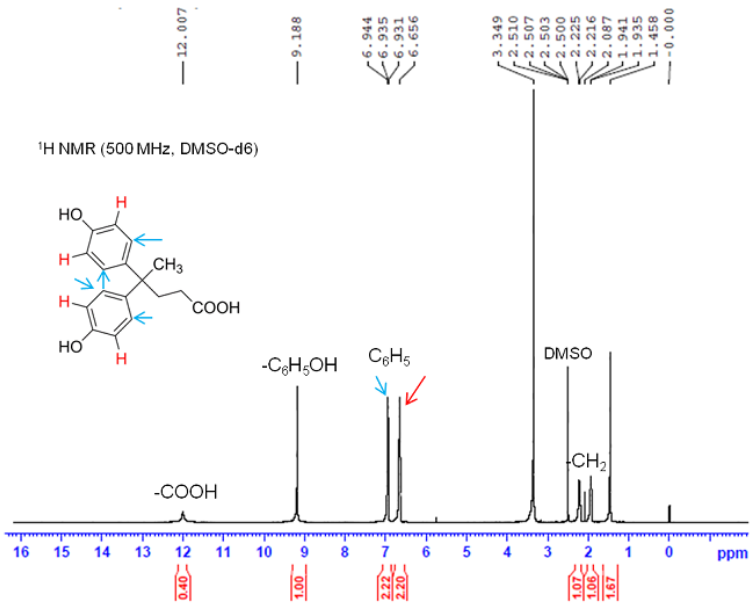

Figure 31. ^{1}H NMR spectrum of BHP

Whereas, the chemical shift values obtained for IBHP are:

δ = 12 ppm (-COOH), δ = 9.48 ppm (-C_6H_5OH), near δ = 2 ppm (-CH_2), δ = 7.45 ppm (-C_6H_5) (Figure 32). The downfield shift of phenolic proton in IBHP was due to the presence of iodine in the molecule. Aromatic proton peaks observed at 6.65 and 6.9 in BHP were absent in IBHP and a new peak was observed at 7.45 ppm for the aromatic proton. This confirmed the presence of four electron-withdrawing iodine atoms in the ortho position of BHP. A similar kind of downfield shift was reported in 4,4'-isopropylidene bis(2,6-dibromophenol) (Pouchert, 1983) and 4,4'-isopropylidene bis (2,6-diiodophenol) (Kiran et al., 2009).

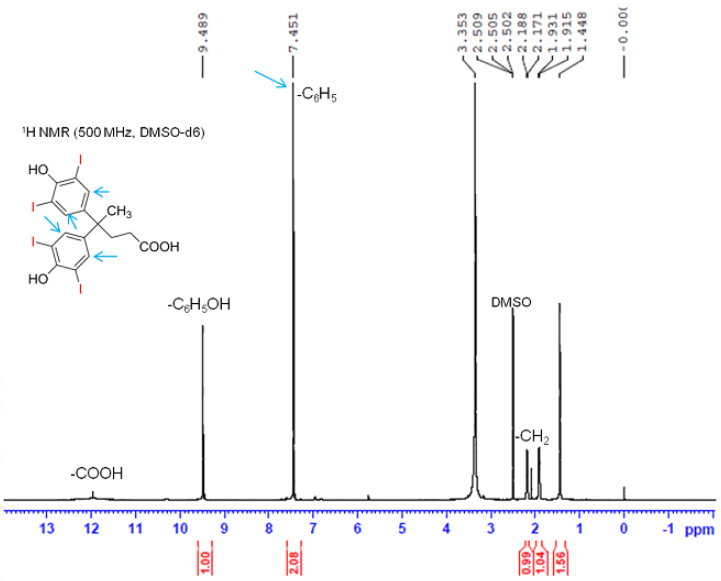

Figure 32. ^{1}H NMR spectrum of IBHP

The functional groups present in BHP and IBHP were analyzed by FTIR spectroscopy. The FTIR spectrum of BHP (Figure 33) showed peaks corresponding to O-H str. of phenolic group at 3296 cm^{-1}, alkane C-H str. at 2972 cm^{-1}, acid C=O str. at 1701 cm^{-1} and aromatic C=C bending at 1512 cm^{-1}. But after iodination, the stretching frequencies of all the functional groups showed a slight increase which is expected as literature reports that when the electron-withdrawing nature of ring substituent increases, the stretching frequency of the functional group also increases (Krueger et al., 1970). The electron-withdrawing iodine atom adjacent to the –OH group showed an increase in stretching frequency from 3296 cm^{-1} to 3415 cm^{-1}. Similarly, all other frequencies shift towards a higher range: alkane C-H str. at 2981 cm^{-1}, acid C=O str. at 1707 cm^{-1}, and aromatic C=C bending at 1529 cm^{-1}. An additional peak obtained for IBHP at 708 cm^{-1} corresponds to C-I str.

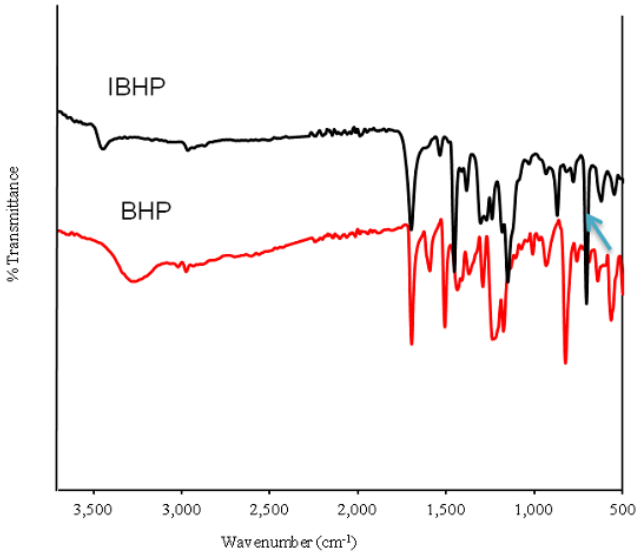

Figure 33. FTIR spectra of BHP and IBHP

The UV-Visible spectra of BHP and IBHP showed primary and secondary absorption bands of the aromatic ring. In BHP the primary band falls at 222 nm and the secondary band falls at 280 nm (Figure 34) while iodination shifts the bands to longer wavelength regions, i.e., the primary band at 227 nm and secondary band at 300 nm (Figure 35). It has been reported that the presence of an electron-donating group increases the λ_{max} and ϵ_{max} values of the secondary band (Kumar, 2021). Iodine being electron-withdrawing in nature donates electrons to the benzene ring and undergoes conjugation with the benzene ring (Bird & Ingold 1938). This explains the observed bathochromic shift of the secondary absorption band from 280 nm to 300 nm.

BHP, λ_{max} (MeOH)/ nm 222 and 280 (ϵ/ dm^3 mol^{-1} cm^{-1} 1, 20,000 and 30,000).

IBHP, λ_{max} (MeOH)/ nm 227 and 300 (ϵ/ dm^3 mol^{-1} cm^{-1} 5, 40,000 and 32,000).

The formation of IBHP was also confirmed by mass spectroscopy analysis. The theoretical molecular mass of BHP is 286 and on tetra iodination, it becomes 790. The

mass spectrum of BHP showed a base peak at 309 (M+23) and a molecular ion peak at 325 (M+40) (Figure 36 (a)). On iodination, the molecular weight of BHP increases, and the base peak of IBHP appeared at 812.69 (M+23) and the molecular ion peak at 834.67 (M+40) (Figure 36 (b)), respectively. The increase in molecular weight of BHP was as expected and indicated successful tetra iodination.

BHP, *m/z* 309 (M^+, 100%), 227 (5), 269 (6), 325 (M^+, 6%)

IBHP, *m/z* 812 (M^+, 100%), 834 (M^+, 18%)

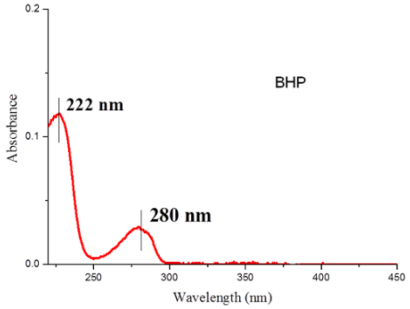

Figure 34. UV-Visible spectrum of BHP

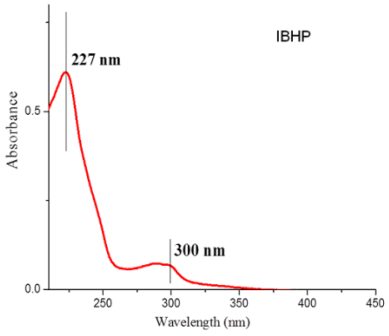

Figure 35. UV-Visible spectrum of IBHP

The iodine content calculated by weight was 64% ((i.e., atomic weight of 4 iodine atoms/ Total molecular weight of IBHP) x 100).

To find the presence of iodine in the molecule, EDX spectroscopic analysis was carried out. The EDX spectrum of IBHP (Figure 37) showed peaks of carbon, oxygen and iodine. The peaks between the regions 3.5-5 keV confirmed the existence of iodine atoms in the molecule (Shiralizadeh et al., 2016).

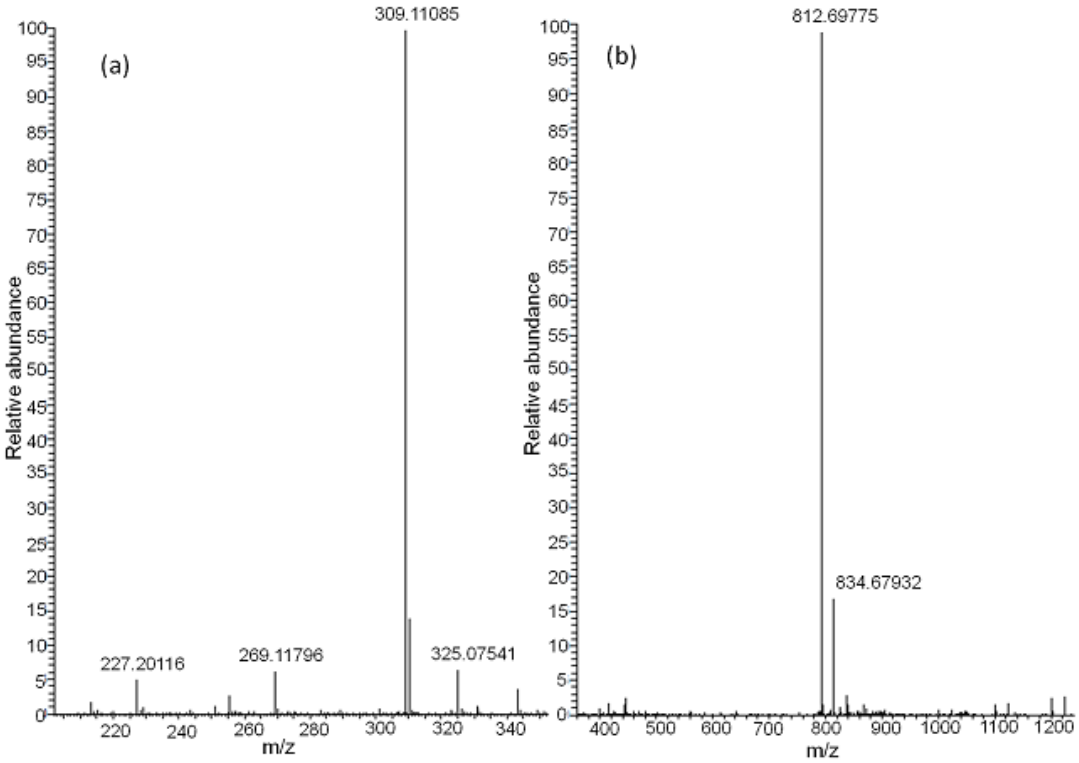

Figure 36. Mass spectra of (a) BHP (b) IBHP

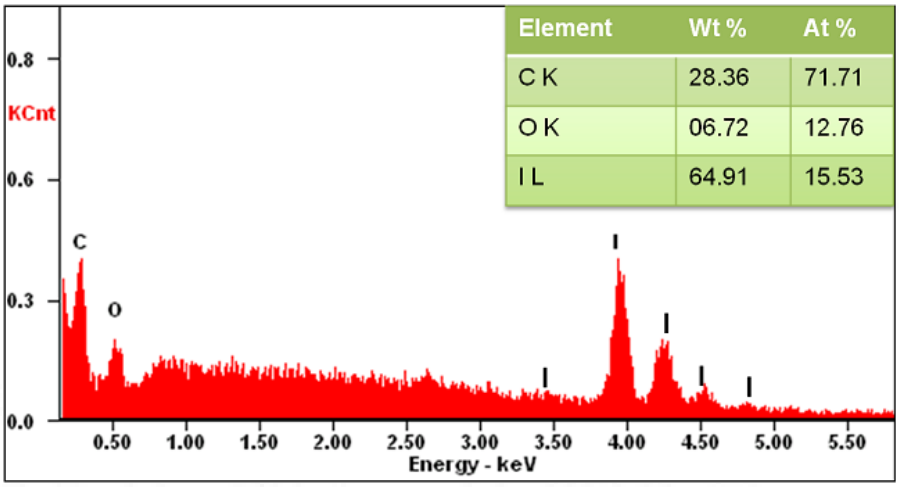

Figure 37. EDX spectrum of IBHP

The thermal stability of IBHP was studied by thermogravimetric analysis. The TGA traces of BHP and IBHP (Figure 38) showed that they undergo one-stage degradation and the major mass loss started at 227.71 ˚C and 180.92 ˚C for BHP and IBHP, respectively. The thermal stability of the compounds decreased due to iodination. During the melting of iodocompounds there was a chance for volatilization of iodine (Goh and Lee, 1990; Moulay, 2013) and this could be the reason for lower thermal stability after iodination. 50% weight loss for IBHP was observed at 264˚C and a similar weight % loss for BHP was observed only at 297˚C. Thus iodination resulted in remarkable changes in thermal stability, molecular weight and UV absorption maxima in BHP.

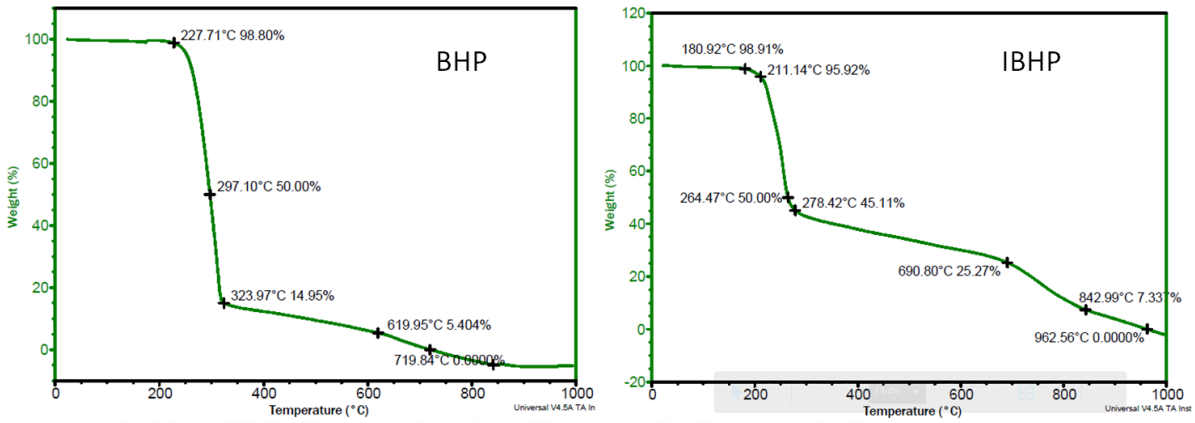

Figure 38. TGA traces of BHP and IBHP

4.1.1.2. In vitro X-ray visibility

Radiopacity is the ability of compounds to absorb X-rays and cast a radiological image. The quantitative measurement of radiodensity used by radiologists in the interpretation of CT images is the Hounsfield Unit (HU). The attenuation range observed for cancellous and cortical bone was 300-400 HU (Birur et al., 2017) and 500-1900 HU (Aamodt et al.,1999; Fat et al., 2012), respectively. La Grutta et al.(2013) compared the attenuation values of different concentrations of iodixanol and iomeprol contrast agents and found that the attenuation value increased with the increase in concentration of iodine load. 10 ml volume of 40, 64, 80 and 160 mg iodine load of iodixanol solution showed 122±6.7, 200.6±6.5, 259.7±6.2 and 473.7±7.3 HU opacity, respectively. Similarly, 10 ml volume of 50, 80, 100 and 200 mg iodine load of iomeprol solution depicted 142.5±8.5, 230.2±7.8, 339.6±7 and 559.8±8.2 HU of opacity, respectively. So compounds having attenuation values in these ranges were visible in X-ray and can be used for imaging applications. Figure 39 shows the computed tomographic images of 5,

10 and 20% solutions of IBHP (solvent: DMSO, iodine load: 321, 643 and 1286 mgI in 10 mL, respectively) and 20% solution of iodixanol solution (solvent: distilled water, iodine load: 980 mgI in 10 mL). The opacity values obtained were 885.15 HU, 1328.8 HU, 1655.78 HU and 1330.74 HU, respectively. The difference in iodine content of iodixanol (49.1 wt %) and IBHP (64 wt %) was reflected in the attenuation value. The 10% solution of IBHP showed an attenuation value (1328.8 HU) similar to the attenuation value of 20% iodixanol solution (1330.74). But the 20% solution of IBHP showed opacity of 1655.78 HU which can be explained due to its higher iodine content.

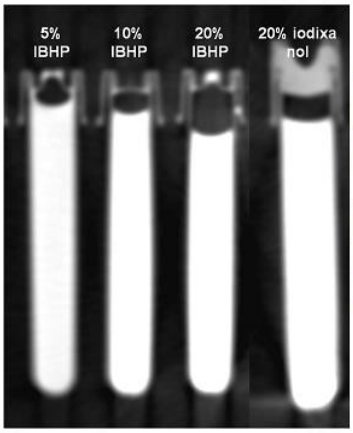

Sample	Mean attenuation (HU)	Standard deviation
5% IBHP	885.15	7.43
10% IBHP	1328.8	12.76
20% IBHP	1655.7	24.4
20% iodixanol (control)	1330.74	2.74

Figure 39. X-ray opacity of different concentrations of IBHP and control material (20% iodixanol).

4.1.2. 4,4-bis (4-hydroxy 3,5-diiodo phenyl) pentanol

The tetra iodo compound with hydroxyl functionality was prepared by the conversion of 4,4-bis(4-hydroxy-3,5 diiodophenyl) pentanoic acid to 4,4-bis (4-hydroxy 3,5-diiodo phenyl) pentanol using borane-THF complex. The hydroxylated iodocompound was yellow in color (Figure 40) and was characterized by FTIR, ^{1}H NMR, mass spectroscopy and thermogravimetry.

Figure 40. 4,4-bis (4-hydroxy 3,5-diiodo phenyl) pentanol

The different types of protons in IBHOH were confirmed by ^{1}H NMR spectroscopy. The spectrum (Figure 41) showed alkyl C-H stretch in the region δ=1-2 ppm, a triplet of alcohol O-H str. at δ=3.3 ppm, phenolic proton peak at δ=9.487 ppm and aromatic proton peak at δ=7.451 ppm. The absence of –COOH peak at δ=12 ppm indicated successful conversion of IBHP to IBHOH.

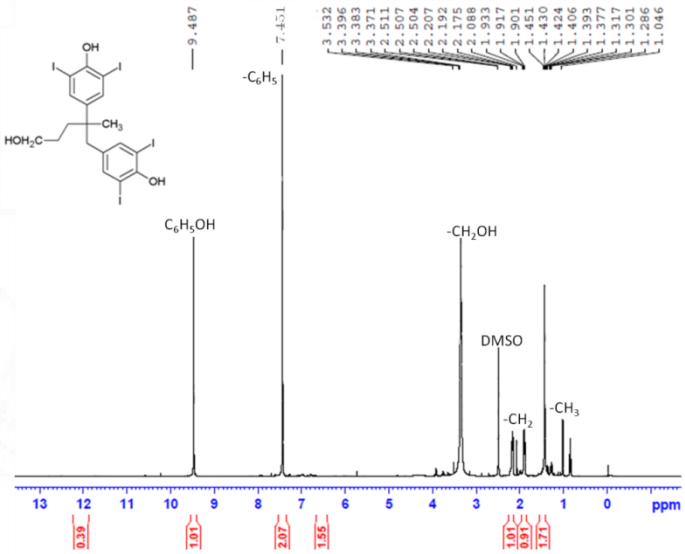

Figure 41. ^{1}H NMR spectrum of IBHOH

On comparing the FTIR spectra of IBHP and IBHOH (Figure 42), a broad peak at 3325 cm^{-1} corresponding to alcohol –OH str. was obtained. The hydrogen bonding in alcohol was responsible for the characteristic broad peak which distinguishes it from other functional groups (Hardas, 1990). The peak corresponding to acid –C=O str. at 1707 cm^{-1} was absent in the case of IBHOH which indicates the successful conversion of IBHP to IBHOH. IBHOH retained the alkane C-H str. and C-H bending vibrations at 2981 and 1529 cm^{-1} respectively. It showed an additional peak at 1123 cm^{-1} of alcohol C-O str, which further confirmed the successful conversion to alcohol. The C-I str. vibration at 708 cm^{-1} in IBHP was also retained.

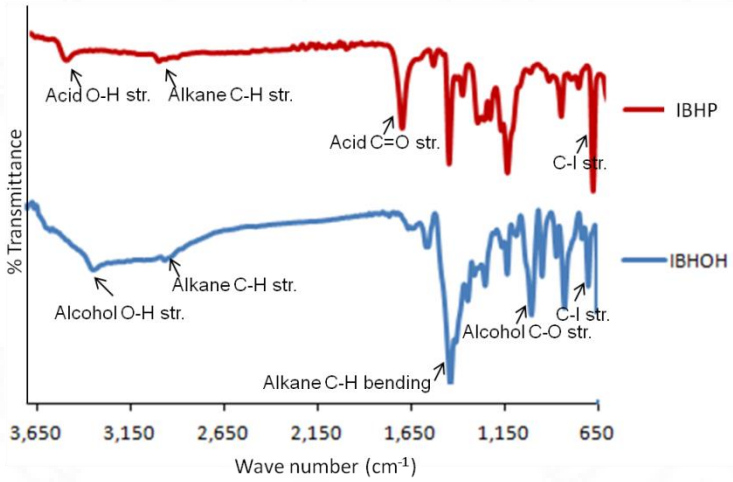

Figure 42. FTIR spectra of IBHP and IBHOH

The conversion and purity of IBHOH was again confirmed by the mass spectroscopic analysis. The mass spectrum of IBHOH (Figure 43) showed a base peak at 783.63 (M+23) and a molecular ion peak at 804.94 (M+40). The reduction in molecular weight of IBHP from 812 (M+23) and 834 (M+40) was also confirmed by the conversion of acidic group to hydroxyl group.

IBHOH, *m/z* 783.63 (M^+, 100%), 804.94 (M^+, 18%).

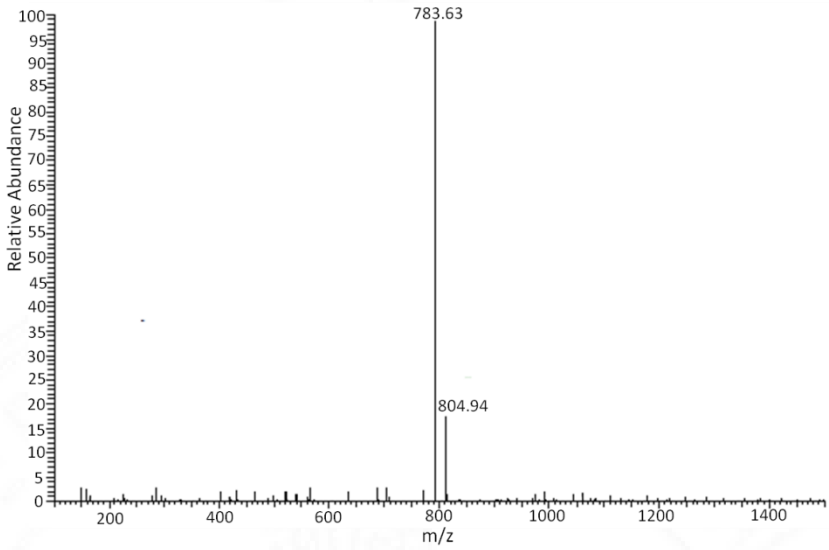

Figure 43. Mass spectrum of IBHOH

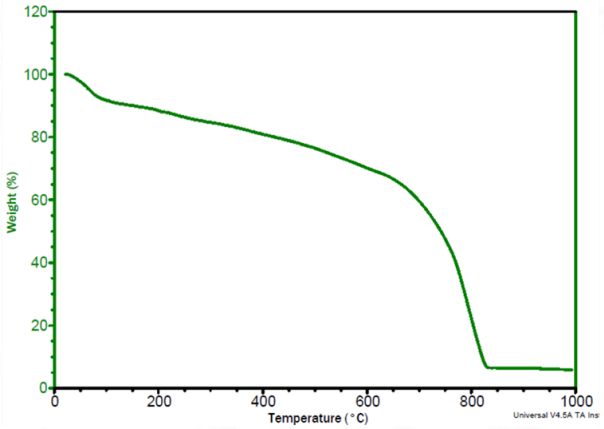

Figure 44. TGA traces of IBHOH

The TGA traces of IBHOH (Figure 44) showed that the first degradation temperature ranged from 25-94˚C which corresponded to the evaporation of moisture. The compound retained around 92% of weight at 94˚C. The second degradation step was observed at temperature ranges of 100-664˚C and the % weight retained at 664˚C was about 65%. The compound then decomposed suddenly up to 825˚C though complete mass loss was not observed. The compound retained a residual mass of 5.7% even after heating at

900˚C. A similar kind of degradation was reported for alcoholic compounds by Teli & Jadhav (2017) and Björklund & Kocherbitov (2017).

The opacity of 10% solution of IBHOH in DMSO was measured with a CT scanner and the attenuation obtained for the solution was 1334±29.7 HU with an iodine load of 325 mgI/mL.

4.1.3. (4-(5-bromo-2-(4-hydroxy-3,5-diiodophenyl) pentan-2-yl)-2,6-diiodophenol

1,4- dibromo butane was used to convert 4,4-bis (4-hydroxy 3,5-diiodo phenyl) pentanol to (4-(5-bromo-2-(4-hydroxy-3,5-diiodophenyl) pentan-2-yl)-2,6-diiodophenol (HR). The obtained HR was a brown liquid (Figure 45) and the conversion confirmed by ^{1}H NMR, ^{13}C NMR, FTIR spectroscopy, mass spectroscopy and TGA analysis.

Figure 45. (4-(5-bromo-2-(4-hydroxy-3, 5-diiodophenyl) pentan-2-yl)-2,6-diiodophenol

The proton NMR spectrum of HR (Figure 46) showed methyl proton at 1-2 ppm. The methylene proton attached to ether linkage was found as a multiplet at 4.2 ppm. The C-H proton attached to bromine was found at 3.3 ppm. The phenolic proton was present at 8.1 ppm and the aromatic proton was noticed at 7.5 ppm.

The different types of carbon atoms in the molecule and their alkylation were confirmed by ^{13}C NMR spectroscopy. HR contains 12 different types of carbon atoms which are labeled and marked in the ^{13}C NMR spectrum (Figure 47). The peak at 44 ppm was due to the carbon attached to the bromine group. The peaks at 63 and 64 ppm correspond to carbon-oxygen single bond in ether linkage. The carbon atoms found in different environment (CH_2 group) were found in the region 24-44 ppm. The aromatic carbon attached to –OH group and iodine group were found at 138 and 162 ppm, respectively.

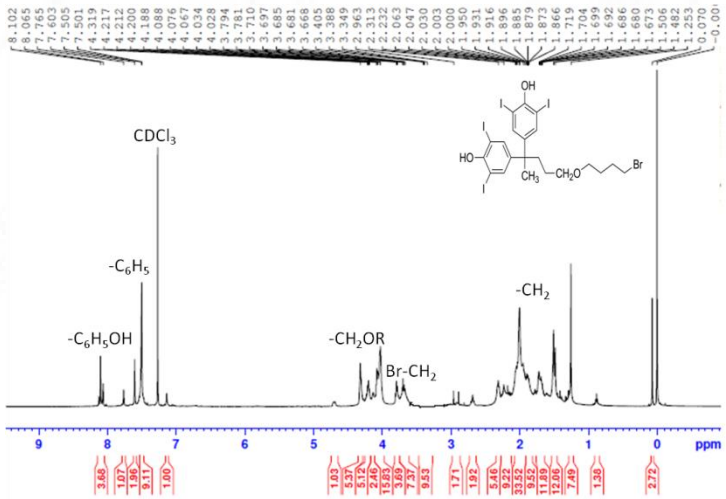

Figure 46. ^{1}H NMR spectrum of HR

The functional group identification of HR was done by FTIR spectroscopy. The FTIR spectrum of HR (Figure 48) was completely different from the starting molecule, IBHOH. The alcoholic stretching was completely absent in the case of HR and it showed C-H str. and C-H bending of alkyl functionality at 2982 and 1529 cm^{-1}, respectively. It also showed a strong peak at 1090 cm^{-1} which indicated the ether C-O str. A new peak at 665 cm^{-1} along with the C-I str. vibration at 708 cm^{-1} indicated the presence of C-Br str.

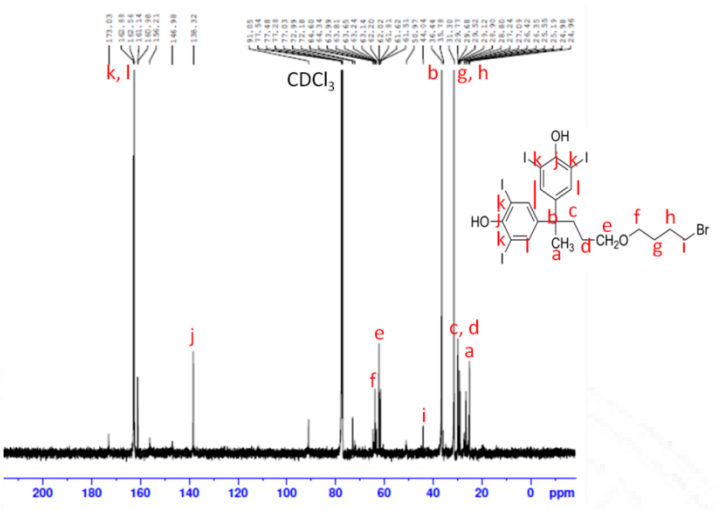

Figure 47. ^{13}C NMR spectrum of HR

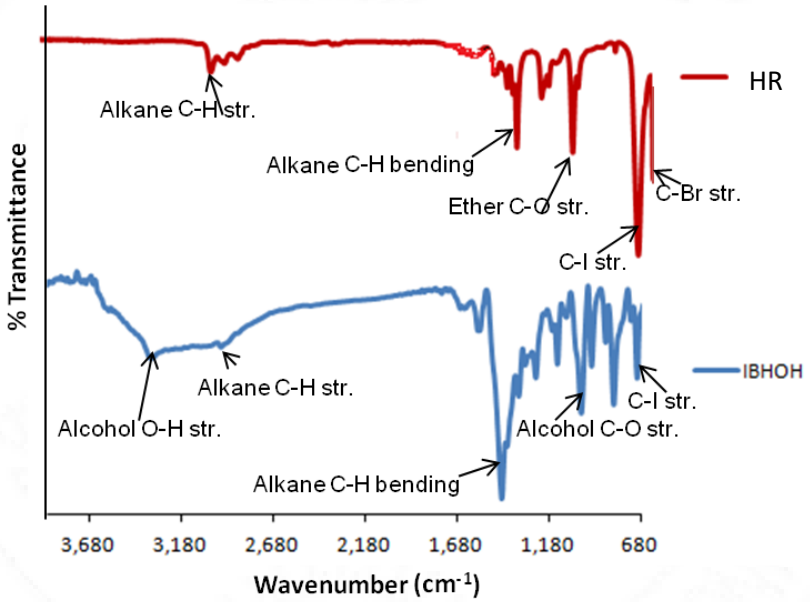

Figure 48. FTIR spectra of HR and IBHOH

The molecular weight confirmation of HR was done by mass spectroscopy. The mass spectrum of HR (Figure 49) showed similar base peak and molecular ion peak at 966.78 (M+23). The increase in molecular weight from 804 to 966 indicated the successful halo alkylation in 4, 4-bis (4-hydroxy 3,5-diiodo phenyl) pentanol.

HR, m/z 966.78 (M^+, 100%), 938.78 (M^+, 14%), 301.16 (M^+, 15%).

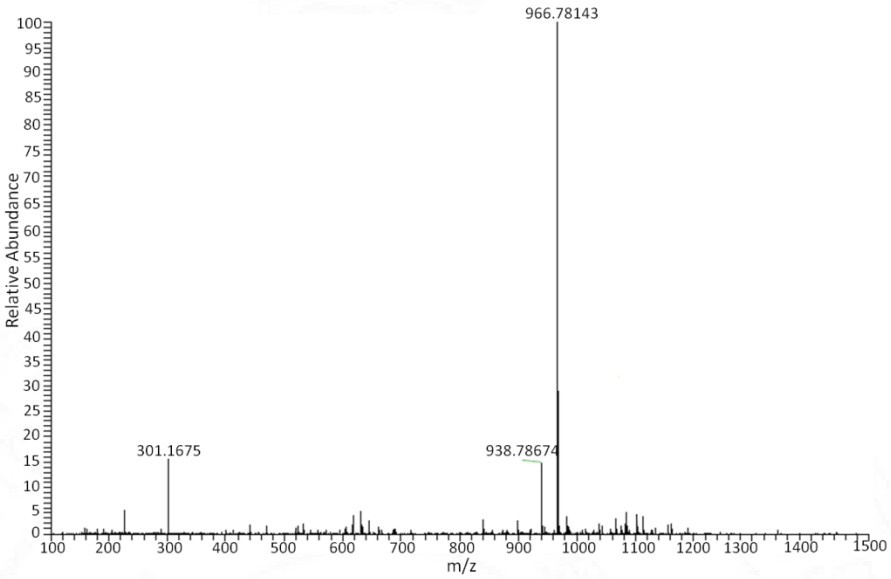

Figure 49. Mass spectrum of HR

The opacity of 10% solution of HR in DMSO was measured in a CT scanner and the attenuation obtained for the solution was 1282±15.7 HU with an iodine load of 270 mgI/mL.

4.2 Characterization of radiopaque polymers

4.2.1. (4-(5-bromo-2-(4-hydroxy-3, 5-diiodophenyl) pentan-2-yl)-2,6-diiodophenol grafted polyvinyl alcohol-co-ethylene (EV-g-HR)

It has been reported that ethers have high chemical stability and the cleavage of ether linkage was very difficult (Roos et al., 1967; Koubsky et al., 2017). So to synthesize radiopaque polymer, ether linkage was selected and this was possible through the reaction of halogenated iodocompound and polymer having hydroxyl functionality. The polymer commercially used for embolization application was polyvinyl alcohol-co-

ethylene which has hydroxyl functionality. Two different grades (38 mol% and 27 mol% ethylene content) of polyvinyl alcohol-co-ethylene were selected and the iodocompound selected for grafting was halogenated (4-(5-bromo-2-(4-hydroxy-3,5-diiodophenyl) pentan-2-yl)-2,6-diiodophenol.

4.2.1.1. Spectral and thermal characterizations

The extent of grafting of HR onto EV was identified from ^{1}H NMR spectroscopy. All grades of EV showed –OH proton peak as a triplet at 4.2, 4.47 and 4.67 ppm due to isotactic, heterotactic and syndiotactic nature of vinyl alcohol units and alkyl proton peak in the region 1-2 ppm. On grafting with HR there were noticeable changes in the NMR spectrum and additional peaks of HR were observed (Figure 50). The –OH proton peak at 4.6 ppm, due to syndiotactic nature of vinyl alcohol unit was absent in the NMR spectrum of grafted polymer which confirms the successful grafting of HR onto EV. The methine proton attached to the hydroxyl group appeared at 3.5-3.9 ppm. Since ether group is electronegative it shifts the methine proton in EV to down field and appears at 2.08 ppm. That was also an indication of grafting. The aromatic proton and phenolic proton in HR were present at 5.7 and 7.4 ppm, respectively.

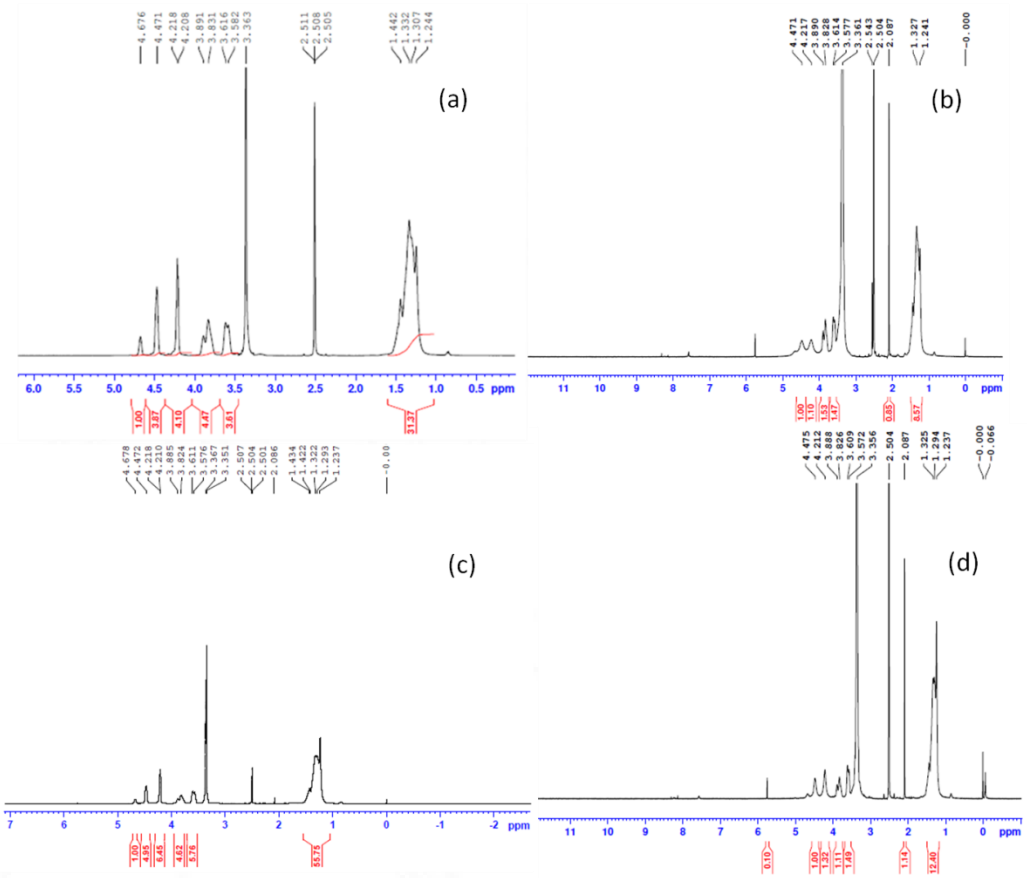

Figure 50. ^{1}H NMR spectra of (a) EV27, (b) EV27-g-HR, (c) EV38, (d) EV38-g-HR

The degree of substitution obtained for EV27-g-HR and EV38-g-HR were 27% and 20%, respectively and the percentage iodine content obtained for the same were 45 wt% and 41.6 wt%, respectively.

Agusti et al. (2015) synthesized and evaluated monoiodo and triiodo benzyl ethers of polyvinyl alcohol (PVA) and found the % iodine content from ^{1}H NMR spectra using a similar formula. The iodine content obtained by them was 43 wt% and 68 wt%, respectively for monoiodo and triiodo benzyl ethers of PVA. The degree of substitution obtained was 53% and 57%, respectively. However, in our study though the degree of substitution obtained was 27%, the tetraiodo compound could achieve more iodine

content than mono or triiodo compounds. This substantiates the successful selection of tetraiodo compound for radiopaque polymer synthesis.

Grafting of HR onto EV through the ether linkage was also confirmed by FT-IR spectroscopy. FT-IR spectra of both grades of EV showed O-H str. around 3440 cm^{-1}, C-H str. at 2920 cm^{-1} and C-H bending around 1470 cm^{-1}. But after grafting the intensity of O-H str. frequency with respect to C-H str. frequency decreased which is due to the consumption of O-H group for grafting. EV38-g-HR also showed the characteristic peaks at 3302 cm^{-1} (O-H str.), 2912 cm^{-1} (C-H str.), 1442 cm^{-1} (C-H bend), 1065 cm^{-1} (ether C-O str.) and 708 cm^{-1} (C-I str.) (Figure 51(a)). EV27-g-HR showed peaks at 3289 cm^{-1} (O-H str.), 2906 cm^{-1} (C-H str.), 1433 cm^{-1} (C-H bend), 1084 cm^{-1} (ether C-O str.) and 708 cm^{-1} (C-I str.) (Figure 51(b)).

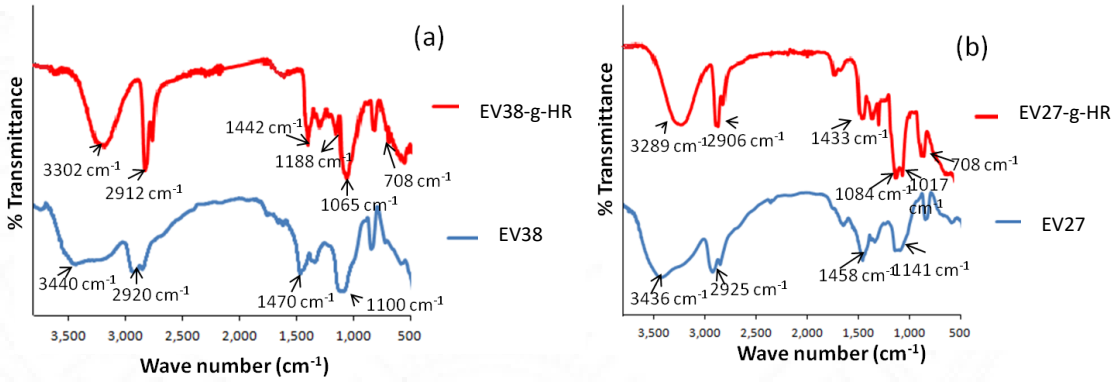

Figure 51. FTIR spectra of EV and EV-g-HR having grades (a) 38 mol% (b) 27 mol%

The thermal stability of the pure and grafted polymer was analyzed by thermogravimetric analysis which serves as an effective tool for studying the thermal behavior of materials. TGA spectra of pure EV and EV-g-HR showed single stage and two step degradation (Figure 52) behaviors, respectively. The initial step occurred

between 100 and 330˚C followed by the second step at around 330 and 470˚C. In the first step the decomposition of the pendant chain occurred, by the breaking of ether linkage followed by the decomposition of the polymer in the second step. Pure EV 27 and EV 38 were thermally stable up to 301˚C and 332˚C, respectively. After grafting the thermal stability reduced to 212.6˚C and 233.9˚C for EV27-g-HR and EV38-g-HR, respectively. The complete decomposition of EV27-g-HR occurred at around 980˚C but EV38-g-HR has 0.3% residual mass after heating up to 1000˚C. The complete decomposition of EV 27 and EV 38 was observed at 469 and 434˚C, respectively. About 50% weight reduction was observed at 387˚C, 375˚C, 395˚C and 415˚C for EV 27, EV27-g-HR, EV 38 and EV38-g-HR, respectively.

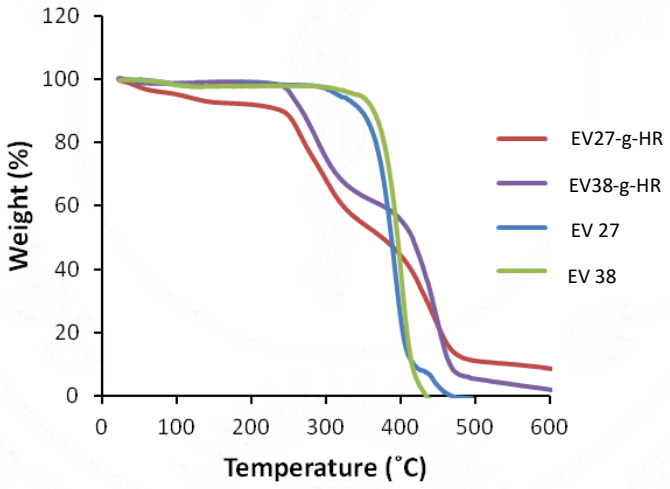

Figure 52. TGA traces of EV and EV-g-HR

The transition temperatures of the pure and grafted EV were analyzed by differential scanning calorimetry. The DSC spectra of pure and grafted EV (Figure 53) showed that grafting decreases the melting point and glass transition temperature of the pure

polymers. The Tg of EV 27 was decreased from 72˚C to 61.9˚C. Similarly the Tg of EV 38 was decreased from 62˚C to 51.7˚C due to grafting. The decrease in Tg was due to the increase in free space between the chains due to the steric hindrance of hanging iodinated organic compounds (Shiralizadeh et al., 2016). The melting points of EV 27 and EV 38 obtained from DSC analysis (Figure 53) were 181.3˚C and 171.9˚C, respectively. The melting points of EV27-g-HR and EV38-g-HR were 161.2˚C and 151.3˚C, respectively. A similar kind of decrease in melting point due to grafting was reported in literatures also (Wang et al., 2020). The degree of crystallinity was responsible for the melting point of the polymer, the higher the crystal defect content, the lower the melting point (Vasanthan et al., 2004; Zhang et al., 2015).

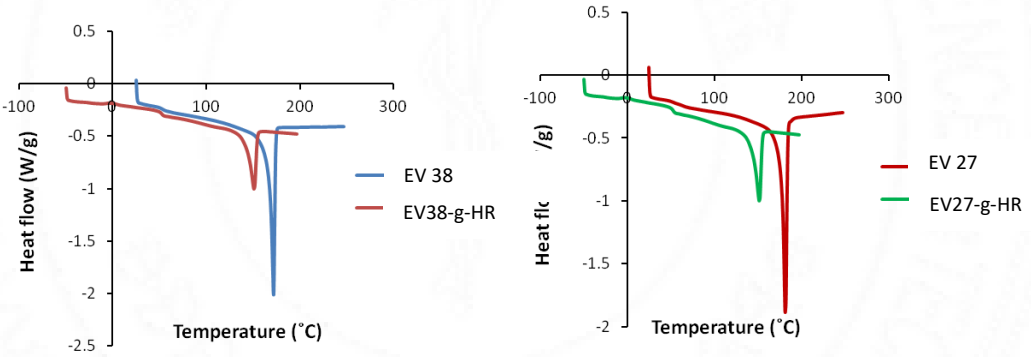

Figure 53. DSC traces of virgin (EV 38 & EV 27) and HR grafted EV (EV38-g-HR & EV27-g-HR)

The phase composition in polymers was analyzed by X-ray diffraction analysis. XRD spectra of pure and grafted EV (Figure 54) showed that grafting caused a slight broadening of the peaks which was brought about by the decrease of crystallite size due to grafting (Ungar, 2004). EV is a highly crystalline polymer (Lagaron et al., 2004)

which retained some amount of crystallite structure in spite of grafting. Similar observations were also obtained in DSC analysis.

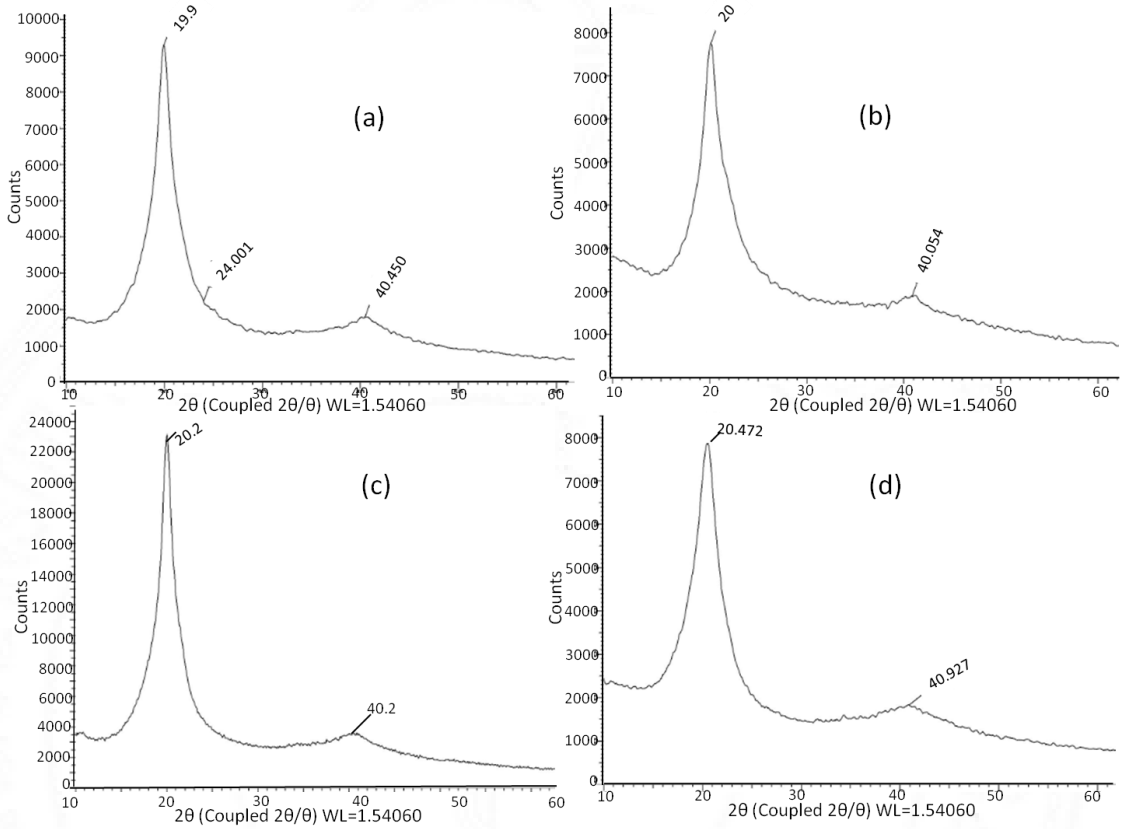

Figure 54. XRD spectra of: (a) EV 27, (b) EV27-g-HR, (c) EV 38, and (d) EV38-g-HR

4.2.1.2. In vitro cell culture cytotoxicity

Test on extract: The cytotoxic responses obtained towards test (EV27-g-HR) and control samples (positive control: dilute phenol, negative control: UHMWPE) are tabulated in the Table 13.

Table 13. Response of L929 cell line towards EV-g-HR.

Sl No.	Sample	Grading	Reactivity
1	Negative control	0	None
2	Positive control	4	Severe
3	IBHR-g-EVOH (24 h extraction)	0	None
4	IBHR-g-EVOH (72 h extraction)	0	None

As per ISO 10993-5, a numerical grade greater than 2 is considered cytotoxic. The EV27-g-HR samples after 24 h and 72 h extraction received numerical grading zero indicating that the material is non-cytotoxic. The morphology of cells after 24 h contact with 24 h and 72 h extracts of EV27-g-HR, negative control and positive control was shown in Figure 55. From the image it is clear that, the cells could retain their morphology after 24 h contact with the material which indicates the non-cytotoxic response of the material towards L929 cells.

MTT assay: The quantitative estimation of cell viability was done by MTT assay. The percentage metabolic activity of L929 cells towards EV27-g-HR is shown in Figure 56. The assay showed that L929 cells after 24 hrs contact with 50%, 25%, 12.5% and 6.25% extract of EV27-g-HR exhibited 95%, 100%, 100% and 110% viability. After 72 h contact, the viability became 96%, 105%, 110% and 120%, respectively. So EV27-g-HR was non-toxic to L929 cells in the measured time periods.

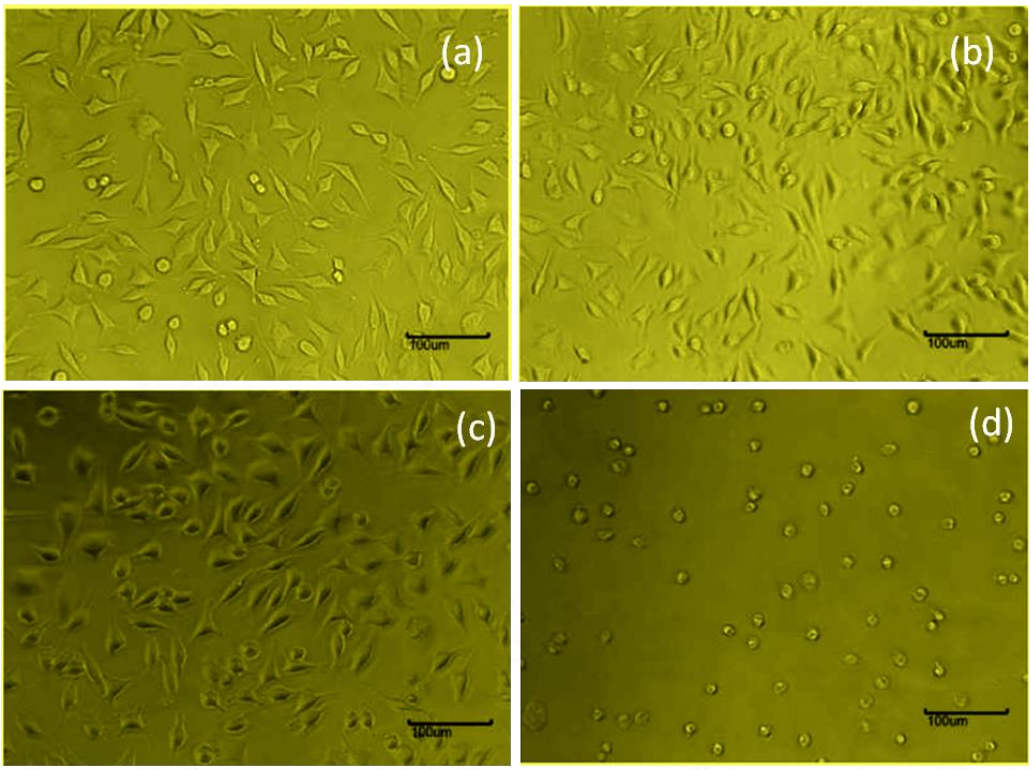

Figure 55. L929 cells after 24 h contact with: (a) 50% extract of EV27-g-HR (24 h extraction), (b) 50% extract of EV27-g-HR (72 h extraction), (c) negative control, and (d) positive control

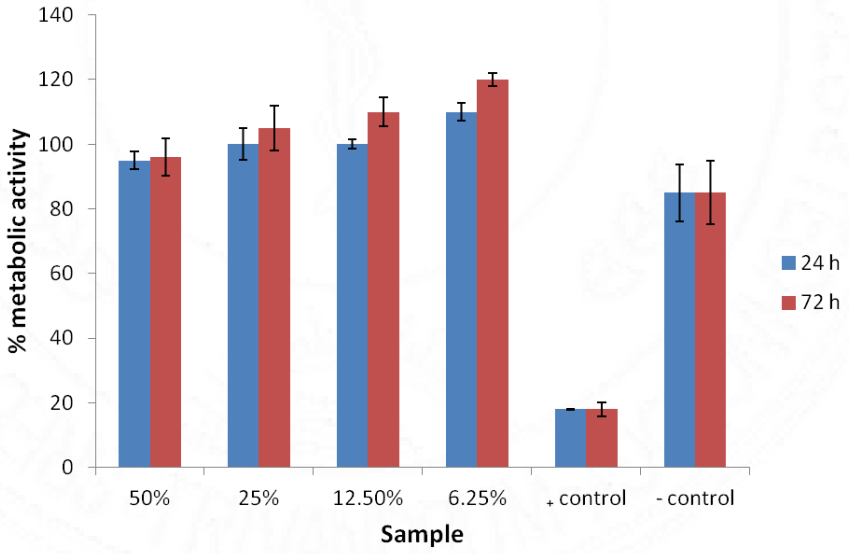

Figure 56. Metabolic activity (%) of EV27-g-HR towards L929 cells.

Since the grafting efficiency and iodine content was low in EV-g-HR, we further grafted 4, 4-bis(4-hydroxy-3,5-diiodophenyl) pentanoic acid onto polyvinyl alcohol-co-ethylene through ester linkage. Arano et al. (1996) reported that the chemical stability of ester bond depended on the chemical structure of the linkages. Ghodke & Punekar (2022) reported that aromatic carboxyl esters are difficult to hydrolyze compared to regular carboxyl esters because of both steric and polar effects. So, the iodocompound containing carboxyl functionality was selected for the synthesis of radiopaque EV.

4.2.2. 4,4-bis(4-hydroxy-3,5-diiodophenyl) pentanoic acid (IBHP) grafted polyvinyl alcohol-co-ethylene (EV-g-IBHP)

The grafting of IBHP was carried out on three grades of EV copolymer, i.e., EV with 27 mol%, 32 mol% and 38 mol% ethylene content. Grafting reaction was carried out by changing the ratios of iodocompound to EV and the by changing the reaction time. In all cases extent of grafting and radiopacity were different. The optimized formulation had EV to iodocompound ratio 1:10 and reaction time 5 days.

4.2.2.1. Spectral and thermal characterizations

The extent of grafting and % iodine content were determined from ^{1}H NMR spectra using the equations (3) and (4). The proton NMR spectra (Figure 57) of all the grades of EV-g-IBHP showed the aromatic proton peak at 6.5-8 ppm and phenolic proton peak at 8.1 ppm which were completely absent in the case of pure EV. The influence of iodocompound in the polymer backbone caused a drastic change in the methylene region (1-2 ppm). The absence of carboxylic acid proton peak in the region 12 ppm indicated

the absence of residual ungrafted iodocompound in the polymer. The isotactic, heterotactic and syndiotactic –OH proton peaks in EV was present at 4.2, 4.47 and 4.67 ppm and the methine proton attached to the hydroxyl group appeared at 3.5-3.9 ppm. These peaks though present in grafted EV also displayed reduction in intensities.

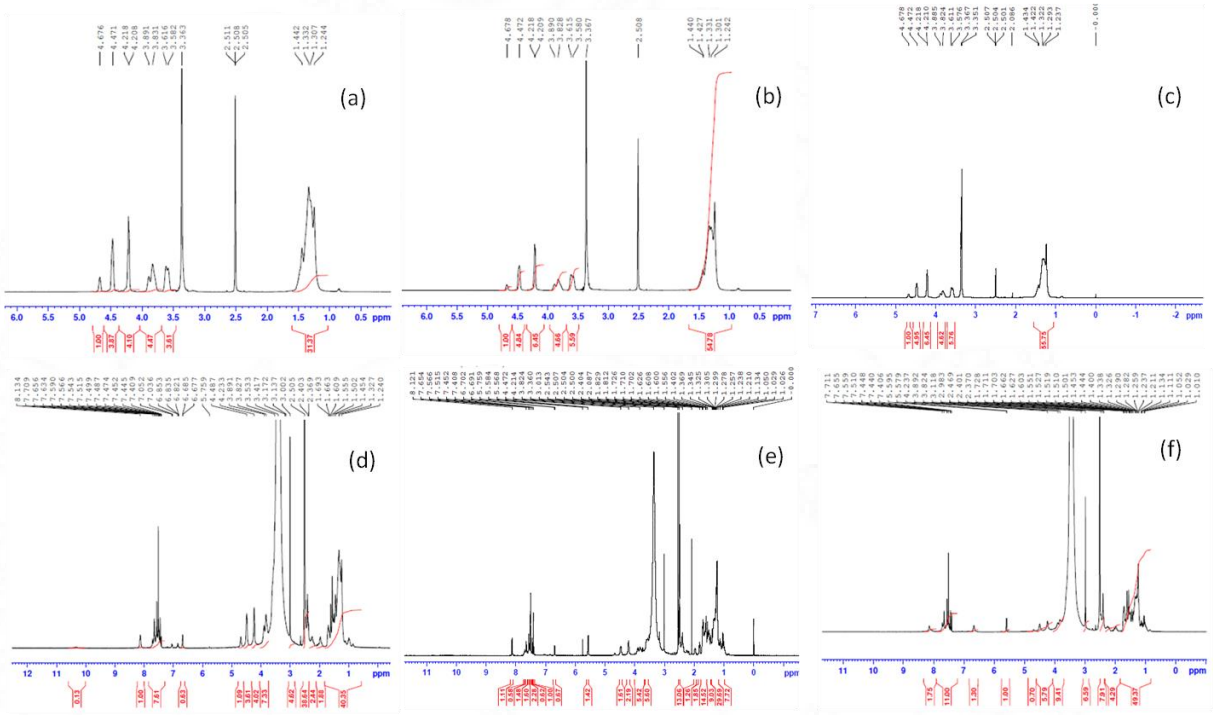

Figure 57. ^{1}H NMR spectra of: (a) EV 27, (b) EV 32, (c) EV 38, (d) EV27-g-IBHP, (e) EV32-g-IBHP, and (f) EV38-g-IBHP

The degree of substitution obtained for EV27-g-IBHP, EV32-g-IBHP and EV38-g-IBHP were 57.5%, 34% and 19.7% respectively. The iodine content (%) obtained for the same were 63.7 wt%, 57.5 wt% and 48.9 wt%, respectively. 27 mol% ethylene containing EV has the highest hydroxyl content (73%) and showed maximum grafting efficiency and maximum iodine content.

The formation of ester linkage was confirmed from FT-IR spectrum. In the FT-IR spectrum of EV-g-IBHP (Figure 58), the peak at 1750 cm^{-1}, 1200 cm^{-1} and 1100 cm^{-1} indicated the presence of ester linkage. The first one was for C=O str. and the latter two were assigned to the C-O str. The spectra retained the –OH str. and methylene symmetric C-H str. of EV at 3300 cm^{-1} and 2963 cm^{-1} but the intensity of –OH peak was reduced due to grafting. All grades of EV showed similar features.

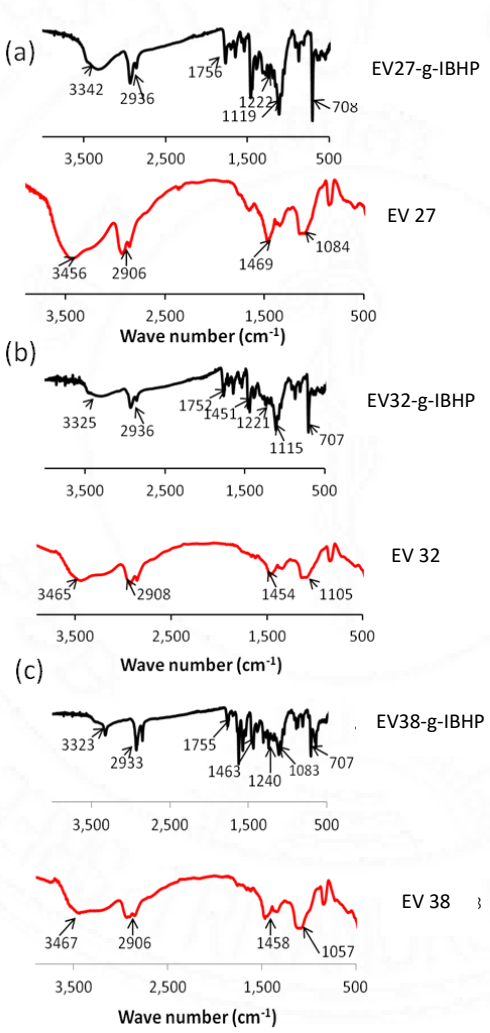

Wave number (cm^{-1})	Functional group
3342 3456	Alcohol O-H str.
2936 2906	Alkyl C-H str.
1756	Ester C=O str
1461 1469	Alkyl C-H bending
1222, 1119	Ester C-O str.
1084	Alcohol C-O str.
708	C-I str.

Wave number (cm^{-1})	Functional group
3325 3465	Alcohol O-H str.
2936 2908	Alkyl C-H str.
1752	Ester C=O str
1451 1454	Alkyl C-H bending
1221, 1115	Ester C-O str.
1105	Alcohol C-O str.
707	C-I str.

Wave number (cm^{-1})	Functional group
3323 3467	Alcohol O-H str.
2933 2906	Alkyl C-H str.
1755	Ester C=O str
1463 1458	Alkyl C-H bending
1240, 1083	Ester C-O str.
1057	Alcohol C-O str.
707	C-I str.

Figure 58. FTIR spectra of: (a) 27 mol%, (b) 32 mol%, and (c) 38 mol% EV and EV-g-IBHP

In the EDX spectra (Figure 59), the peaks present in the region 3.5-5 KeV represented the iodine element in the polymer chain (Shiralizadeh et al., 2016).

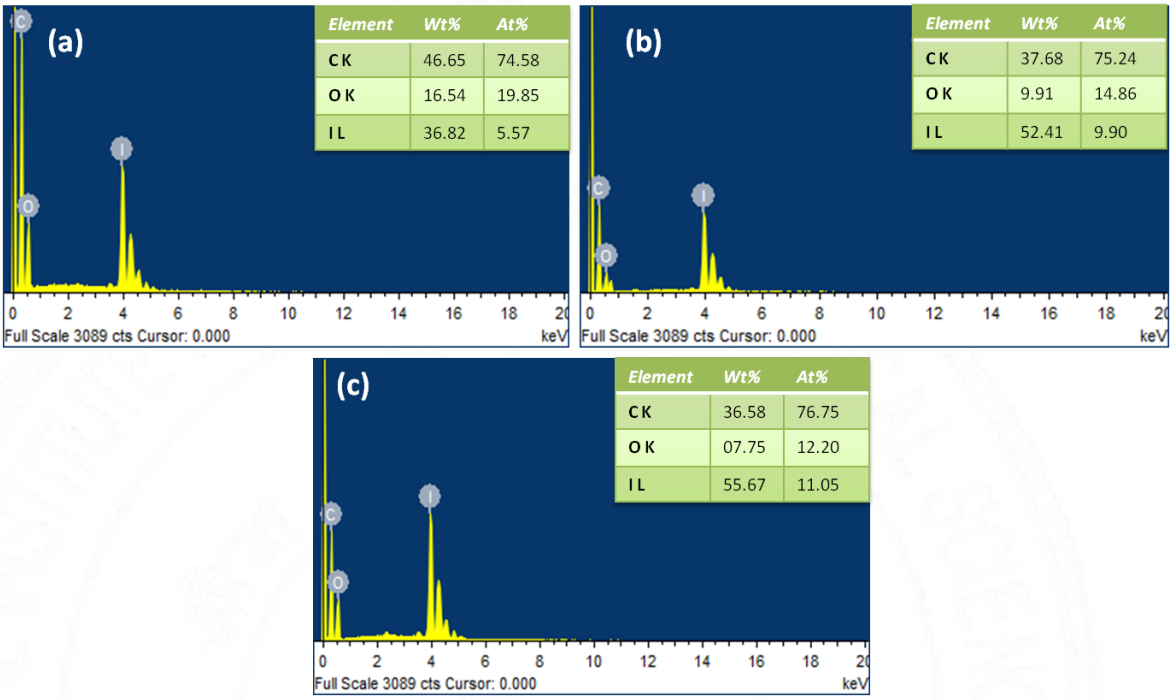

Figure 59. EDAX spectra of: (a) EV38-g-IBHP, (b) EV32-g-IBHP, and (c) EV27-g-IBHP

Thermal stability of radiopaque polymers was studied by thermogravimetric analysis. In all the grades of EV evaluated, the decomposition temperatures of the grafted polymers showed a tremendous decrease. The TGA traces (Figure 60) showed that virgin EV 27, EV 32 and EV 38 were degraded at 301.4°C, 293.45°C and 332.1°C, respectively, but EV27-g-IBHP, EV32-g-IBHP and EV38-g-IBHP were degraded at 192.5°C, 191.2°C and 174°C, respectively. The thermal stability of the polymer increased on increasing the IBHP units in the grafted polymer. A similar observation was noticed by Cankaya & Temuz 2014 in N-cyclohexylacrylamide and methyl methacrylate (MMA) grafted cellulose. They found that thermal stability of cellulose increased with an increase in

MMA units. The pure polymers: EV 27, EV 32 and EV 38 lost their complete mass at 469, 490 and 434˚C but the grafted counterparts retain a residual mass of 11-18.9 % even after heating at 600˚C. So the decomposition of grafted polymers was not complete in inert conditions (Worzakowska, 2016).

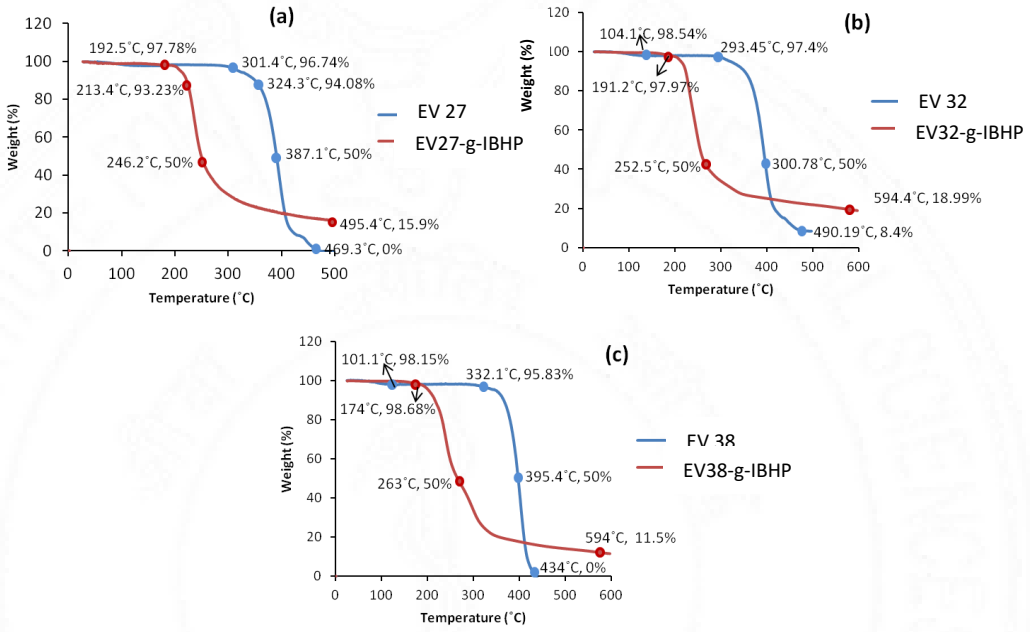

Figure 60. TGA traces of: (a) 27 mol%, (b) 32 mol%, and (c) 38 mol% EV and grafted EV

The particular end use of a polymer depends on its glass transition temperature (Tg). Tg of the polymers was identified using differential scanning calorimetry. DSC traces (Figure 61) showed that the Tg of EV 27 and EV 38 was reduced from 72˚C to 64.56˚C and 62˚C to 51.11˚C respectively. EV 32 showed a Tg of 69˚C but after grafting it didn't show any particular transition temperature. The steric hindrance experienced due to the pendent iodinated groups caused an increase in free space between the chains (Shiralizadeh et al., 2016). This was the reason proposed for the observed reduction in Tg in IBHP grafted polymers. In addition, grafting replaced the hydroxyl group on the

main chain with ester groups and this reduced the intra molecular interactions and the Tg.

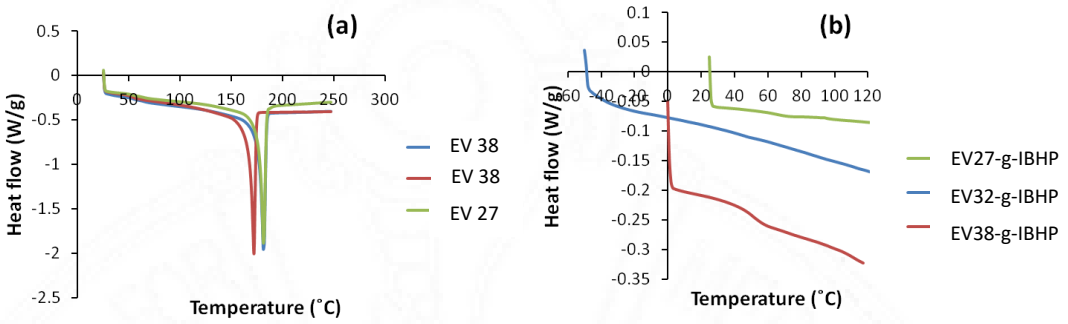

Figure 61. DSC traces of different grades of: (a) EV, and (b) EV-g-IBHP

The sharp melting points of EV 27 (181.36˚C), EV 32 (181.39˚C) and EV 38 (171.92˚C) (Figure 61) were not found in the grafted polymers. These polymers found to decompose prior to melting due to weak covalent interactions between iodocompound and polymer. The melting temperature was attained only when thermal motion could break these intermolecular interactions. Further the crystallinity of the polymer was distorted due to grafting and this explained the absence of a sharp melting point in the case of grafted polymers.

EV is a highly crystalline polymer (Lagaron et al., 2004). The XRD images (Figure 62 (a)) of all grades of EV showed a high intensity peak at 20˚ and a low intensity peak at 40˚. After the iodocompound was introduced, the sharp peak at 20˚ turned into a broad one and the peak at 40˚was not distinguishable (Figure 62(b)). These were due to the decrease in crystallite size (Chauhan, 2015) and so grafting disrupts the ordered arrangement and it becomes amorphous.

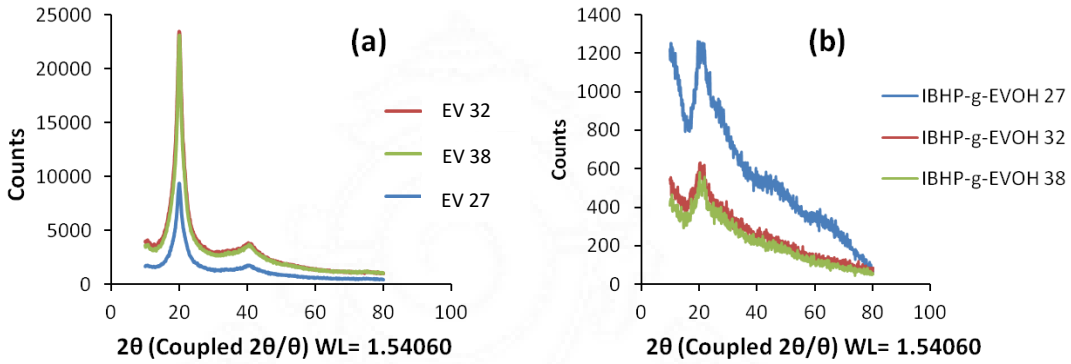

Figure 62. XRD spectra of different grades of: (a) EV, and (b) EV-g-IBHP

4.2.2.2. In vitro cell culture cytotoxicity of EV27-g-IBHP against fibroblast cells

The response of cells to EV27-g-IBHP-120h was studied through *in vitro* cell culture cytotoxicity tests such as test on extract, MTT assay and direct contact assay on L929 fibroblastic cells. Figure 63 showed the survival of cells after contact with 50% extract of EV27-g-IBHP-120h. The original morphology of the cells was retained even after contact with the extract of the polymer (extraction time: 72h).

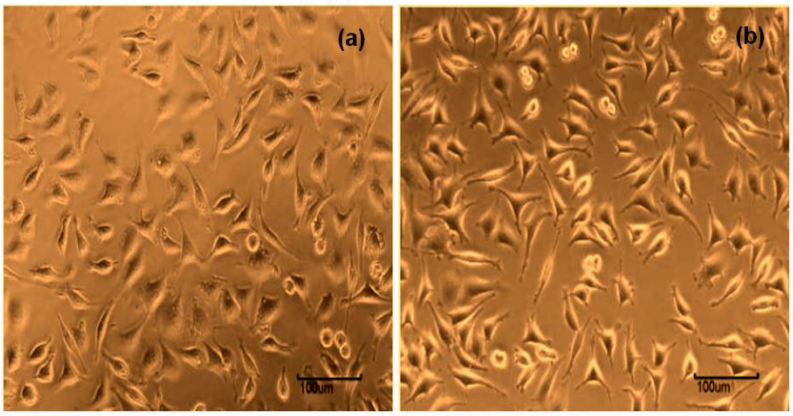

Figure 63. L929 cells after 24 h contact with 50% extract of EV27-g-IBHP-120h: (a) 24h extract, and (b) 72h extract

The cytotoxic reactivity of test and control sample was evaluated under an inverted phase contrast microscope and the observations were tabulated in the Table 14.

Table 14. Response of L929 cell line towards extract of EV27-g-IBHP.

Sl No.	Sample	Grading	Reactivity
1	Negative control	0	None
2	Positive control	4	Severe
3	EV27-g-IBHP-120h (24 h extraction)	0	None
4	EV27-g-IBHP-120h (72 h extraction)	0	None

As per ISO 10993-5, the numerical grading above 2 is considered toxic. EV27-g-IBHP-120h had a numerical grading of 0 indicating that the material was not toxic towards L929 fibroblast cells.

The MTT assay of fibroblastic cell lines after contact with 50%, 25%, 12.5% and 6.25% extracts of EV27-g-IBHP-120h showed 88.83%, 112.59%, 113.48% and 107.44% metabolic activity for 24 hrs extract (Figure 64), 92.90%, 105.54%, 109.75% and 112.65% metabolic activity for 72 hrs extracts. Reagent control showed 94.11%, positive control showed 21.94% and negative control showed 89.13% metabolic activity. So the MTT assay also proved that the material was nontoxic in nature.

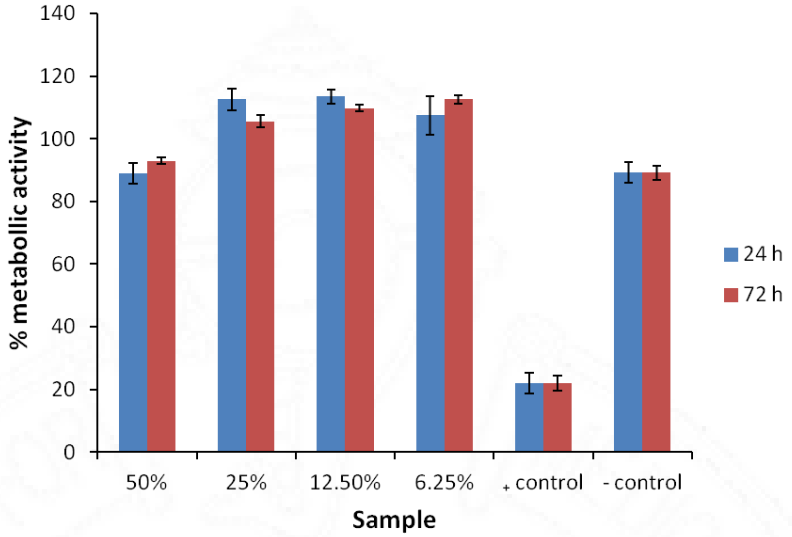

Figure 64. Metabolic activity of 24 h and 72 h extract of EV27-g-IBHP-120h towards L929 cells.

Direct contact assay: The toxicity of the material in disc form was again evaluated by direct contact assay. Direct contact assay is highly sensitive and can also detect weak cytotoxicity (Srivastava et al., 2018). The grading based the response of L929 cells towards the material is tabulated in Table 15.

Table 15. Reactivity of L929 cells towards EV27-g-IBHP-120h

Sample	Grading	Reactivity
Negative control	0	None
Positive control	4	Severe
IBHP-g-EVOH	0	None

Here the test material got zero grading indicating its non-toxic nature. Figure 65 (a), (b) and (c) show the viability of L929 cells on contact with EV27-g-IBHP-120h disc, negative control and positive control, respectively.

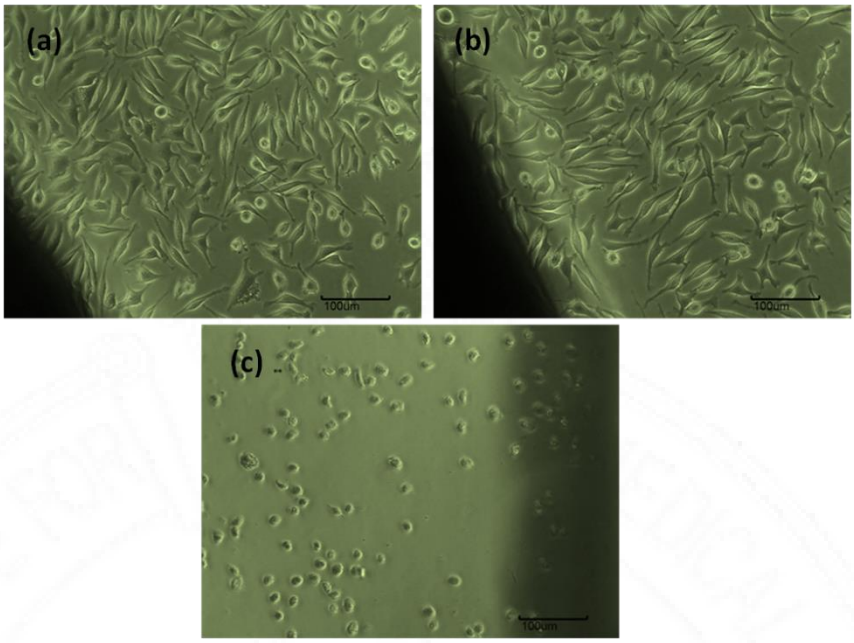

Figure 65. L929 cells after 24 h contact with: (a) EV27-g-IBHP-120h, (b) UHMWPE (negative control), and (c) PVC disc (positive control).

4.2.2.3. In vitro cell culture cytotoxicity study of EV27-g-IBHP-120h using endothelial cells

The response of endothelial cell lines (EA.hy926) towards EV27-g-IBHP-120h was also studied. In the direct contact assay with the grafted polymer disk, the cell response grading was zero with no detectable zone of lysis (Figure 66). The cells retained their morphology after 24 h contact with the material. So the IBHP grafted EV copolymer was considered as non-cytotoxic.

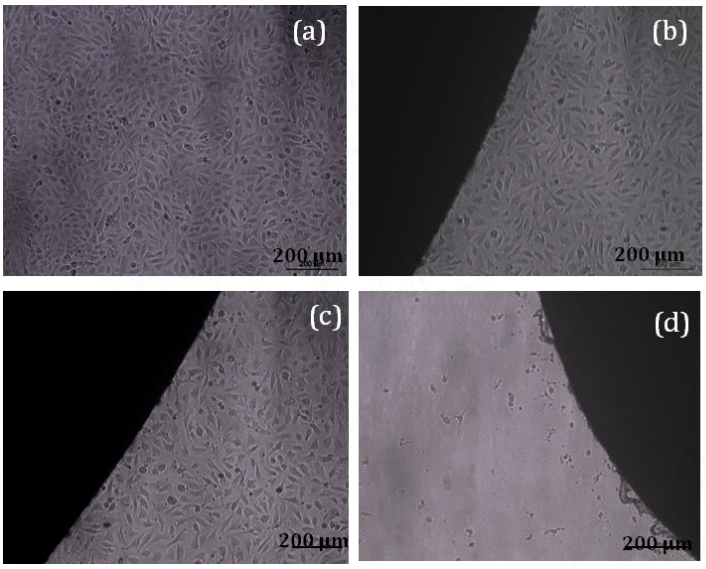

Figure 66. Morphology of EA.hy926 endothelial cell lines: (a) Cells only, after 24 h contact, (b) with test sample, (c) with negative control, and (d) with positive control

The quantitative analysis of cell viability was done by alamar blue assay. After 24 h incubation, 0.3g, 0.2g and 0.1g of EV27-g-IBHP-120h pellets showed 84.8±1.55%, 85.2±0.09% and 85.9±1.88% cell viability, respectively, which are close to the viability of negative control, i.e., 84.99 ± 1.5 %. Positive control showed 15.9 ± 0.89 % viability (Figure 67). According to ISO-10993-5, percentage cell viability above 80% is considered as non-cytotoxic. Here the test material attained a viability of more than 80% and was considered non-cytotoxic toward endothelial cell lines.

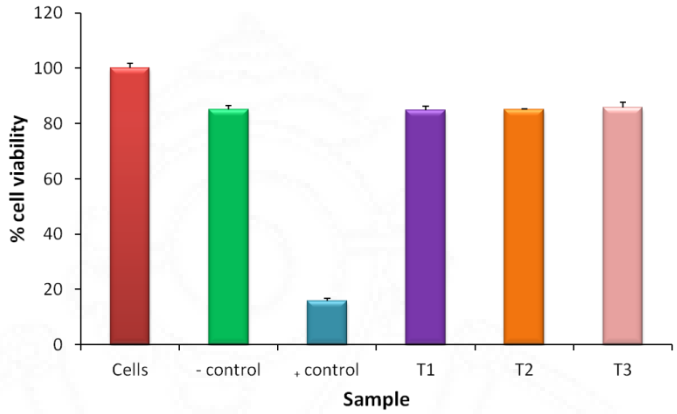

Figure 67. Cell viability (%) of EA.hy926 cell line towards 24 h incubated samples (T1, T2 and T3 are pellets of EV27-g-IBHP-120h each weighing 0.3g, 0.2g and 0.1g, respectively)

4.3 Characterization of liquid embolic systems

The maximum grafting efficiency and percentage iodine content were obtained for 27 mol% grade EV for both systems. So it was chosen for formulating liquid embolic systems (LES).

4.3.1. LES from EV27-g-HR

Since the grafting efficiency obtained for 27 mol% grades was more, it was chosen for the preparation of liquid embolic formulation. Different concentrations of EV27-g-HR were prepared according to the formulation in Table 2 and analyzed for its viscosity, precipitation behavior and radiopacity. The maximum concentration of solution that could be prepared was 20% (w/v). Above this concentration, the polymer remain insoluble in DMSO. All concentrations of EV-g-HR were dark brown color as shown in Figure 68.

Figure 68. EV27-g-HR-48h-20%

4.3.1.1. Radiopacity analysis

Radiopacity enables easy identification of the location of the material in the body and is a highly desirable feature required of liquid embolic agents. Quantitative measurement of radiopacity could be achieved through computed tomography (CT) scan and the results are expressed in Hounsfield Units (HU). For radiopacity measurements, 2 ml solutions of different formulations were prepared and scanned in a CT scanner. The radiopacities obtained were tabulated in table 16.

Table 16. Radiopacity analysis of different formulations of EV27-g-HR

LEA formulation code	Attenuation (HU)
EV27-g-HR-24h-10%	317±1
EV27-g-HR-48h-5%	312±4
EV27-g-HR-48h-10%	399±20
EV27-g-HR-48h-15%	509±10
EV27-g-HR-48h-20%	625±14
EV27-g-HR-72h-10%	309±16

Radiopacity analysis of 10 % formulations (table 16) showed that the opacity reached its maximum when the reaction time was 48 h. After that, the opacity values found to decrease. So the optimum time duration required for grafting reaction was 48 h.

Different concentrations of '48 h' samples showed that the maximum concentration that can be prepared from EV27-g-HR-48h was 20% and the highest opacity showed was 625±14 HU.

4.3.1.2. Viscosity analysis

Different concentrations of EV27-g-HR-48h were prepared and their viscosities were analyzed in a rolling ball viscometer. The results compiled in Table 17.

On analyzing the Table, it was clear that the LEA prepared from IBHR-g-EVOH has higher viscosity (more than 100 cSt.) than parent polymer (Table 18) and was not suitable for embolization of smaller blood vessels found in the disease condition known as arteriovenous malformation (AVM). However, it could be used to block blood flow into aneurysms. Commercially available Onyx® HD-500 is widely used for the treatment of intracranial aneurysms (Dalyai et al., 2012).

Table 17. Viscosity data of different concentrations of EV27-g-HR-48h

Concentration (%, w/v)	Density g/cm^3)	Temperature (˚ C)	Dynamic viscosity (mPas)	Kinematic viscosity (m^2/s)	Shear rate (s^{-1})
5	1.409	25	527.8	374.6	784.5
		37	331.9	235.6	514.3
		40	215.3	152.8	435.2
10	1.427	25	584.3	409.5	714.2
		37	371.3	260.2	486.1
		40	286.2	200.6	400.9
15	1.432	25	625.4	436.7	691.5
		37	405.3	283.0	451.7
		40	315.7	220.5	396.4
20	1.480	25	684.9	462.8	684.9
		37	425.4	287.4	425.4
		40	374.7	253.2	374.7

Table 18. Viscosity data of different grades of EV.

EV Grade and concentration	Temperature	Viscosity (cSt.)
EV 27-5%	25	24.4
	37	17.4
	40	16.2
EV 32-5%	25	28.9
	37	20.8
	40	19.4
EV 38-5%	25	16.1
	37	11.6
	40	10.5

EV27-g-HR-48h-20% could form a cohesive lump on precipitation and could be suitable for embolization of arteriovenous malformation. However, it did not have suitable viscosity and radiopacity required for AVM embolization. The viscosity values were rather high and were not suitable to inject through tiny blood vessels. Since our aim was to study the embolization in smaller blood vessels the embolic compositions were formulated using the other polymer systems.

4.3.2. LES from EV27-g-IBHP

The grafting efficiency was found to be higher for EV27 grade copolymer. So the liquid embolic system was prepared from EV27-g-IBHP. Different concentrations of EV-g-IBHP were prepared and tested for their properties. The maximum concentration that could be prepared using this radiopaque polymer system was 35.5% (Figure 70).

Figure 69. EV27-g-IBHP-120h-35.5% in DMSO

4.3.2.1. Radiopacity of the LES

For radiopacity measurements, 2 ml solutions of different formulations of EV27-g-IBHP were prepared and tested. The attenuation values obtained from the CT scan measurements were tabulated in Table 19. The radiopacity data was compared against reaction times for 10% solutions and the data showed that opacity reached its maximum when the reaction time was 120 h. Concentration based radiopacity data showed that maximum opacity of 3988±8 HU could be achieved with 35.5% solution. Further increase in concentration was not possible with the polymer.

Table 19. Attenuation values of different formulations of EV27-g-IBHP in DMSO

LES Formulation code	Attenuation (HU)
EV27-g-IBHP-24h-10%	1335±5
EV27-g-IBHP-48h-10%	1387±6
EV27-g-IBHP-72h-10%	1528±8
EV27-g-IBHP-96h-10%	1591±4
EV27-g-IBHP-120h-10%	1659±5
EV27-g-IBHP-144h-10%	1583±2
EV27-g-IBHP-120h-20%	2626±5
EV27-g-IBHP-120h-30%	3263±1
EV27-g-IBHP-120h-35%	3965±3
EV27-g-IBHP-120h-35.5%	3988±8

4.3.2.2. Viscosity analysis

Viscosity of different concentrations of EV27-g-IBHP-120h at different temperatures are plotted in Table 20. The viscosity measurements were carried out using a micro-viscometer. The concentrations selected for viscosity analysis were 5, 10, 15, 20, 25, 30, 35 and 35.5% (w/v).

Table 20. Viscosity data of different concentrations of EV27-g-IBHP-120h

Concentration (%, w/v)	Density (g/cm^3)	Temperature (˚C)	Dynamic viscosity (cP)	Kinematic viscosity (cSt)	Shear rate (s^{-1})
5	1.2148	25	0.29	0.24	2112
		37	0.23	0.18	2718
		40	0.21	0.17	2878
10	1.255	25	6.98	5.56	334.9
		37	5.16	4.11	452.4
		40	4.80	3.83	485.8
15	1.2868	25	11.3	8.78	205.9
		37	8.49	6.60	273.5
		40	7.93	6.16	292.8
20	1.2982	25	18.3	14.1	126.8
		37	13.2	10.2	175.5
		40	12.2	9.40	189.9
25	1.322	25	29	21.9	79.8
		37	20.8	15.7	111.2
		40	19.3	14.6	119.7
30	1.2936	25	34.6	26.8	67.13
		37	24.1	18.6	96.16
		40	22.1	17.0	105.2
35	1.332	25	52.9	39.8	43.6
		37	36.2	27.2	63.69
		40	33.1	24.9	69.56
35.5	1.3722	25	55.1	40.2	41.51
		37	37.2	27.4	61.60
		40	33.9	25.2	67.68

The reported viscosity range of a commercially used liquid embolic agent (Onyx®) is 18-34 cSt. at 40˚C (Seikmann, 2005). The concentrations 30, 35 and 35.5% depicted

similar viscosity range. It was noted that the radiopaque polymer solutions exhibited lower viscosity than the parent polymer (Table 18).

4.3.2.3. Nature of precipitation

The nature of precipitation of EV27-g-IBHP-120h-35.5% was tested in saline and the precipitate formed was a cohesive lump which was not easy to break (Figure 71). The overall assessment of viscosity, radiopacity and precipitation behavior of EV27-g-IBHP-120h indicate that the system is suitable for the application in the arteriovenous malformation. It had low viscosity, good radiopacity and optimum precipitation characteristics. The viscosity of EV27-g-IBHP-120h-35.5% was 25.2±3.5 cSt, which was in the range of commercially available liquid embolic agent, Onyx® (18-34 cSt.) and the radiopacity obtained for 35.5% solution was 3988±7.6. Therefore, this system was selected for detailed study and for subsequent implantation in swine rete mirabile.

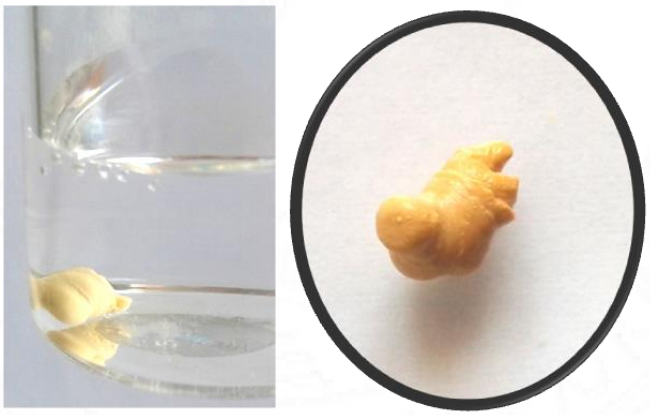

Figure 70. Precipitation of EV27-g-IBHP-120h-35.5% in saline and the precipitate taken out from saline

4.3.2.4. Flow behavior analysis

Suitable viscosity and opacity values were obtained for 35.5% concentration, and this concentration was chosen for further studies. The rheology profile (shear stress and viscosity across a range of shear rate) of EV27-g-IBHP-120h-35.5% and control material Onyx® was measured in a rheometer in the shear rate range 0.1-500 s^{-1}. The rheology curves obtained for the same were plotted in Figure 72. Figure (a) and (c) were the viscosity vs. shear rate plot for EV27-g-IBHP-120h-35.5% and Onyx® 18 liquid embolic agents, respectively. Figure (b) and (d) represented the flow curve (shear stress vs. shear rate) of EV27-g-IBHP-120h-35.5% and Onyx®18, respectively. From the figures it was clear that the in-house developed system also followed the same type of flow behavior as Onyx® 18.

At low shear rates, the viscosity decreased with increase in shear rate and after reaching a particular shear rate, it remained almost constant. The decrease in viscosity was drastic in the case of Onyx®, but the EV27-g-IBHP-120h-35.5% followed a steady, slow decrease which is an indication of the ease of handling of the material.

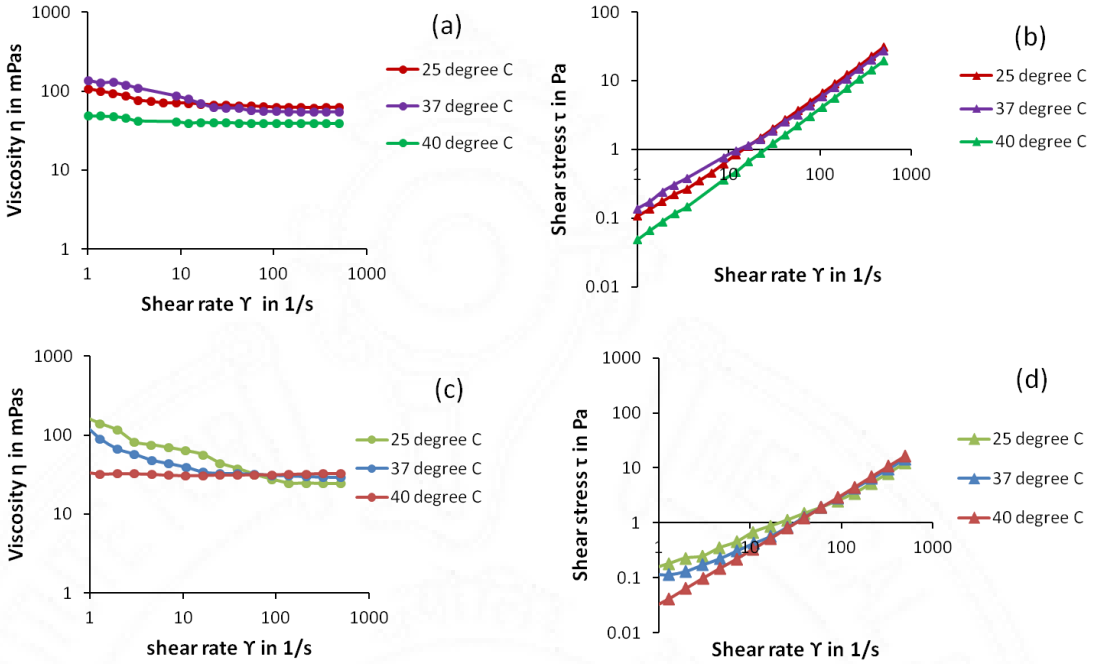

Figure 71. Rheological behaviour of: (a) and (b) EV27-g-IBHP-120h-35.5%, (c) and (d) Onyx® 18 (control material)

4.3.2.5. Precipitation behavour in an artificial nidus and fluoroscopic analysis

A good liquid emboli material must precipitate immediately on contact with biological fluid. To check the precipitation *in vitro*, an artificial nidus model was constructed. Figure 73 (a) shows the image of the in-house developed artificial nidus. On passing LEM through this, it showed a smooth flow in the inter-pillar space and undergone precipitation. An off-white colored precipitate was obtained (Figure 73 (b)). The individual compartment of nidus was not visible under fluoroscopy before the filling of the material (Figure 73 (c)), but after filling with LEM each compartment of the nidus was visible (Figure 73 (d)). Figure 73 (e) shows the filling of Onyx® 18 in the nidus. From the image it was clear that the opacity was not uniform in Onyx®-18 due to the presence of heterogeneously dispersed tantalum particles. In some compartments opacity

was high and in other compartments it was not as high depending on the distribution of tantalum particles. But in the case of EV27-g-IBHP-120h-35.5%, the opacity was uniform due to the covalently bound iodine moiety. A similar observation was noticed by Mason et al. (2018) in PHIL™. He compared the radiopacity of Onyx® 18, Squid™ 12, Squid™ 18 using PHIL™ as control material and found that covalently bonded iodine based embolics, PHIL™ revealed constant radiopacity over time.

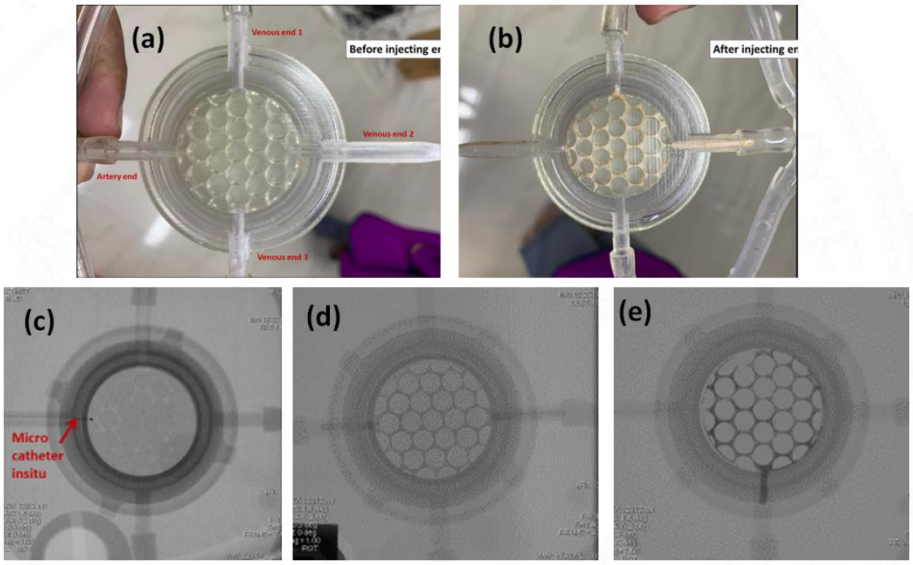

Figure 72. Nature of precipitation of LES in an artificial nidus model: (a) Nidus before filling with LES, (b) Nidus after filling with LES. Fluoroscopic image of nidus after filling with: (c) saline, (d) EV27-g-IBHP-120h-35.5%, and (e) Onyx® 18 (control)

4.4 Biological Safety Evaluation of LEA

4.4.1. In vitro hemocompatibility

Hemocompatibility is an important property that has to be measured for blood contacting devices. The average % hemolysis value obtained for the plasma sample after exposure to radiopaque polymeric material was as low as 0.02±0.01% (n=3). According

to ISO 10993-4, the percentage hemolysis less than 1 can be considered as hemocompatible and can be safely used in the blood stream.

4.4.2. *In vitro* bacterial reverse mutation assay (Ames test)

The Ames test is based on the principle that the small amount of histidine in the growth medium allows the bacteria to grow for an initial time and have the opportunity to mutate. When all the histidine were used only bacteria that have mutated to gain the ability to produce its own histidine will survive. The number of colonies is proportional to the mutagenicity of the substance.

Here the viable count of revertants in each strain is tabulated in tables 21-30. On analyzing the tables we can see that the number of revertants in positive and negative control plates was in agreement with the historical data of lab. Therefore we can conclude that the test material did not exhibit any mutagenic activity against S. typhimurium TA98, TA100, TA1535, TA1537 and TA102 strains tested both with and without metabolic activation. Back ground lawn was present in all the plates.

Table 21. Viable count of TA98 without S9 activation.

Sample group	Dose and volume per plate	Number of replicate plates	Mean revertants per plate
Solvent control	50 µL	3	17±5
Positive control (2-nitrofluorene)	10 µg	3	664±14
Test sample	50 µL	3	23±5

Table 22. Viable count of TA98 with S9 activation.

Sample group	Dose and volume per plate	Number of replicate plates	Mean revertants per plate
Solvent control	50 µL	3	24±6
Positive control (2-aminoanthracene)	5 µg	3	695±15
Test sample	50 µL	3	31±3

Table 23. Viable count of TA100 without S9 activation.

Sample group	Dose and volume per plate	Number of replicate plates	Mean revertants per plate
Solvent control	50 µL	3	112±8
Positive control (Sodium azide)	1 µg	3	531±11
Test sample	50 µL	3	118±9

Table 24. Viable count of TA100 with S9 activation.

Sample group	Dose and volume per plate	Number of replicate plates	Mean revertants per plate
Solvent control	50 µL	3	114±6
Positive control (Sodium azide)	1 µg	3	543±21
Test sample	50 µL	3	114±7

Table 25. Viable count of TA1535 without S9 activation.

Sample group	Dose and volume per plate	Number of replicate plates	Mean revertants per plate
Solvent control	50 µL	3	17±4
Positive control (Sodium azide)	1 µg	3	224±16
Test sample	50 µL	3	20±7

Table 26. Viable count of TA1535 with S9 activation

Sample group	Dose and volume per plate	Number of replicate plates	Mean revertants per plate
Solvent control	50 µL	3	9±2
Positive control (Sodium azide)	1 µg	3	210±21
Test sample	50 µL	3	17±2

Table 27. Viable count of TA1537 without S9 activation

Sample group	Dose and volume per plate	Number of replicate plates	Mean revertants per plate
Solvent control	50 µL	3	7±2
Positive control (Sodium azide)	1 µg	3	204±8
Test sample	50 µL	3	9±3

Table 28. Viable count of TA1537 with S9 activation

Sample group	Dose and volume per plate	Number of replicate plates	Mean revertants per plate
Solvent control	50 µL	3	12±3
Positive control (Sodium azide)	1 µg	3	234±13
Test sample	50 µL	3	11±2

Table 29. Viable count of TA102 without S9 activation

Sample group	Dose and volume per plate	Number of replicate plates	Mean revertants per plate
Solvent control	50 µL	3	134±11
Positive control (Sodium azide)	1 µg	3	505±8
Test sample	50 µL	3	141±9

Table 30. Viable count of TA102 with S9 activation

Sample group	Dose and volume per plate	Number of replicate plates	Mean revertants per plate
Solvent control	50 µL	3	142±5
Positive control (Sodium azide)	1 µg	3	485±26
Test sample	50 µL	3	134±6

4.4.3. Acute systemic toxicity

According to ISO 10993-11, acute systemic toxicity is the adverse effects occurring at any time within 72 h after single, multiple or continuous exposures of a test sample for 24 h. For this test, material extract was dosed intravenously and/or intraperitoneally to the animals and then observed at 24±2, 48±2 and 72±2 h for various signs of toxicity.

The materials used for evaluation were cotton seed oil (non-polar) and physiological saline (polar) extract of grafted polymer. Since these media are non-toxic in nature, any toxicity identified during the procedure would be due to the test material. The two methods selected for administration were intraperitoneal and intravenous. In intraperitoneal, the injection was given in the lower left or right quadrant of the abdomen where vital organs were absent. Intravenous injection was given in the right/left lateral tail vein of mice. Here the fluid was directly injected into the venous system to obtain fastest absorption rate.

4.4.3.1. Acute intraperitoneal application of cotton seed oil extract of grafted polymer in albino mice

Acute systemic toxicity was evaluated on the basis of toxic signs, symptoms, body weight reduction or death of the animal. The observed clinical signs were tabulated in Table 31.

Table 31. Clinical observations made in mice after intraperitoneal injection of cotton seed oil extract.

Clinical observations		Test (n=5)	Control (n=5)
Body weight (g)	Initial	22.9	22.85
Respiratory	Imm/4 h	N	N
	24 h	N	N
	48 h	N	N
	72 h	N	N
Motor	Imm./4 h	N	N
	24 h	N	N

	48 h	N	N
	72 h	N	N
Convulsion	Imm./4 h	N	N
	24 h	N	N
	48 h	N	N
	72 h	N	N
Reflexes	Imm./4 h	N	N
	24 h	N	N
	48 h	N	N
	72 h	N	N
Ocular signs	Imm./4 h	N	N
	24 h	N	N
	48 h	N	N
	72 h	N	N
Cardiovascular signs	Imm./4 h	N	N
	24 h	N	N
	48 h	N	N
	72 h	N	N
Salivation	Imm./4 h	N	N
	24 h	N	N
	48 h	N	N
	72 h	N	N
Piloerection	Imm./4 h	N	N
	24 h	N	N
	48 h	N	N

	72 h	N	N
Analsesia	Imm./4 h	N	N
	24 h	N	N
	48 h	N	N
	72 h	N	N
Muscle tone	Imm./4 h	N	N
	24 h	N	N
	48 h	N	N
	72 h	N	N
Gastro intestinal	Imm./4 h	N	N
	24 h	N	N
	48 h	N	N
	72 h	N	N
Skin	Imm./4 h	N	N
	24 h	N	N
	48 h	N	N
	72 h	N	N
Body weight	Final	26.45	27.17
Death		Nil	Nil

From the table it was evident that the cotton seed oil extract of the grafted polymer and control injected animal didn't show any abnormalities or significant loss in body weight during the observation period. So the material was nontoxic.

4.4.3.2. Acute intravenous application of physiological saline extract of grafted polymer in albino mice

The acute systemic toxicity was evaluated in the same manner as that of cotton seed oil extract. Table 32 comprises the clinical observations during the study period.

Table 32. Clinical observations after intravenous injection of physiological saline extract

Clinical observations		Test (n=5)	Control (n=5)
Body weight (g)	Initial	20.55	20.75
Respiratory	Imm./4 h	N	N
	24 h	N	N
	48 h	N	N
	72 h	N	N
Motor	Imm./4 h	N	N
	24 h	N	N
	48 h	N	N
	72 h	N	N
Convulsion	Imm./4 h	N	N
	24 h	N	N
	48 h	N	N
	72 h	N	N
Reflexes	Imm./4 h	N	N
	24 h	N	N
	48 h	N	N
	72 h	N	N
Ocular signs	Imm./4 h	N	N

	24 h	N	N
	48 h	N	N
	72 h	N	N
Cardiovascular signs	Imm./4 h	N	N
	24 h	N	N
	48 h	N	N
	72 h	N	N
Salivation	Imm./4 h	N	N
	24 h	N	N
	48 h	N	N
	72 h	N	N
Piloerection	Imm./4 h	N	N
	24 h	N	N
	48 h	N	N
	72 h	N	N
Analsesia	Imm./4 h	N	N
	24 h	N	N
	48 h	N	N
	72 h	N	N
Muscle tone	Imm./4 h	N	N
	24 h	N	N
	48 h	N	N
	72 h	N	N
Gastro intestinal	Imm./4 h	N	N
	24 h	N	N

	48 h	N	N
	72 h	N	N
Skin	Imm./4 h	N	N
	24 h	N	N
	48 h	N	N
	72 h	N	N
Body weight	Final	25.42	24.34
Death		Nil	Nil

From the table it was clear that the test material and control material injected animals did not show any abnormalities or body weight loss during the observation period. So physiological saline extract of grafted polymer was also non-toxic in nature.

4.4.4. *In vivo* toxicokinetic study

The systemic exposure of the polymer sample was analyzed by collecting the blood sample of rabbit in different periods. The UV-spectrophotometric measurement showed that the spiked blood had an extra peak at 280 nm (Figure 74 (a)) in addition to the pure blood peak (206 nm). So the acetonitrile can extract the polymer component, if any, from the blood. The blood samples collected at different periods had the same peak as obtained for pure blood collected before the injection of the material (Figure 74 (b)).

In the HPLC analysis, spiked plasma shows two peaks each of which at retention times 1.291 and 1.567 minutes (Figure 75). The peak at 1.567 is broad which is easy to detectable. That peak was absent in all the plasma collected at different periods.

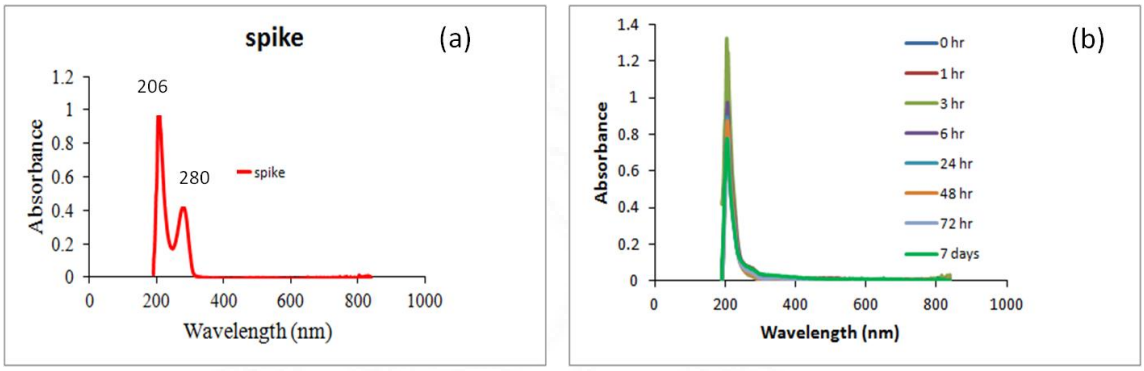

Figure 73. UV-visible spectra of: (a) sample spiked plasma, (b) plasma collected at different periods

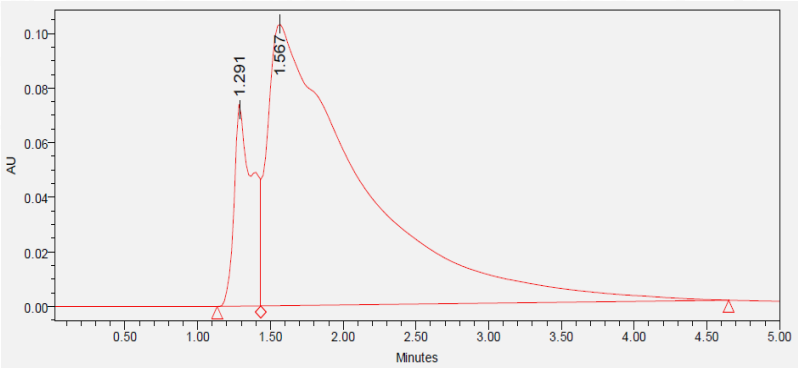

Figure 74. HPLC chromatogram of sample spiked plasma

The HPLC chromatogram of blank plasma shows a peak at 1.288 min. and a shoulder peak at 1.375 min. The plasma samples collected at different periods also shows the same peak of pure plasma and no extra peaks were observed as in spiked plasma (Figure 76). This indicated that no extractables were coming out from the injected materials into the blood.

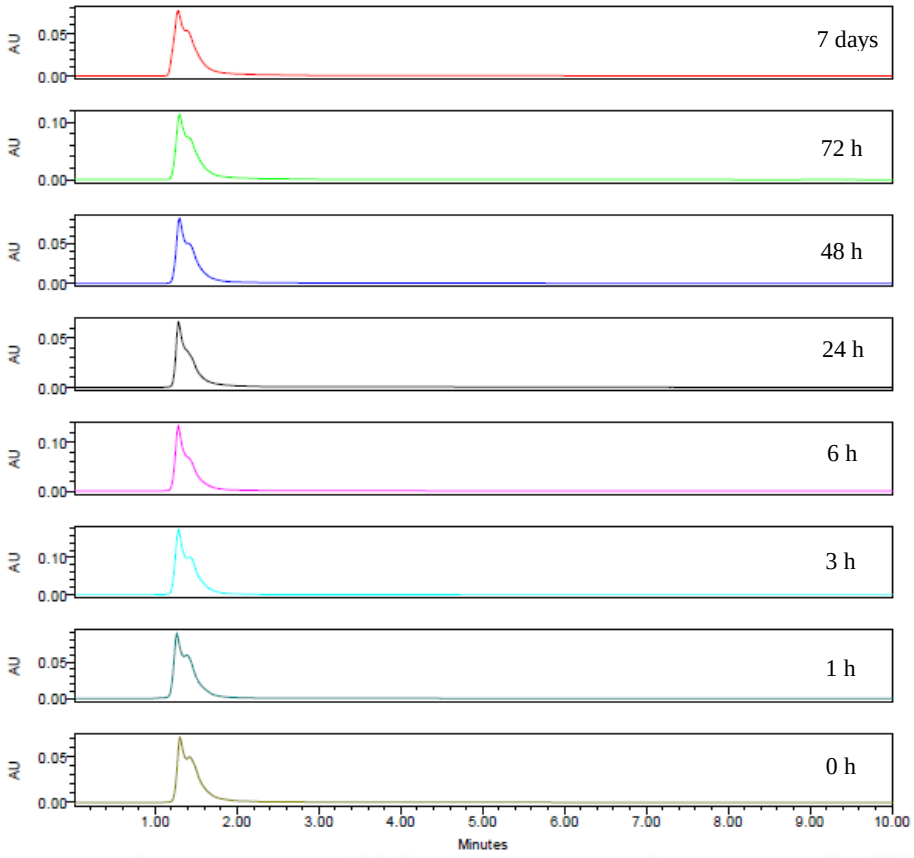

Figure 75. HPLC chromatogram of plasma collected at different periods.

4.4.5. Muscular implantation of LEA in rabbit model

After the muscular implantation, the general physical condition of the animals were observed and was found normal in the entire study period (from beginning to 12 weeks). The body weight increase and feed intake of the animals were also normal and none of the animals showed any abnormality or behavioral changes. At the end of each observation period animals were sacrificed and the implantation sites were clearly visible with black cast for control material and light yellow cast for test material (Figure 76 (a) and (b)). The implants with surrounding tissues were collected for histopathological studies and were depicted in Figure 76 (c) and (d). There was no

evidence of hemorrhage, encapsulation, discoloration, necrosis or infection at the implant site during any of the observation periods. The tissue was collected with test and control materials and subjected X-ray analysis. The implanted materials were clearly visible under X-ray (Figure 77). X-ray images revealed that the materials were present not as a single lump but were spread around each injection site.

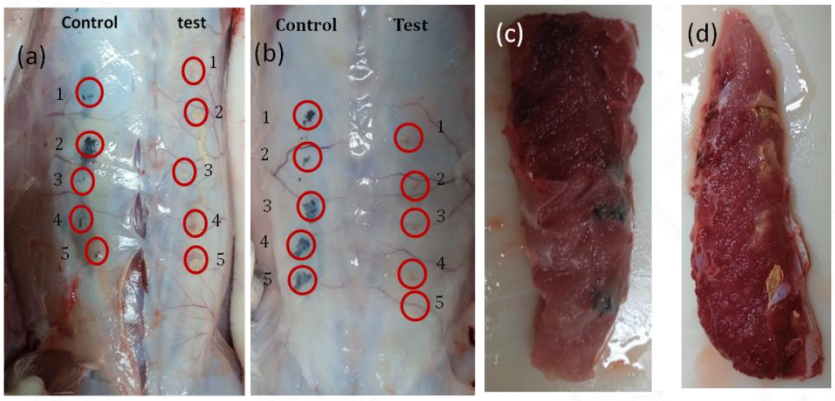

Figure 76. Injection sites and muscle tissues of rabbit after explantation:Implantation sites after: (a) 1 week, and (b) 12 weeks. Explanted muscles with: (c) control material, and (d) test material.

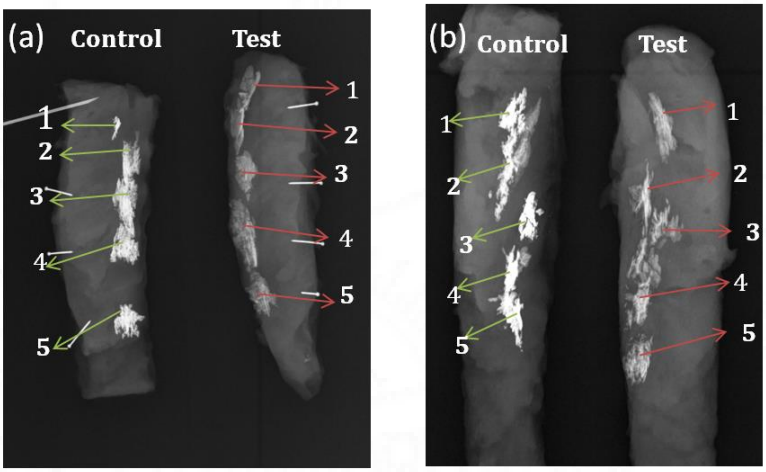

Figure 77. X-ray images of explanted rabbit muscles after: (a) 1 week, and (b) 12 weeks.

Macroscopically there was no hemorrhage, encapsulation, discoloration, necrosis or infection at the implant site during any of the observation periods.

Gross observation of test material implanted muscular region, in both periods, revealed that the implant material was widely spread in the deep muscle region. The implant appeared as a white opaque material and it was not possible to measure implant dimensions. The muscle region adjacent to the implant appeared pale and it was not possible to remove the implant from the precipitated site. So, sections of implant site perpendicular to the implant were taken for histopathological evaluation.

In control group also the implant material was found to be spread widely in the deep muscle region. Implant material appeared black in color and it was not possible to measure implant dimensions. As previously seen, muscle region adjacent to the implant appeared as pale. Control material could not be removed from the muscular region and sections perpendicular to the implant were taken for histopathological evaluation.

4.4.5.1. Histological analysis of LEA implanted rabbit muscular tissue

Histological analysis of test and control LEA implanted tissues showed severe acute inflammation in one week (Figure 78) which is a normal phenomenon in wound healing process. Implant and tissue interfaces showed degeneration of muscle fibers and necrotic changes. There was fibrosis with blood capillaries and this indicated the initiation of healing process. Severe infiltration of neutrophils, lymphocyte, macrophages and plasma cells were observed at the implanted site. Moderate infiltration of multinucleated giant cells was also observed which were formed by the fusion of monocytes/macrophages.

The implantation sites were filled with some exudates which is usual from the areas of infection or inflammation.

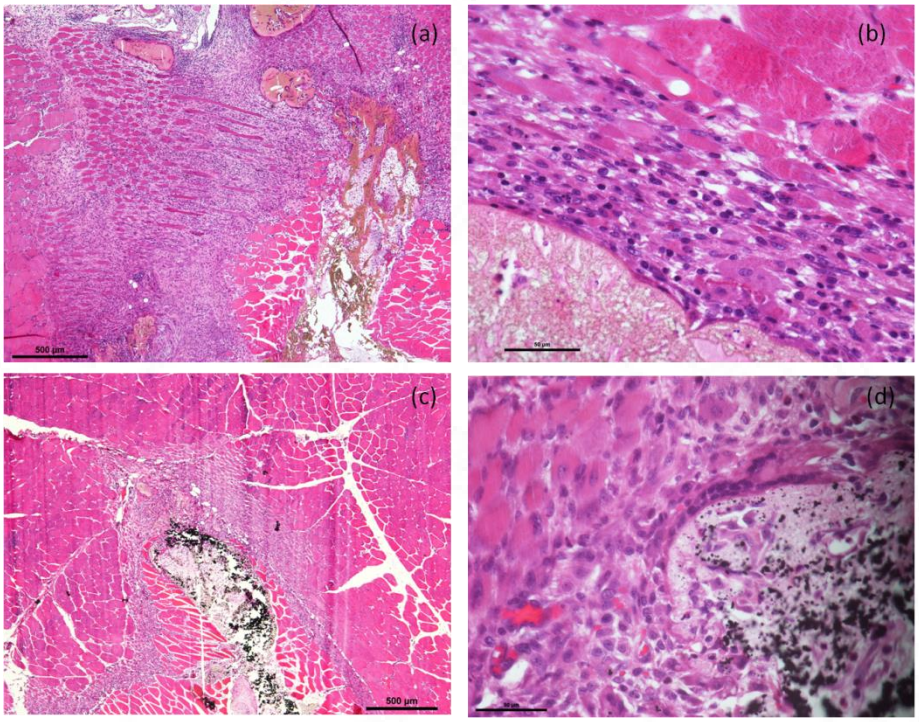

Figure 78. H&E stained histological images of muscular tissues along with implant after 1 week implantation. (a) & (b) are test materials, and (c) & (d) are control materials. For (a) & (c) magnification is 500X, and for (b) & (d) magnification is 50X.

At 12 weeks, both in test and control, degeneration and necrosis were absent which indicates the proper healing of the implantation site (Figure 79). The healing process was also confirmed by the presence of a moderately thick fibrous capsule. The fibrous capsules were identified with a few blood capillaries. The infiltration of neutrophils was reduced in the twelfth week since they are the first inflammatory cells recruited at the site of a wound (Wilgus et al., 2013) and a moderate infiltration of lymphocyte, macrophages and plasma cells was noted but it was lesser than that observed in the first week. There was no change noted in the infiltration of multinucleated giant cells

compared to first week. They are important mediators of tissue remodeling and repair and are also responsible for the removal of non-phagocytosable foreign materials (Quinn et al., 2009). Tissue ingrowths into the cavities of implant material were observed in the test and control groups. The mean average scores obtained for 1 week and 12 weeks are 3.3 and 2.6, respectively. According to ISO-10993 (6), a material attaining 0.0-2.9 score is considered having minimal/or no reaction and 3.0-8.9 score is considered having slight reaction. So, here the material was considered as a slight irritant (3.3) at one week and non-irritant (2.6) at 12 weeks.

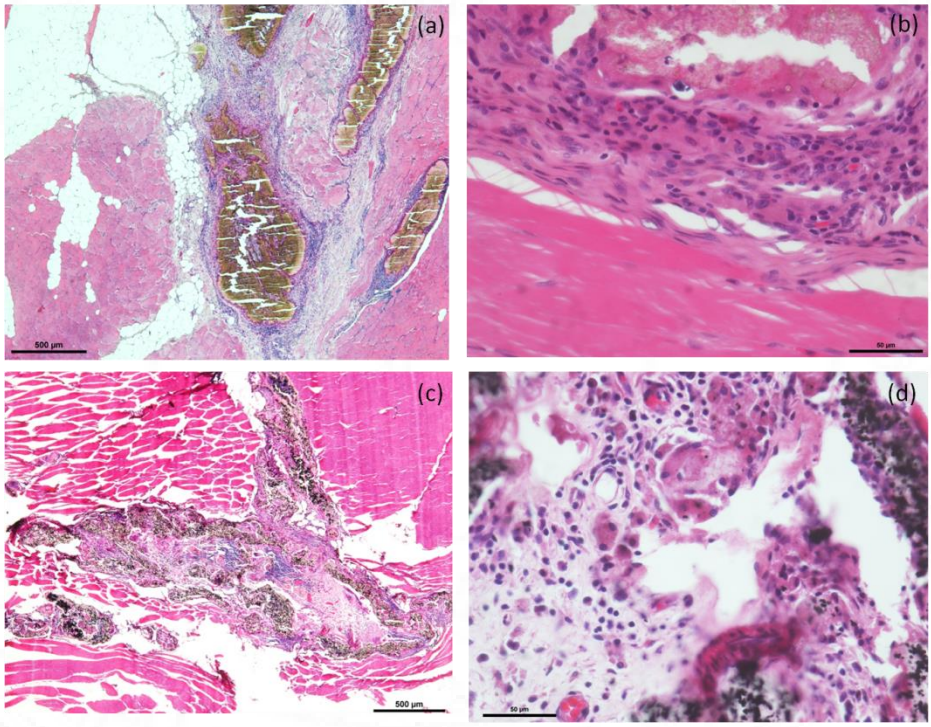

Figure 79. H&E stained histological images of muscular tissues along with implant after 12 weeks implantation. (a) & (b) test materials, and (c) & (d) control materials. For (a) & (c) magnification is 500X, and for (b) & (d) magnification is 50X.

4.4.5.2. Genomic study of FFPE rabbit muscular tissue

The muscular tissues collected after 1 week and 12 weeks of explantation were selected for the comparison of gene expression levels. The relative expressions of various cytokines observed in test and control materials in the two periods were plotted in Figure 80.

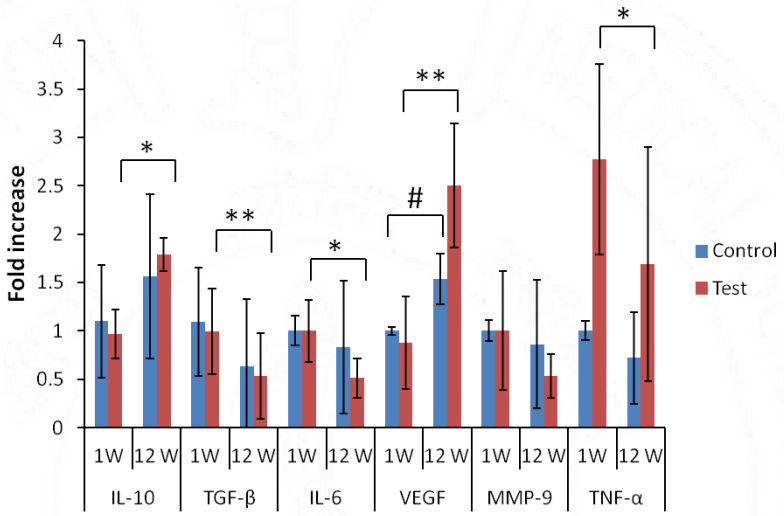

Figure 80. Relative expressions of various cytokines in rabbit muscular tissue.

After every injury, an immune inflammatory response would be initiated immediately and cytokines appear and function as a regulator of immunity (Hsing & Wang 2015). In the early stages of wound healing the pro-inflammatory cytokines such as IL-6, TNF-α, etc. (Kishimoto, 1989; Lin et al., 2003); pleiotropic cytokines such as TGF-β and matrix metalloproteinase (MMP) were predominant but in the remodeling phase their expressions get reduced (Johnson et al., 2020; Lan et al., 2021) and the angiogenic cytokines such as VEGF, PECAM, etc. and the anti-inflammatory cytokines such as IL-10 were increased (Li et al., 2005; Daniela et al., 2009; Xu et al., 2020).

Here the expression of IL-6, TNF-α, MMP-9 and TGF-β were high in the first week and got reduced in the twelfth week. The reduction in pro inflammatory cytokines in twelfth week was more in test material compared to the control material.

The expressions of angiogenic cytokine, VEGF, and anti-inflammatory cytokine IL-10 were increased in the twelfth week both in control and in the test but VEGF were more expressed in test material compared to control material. IL-10 was increased in similar amount both in test and control materials. Highly expressed VEGF and IL-10 and less expressed IL6, TNF-α, TGF-β and MMP-9 suggested that better healing was initiated by the test material compared to control material.

4.5 In vitro degradation

The % weight remaining after each period of the degradation study was more than 97 % and no significant weight loss was observed during this period. Figure 81 (a) shows the degradation profile of EV27-g-IBHP-120h-35.5% pellet. Figures 81 (b) and (c) represent the nature of the pellet in the beginning and after 1 year of degradation study. The pellet retained its shape and size during the complete study. Even on removal from the PBS medium the pellet was hard and cohesive and no breakdown was observed.

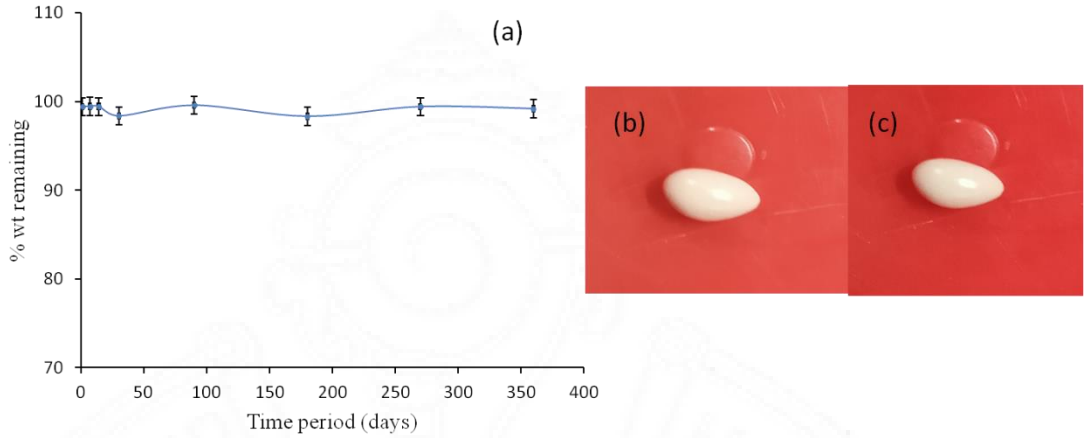

Figure 81. Results of the in vitro degradation study. Sample weight remaining at different time periods. (a) Weight retention profile of EV27-g-IBHP-120h-35.5% pellet, (b) appearance of the pellet at the beginning of the experiment, and (c) that after one year

4.6 Storage Stability of LEA

The stability of the LEA composition, EV27-g-IBHP-120h-35.5%, on storage was studied by storing LEA at room temperature and at 37 °C and following its viscosity, precipitation behavior, and IR spectral features. The studies were conducted for one year. After each time period, the viscosity of the samples was analyzed with a micro viscometer and recorded. The results obtained are shown in Figure 82.

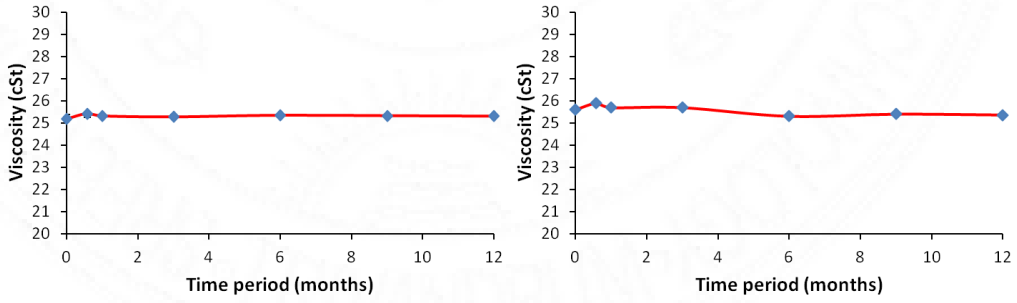

Figure 82. Viscosity profile of EV27-g-IBHP-120h-35.5% stored at (a) RT and (b) 37˚C

From Figure 83, it was clear that both the samples kept at room temperature and 37 °C retained the same viscosity during the study period. So the samples were stable with respect to viscosity for the evaluated time period of 1 year.

In each period of the aging, the precipitation behavior of the LEA was also checked and it was confirmed that the LEA formed a cohesive, lump mass of precipitate irrespective of evaluated time periods (Figure 83). The samples kept at both temperatures showed similar behavior and there was no tendency to dissociate into powder particles.

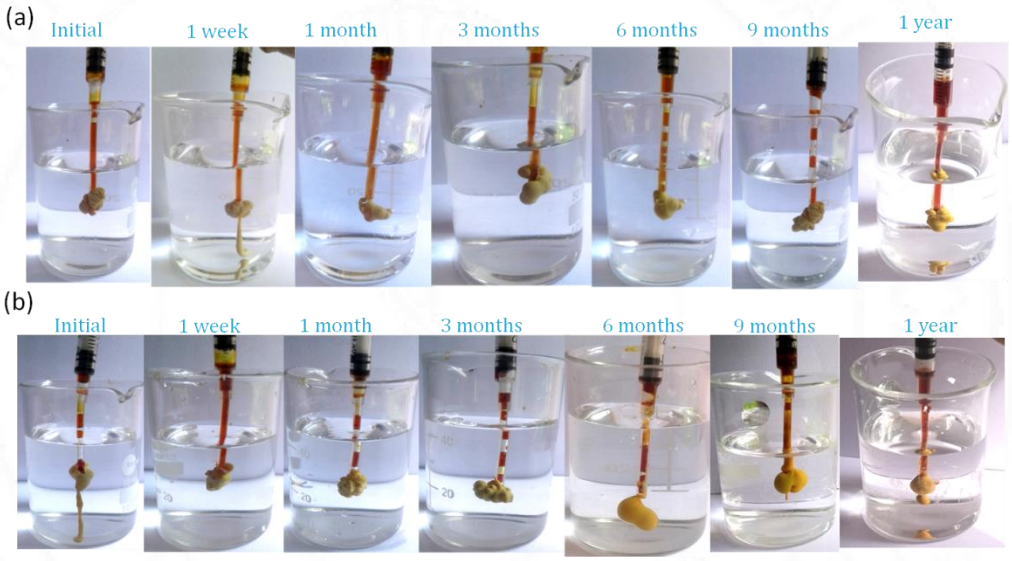

Figure 83. Nature of precipitation of EV27-g-IBHP-120h-35.5% stored at (a) RT, and (b) 37˚C

For spectroscopic analysis, after each storage period the LEAs were precipitated in distilled water under vigorous stirring. The powder form of the radiopaque polymer obtained was then washed, dried, and used for FTIR spectroscopic analysis. There were no apparent changes in the FTIR spectra during the whole storage period (Figure 84) indicating that the material was stable during this period.

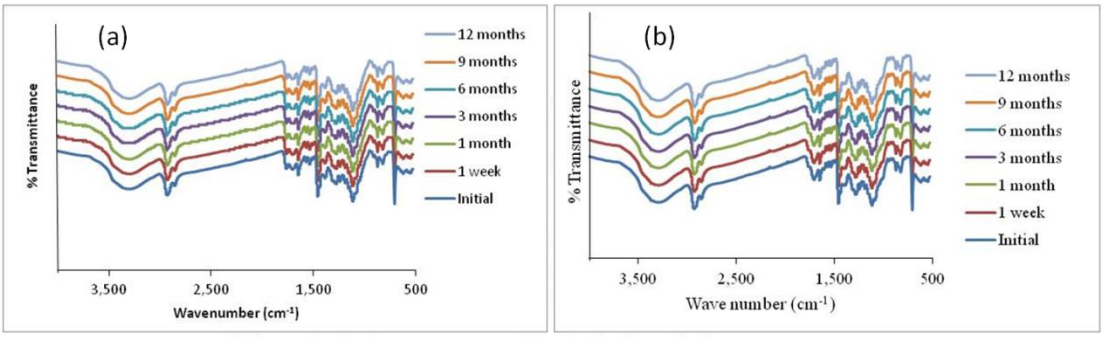

Figure 84. FTIR spectra of LEA samples stored at: (a) room temperature, and (b) 37˚C.

4.7 Preclinical Functional Evaluation of LEA

4.7.1. Clinical observation and angiography

According to literature swine would be a suitable animal model for arteriovenous malformation studies (Eliyas et al., 2016). The rete mirabile (RM) of swine could be embolized for effective evaluation of the material. The network of arteries consists of ascending pharyngeal arteries which supply the RM and the internal carotid arteries. So to stop the supply of blood into rete mirabile the feeding arteries must be initially embolized. Non-adhesive liquid embolic agents are preferred because of the minimal risk of gluing and multiple injections through a single catheter (Murayama et al., 1998; Tokunaga et al., 1999). The LEA formulated in this work was also non-adhesive and does not experience any catheter entrapment and gluing like those manifested by commercial products. In the case of Onyx®, catheter withdrawal was difficult and the catheter got blocked during the procedure but the test material doesn't manifest such difficulties. In addition, the non-adhesive nature of the material also provided for slow and controlled injection. Compared with the control there were no significant changes noted in the injection force. Test material took less time for complete occlusion than for the control material. The density of tantalum powder caused some difficulty in the

injection of control material (Van Rooij et al., 2007). However, the test material demonstrated good ante-grade percolation without any proximal reflux and no significant resistance was observed during injection.

Since DMSO compatible Marathon microcatheter (ev3) was used, the microcatheter could withstand damage or dissolution. To overcome the toxic effects of higher volumes of DMSO it was normally diffused into the circulating blood and distributed in the total body water. The metabolized products, dimethyl sulphur dioxide ($DMSO_2$) and dimethyl sulphide (DMS) were excreted through urine and exhalation, respectively. The toxicity of EV and DMSO were found to be dose-dependent (Ozdol et al., 2015).

No premixing/shaking was needed for this material, unlike Onyx®. The uniform and inherent opacity obtained with the covalently bound iodine moiety coupled with no loss in homogeneity during prolonged injections allowed safe monitoring of the embolic material. The rete mirabile was successfully embolized in all eleven animals and the animals remained healthy throughout the period, except for two animals in which one died after the first day of embolization with frothy fluid in the nostrils and tracheal lumen. The gross observation showed emphysema of lung, cerebral edema and congestion and the death was caused by asphyxia and neurogenic shock. In another animal neurological deficit was observed after 5 days of embolization. It was sacrificed and the gross observation showed occlusion of lumen of right internal carotid artery and associated infarct in the cerebral region. No other animals showed any problem related to embolization and greater than 95% angiographic reduction of rete mirabile size was

observed for test sample in all animals. In control, only around 80% embolization was observed. In both case there were no uncontrolled bleeding, medication reaction, hypotension/ hypertension, cardiac arrhythmia and stroke observed during the procedure. After the embolization procedure there was no fever, transient or persistent irritability, limb ischemia, local site hematoma and ischemia observed in any animal. The overall observations obtained after embolization in all animals were tabulated in Table 33.

Table 33. Clinical observations after embolization

	Test									Control	
Animal No.	20695	20702	20727	20682	20732	20733	20701	20729	20734	20680	20725
Sex	M	M	M	F	M	M	M	M	F	M	M
Body weight (Impl.), Kg	65	64	62	71	44	79	55	47	50	50	49
Body weight (Expl.), Kg	68	68	Dead on next day	78	53	85	61	Terminated on 5th day due to neurologic deficit	56	58	56
Access area	Rt.	Rt.	Rt.	Rt.	Rt.	Rt.	Lt.	Rt.	Lt.	Lt.	Rt.
Angiographic reduction in RM size of 50 % or greater	√	√ Through right left side also embolized (100% of entire RM)	√	√	√ 50 %	√ 100 %	√	√ >90 %	√ 100 %	√ 60 -70 %	25 %
Serious adverse events											
Intra-procedure											
Death	×	×	√	×	×	×	×	× Prematu	×	×	×

								re terminat ion			
Worsening of neurologic status	×	×	NA	×	×	×	×	√	×	×	×
Infection	×	×	NA	×	×	×	×	×	×	×	×
Deteriorati on in health-resulting in permanent impairemen nt of body function	×	×	NA	×	×	×	×	√	×	×	×
Distal embolizati on of material into ICA	×	×	√ Lt CCA	×	×	×	×	√	×	A small embol i at necro psy	×
Rupture of APA	×	×	×	×	×	×	×	×	×	×	×
Recanaliza tion	×	×	×	×	×	×	×	×	×	×	×
Other adverse events											
Poor visibility of material under road map and under subtractio n	Poo r	×	×	×	Adequa te	×	Less visible undue road map good visibility under subtract ion	Adequa te	Adequ ate	Good	×
Poor or inadequate percolatio n of material	×	×	×	×	Inadequ ate	×	×	Good percolat ion	×	×	Yes only 25% niches filled
Early proximal reflux of the material	×	×	×	×	√	Late reflux into proxi mal 2/3rd of APA	×	×	×	×	Yes
Delivery catheter removal	×	×	×	×	×	×	×	×	×	Mild difficu lty	×

difficulty											
Premature precipitation time	×	×	×	×	×	×	×	×	×	×	Yes, catheter blocked at 13 min. after injection
Post-procedure											
Prolonged fever	×	×	NA	×	×	×	×	NA	×	×	×
irritability	×	×	NA	×	×	×	×	√	×	×	×
Limb ischemia	×	×	NA	×	×	×	×	×	×	×	×
Local site hematoma	×	×	NA	×	×	×	×	×	×	×	×
Seizures	×	×	NA	×	×	×	×	×	×	×	×

×: Absent; NA: Not applicable; √: Present

Figure 85 A and B shows the pre-embolization and post-embolization angio of rete mirabile of swine, respectively. On comparing the two it was understood that LEA can embolize the right rete mirabile and right ascending pharyngeal artery by retaining the right internal carotid artery (red arrowhead) and the left rete mirabile, left ascending pharyngeal artery and left internal carotid artery. The embolized EV27-g-IBHP-120h-35.5% can be seen as a radiopaque cast (white arrow) on the nonsubtracted image (Figure 85 C). Three months follow-up angiogram (Figure 85 D) showed that the embolized cast had no change and the recanalization of blood vessels didn't take place. A similar observation was noted by Murayama et al. (1998) after experimental embolization of 26 swine rete with Onyx®. But in the experiments done by Gruber et al. (1996) and Arakawa et al. (2007) with n-BCA and Eudragit-E 100, respectively, recanalization was observed.

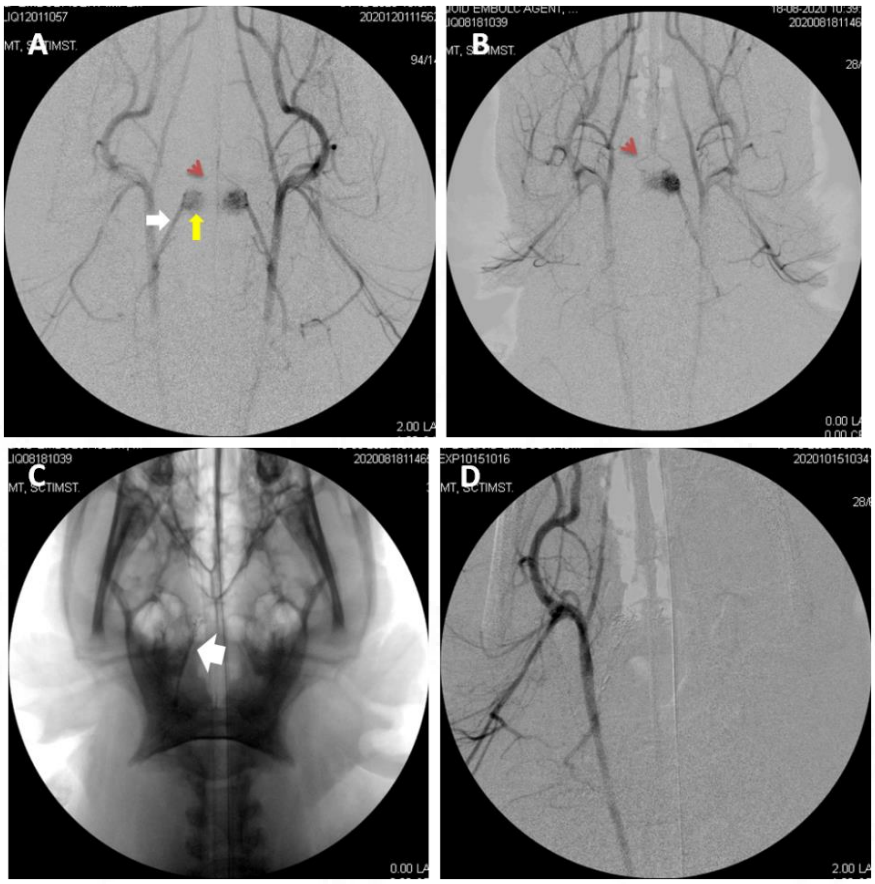

Figure 85. Angiogram of swine rete: A) before embolization, B) Immediately after embolization with EV27-g-IBHP-120h-35.5%, C) Embolized EV27-g-IBHP-120h-35.5% as radiopaque cast on non-subtracted image (white arrow), and D) 3 months after angiogram shows complete obliteration of right RM.

PHIL^{TM} is another commercially available liquid embolic agent available only in Europe which also uses iodinated contrast to provide radiopacity (Varadharajan et al., 2017). Like PHIL^{TM}, EV27-g-IBHP-120h-35.5% is also free from tantalum powder so the need of prior agitation is not needed in these cases. Onyx® can penetrate into the vessel up to 5 µm in comparison to n-BCA which has 20 µm penetrations (Natarajan et al., 2009). EV27-g-IBHP-120h-35.5% can also achieve deeper penetration like Onyx®.

4.7.2. Micro CT analysis

Figure 86A is the micro CT reconstruction image of EV27-g-IBHP-120h-35.5% embolized rete and illustrates the high visibility and potential for assessment of the spatial distribution of LEA cast within the rete mirabile. The same was observed for Onyx® also (Figure 86B). Figures 86C and 86D represent the 3D reconstructed images of EV27-g-IBHP-120h-35.5% and Onyx® LEA embolized rete, respectively.

4.7.3. Histological assessment

The gross analysis of EV27-g-IBHP-120h-35.5% and Onyx® embolized RM showed light yellow colored and black opaque polymer casts respectively in the middle and distal regions of right RM, right common carotid artery and right ascending pharyngeal artery. Embolic casts were absent on the left side (Figure 87).

Gross observations revealed that the cerebrum and cerebellum did not show any abnormality. Cerebral arteries did not reveal any visible polymer cast in the lumen. Other organs such as the heart, liver, kidney, and spleen did not show any abnormality.

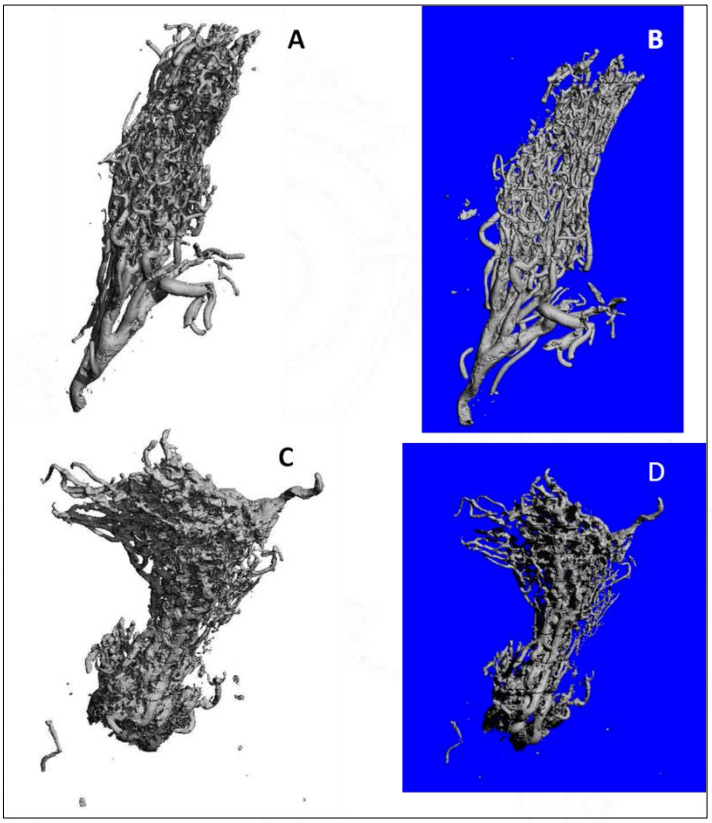

Figure 86. MicroCT scan images of embolized rete: 3D reconstructed images of (A) & (B) EV27-g-IBHP-120h-35.5% embolized rete (C) & (D) Onyx® embolized rete

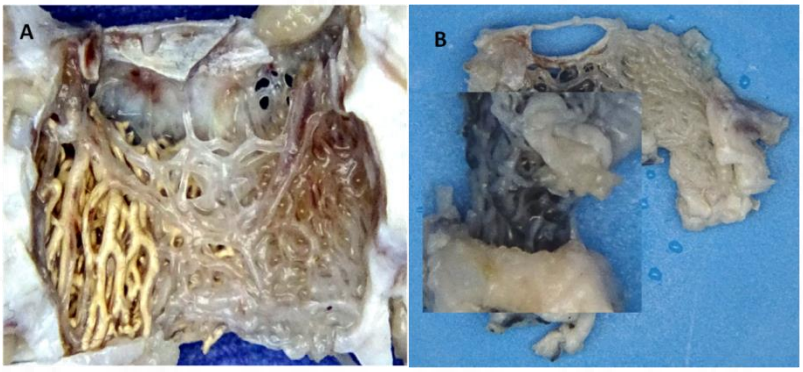

Figure 87. Gross images of rete embolized with A) EV27-g-IBHP-120h-35.5% B) Onyx® (right rete got embolized in both cases and left rete intact)

The histological image of a normal rete shows thick tunica adventitia (Figure 88 (a)) which differs from the rete vessels from normal vessels. The histological assessment of test material embolized rete mirabile showed many grey polymers cast-filled dilated blood vessels and tissue infiltration in the lumen (Figure 88 (b)). Tunica intima was not appreciated here. There was infiltration of fibrocytes, foreign body type giant cells, macrophages, and lymphocytes noted in the lumen. There was angiogenesis noted in the lumen (Figure 88 (c)). Tunica media was atrophied and internal elastic lamina (IEL) was disrupted. The adventitia and periadventitial region revealed fibrosis and mild infiltration of mononuclear cells. There was mild inflammatory cell infiltration of neutrophils, lymphocytes and macrophages in the intervessel area and the periadventitial region. Angiogenesis was also noted (Figure 88 (d)). Blood vessels without polymer cast revealed intima lined by endothelium, intact IEL, thick media consisting of smooth muscle cells and loosely arranged fibrous adventitia. The cerebral parenchyma of ventral frontal lobe region did not reveal any abnormality.

The histological assessment of control materials embolized rete showed many dilated blood vessels with black particles and tissue infiltration in the lumen (Figure 89 (a)). From the image it was clear that the occlusion was not complete in the case of the control material and much tissue ingrowths were observed compared to the test material. But in the case of EV27-g-IBHP-120h-35.5% the occlusion was greater than 98% and the tissue ingrowth rate was very less compared to control material (Figure 89 (b)).

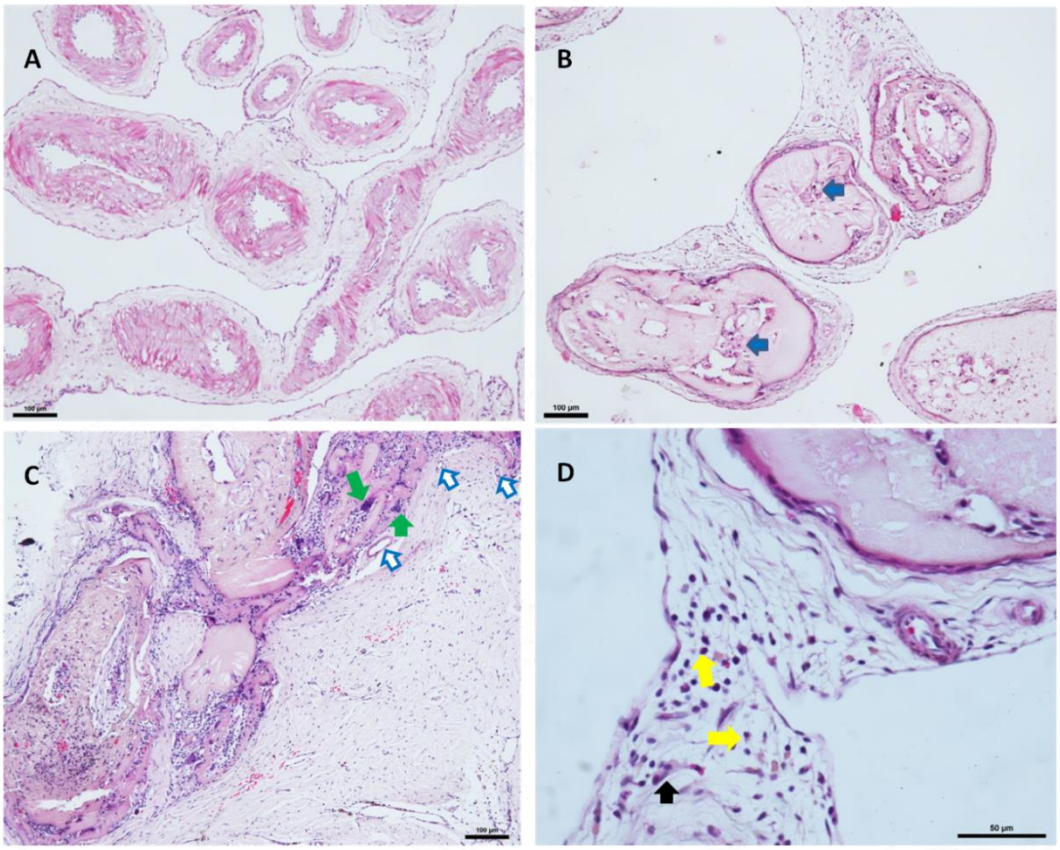

Figure 88. Histo images of (a) normal rete blood vessels (b) IBHP-g-EVOH polymer occluded blood vessels of rete (blue arrow: cellular infiltration) (c) Foreign body type giant cells (green arrow) and angiogenesis (blue outlined arrow) in the lumen (d) Infiltration of mononuclear cells (yellow arrow) and neutrophils (black arrow) in the periadventitial region

In the microscopic image of Onyx® we can see artifacts (Figure 89 (a) yellow line) due to metal particles that affect diagnosis and potentially mimic intracranial hemorrhage (Reiderer et al., 2019). However, the EV27-g-IBHP-120h-35.5% didn't show that type of artifact and the images were very clear due to the absence of metal particles. A similar observation was noticed by Schmitt et al. (2021). They compared the imaging artifacts of non-adhesive liquid embolic agents and made a conclusion that the imaging artifacts were higher for Onyx® and Squid™ compared to the iodine-based PHIL™ (Schmitt et al., 2021).

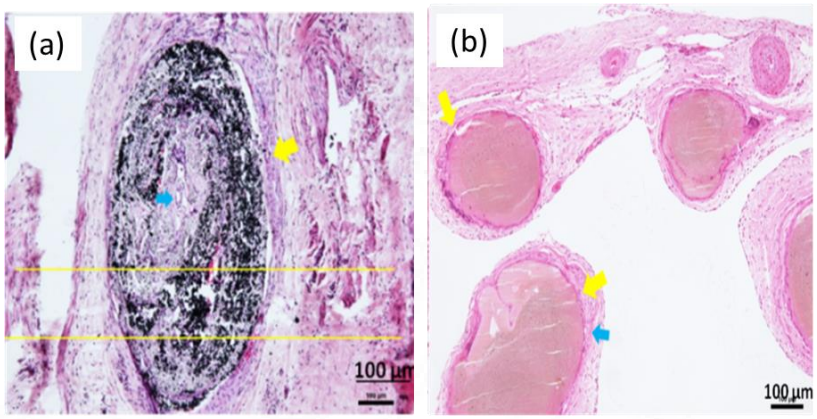

Figure 89. Histo images of (a) Onyx®and (b) EV27-g-IBHP-120h-35.5% embolized rete (blue arrow: angiogenesis; yellow arrow: fibrosis; yellow line: artifact due to metal particles)

Other histological observations of the control material embolized rete were the same as that in the test material. However, the adventitia and periadventitial region revealed severe fibrosis and moderate mononuclear cell infiltration than in the test material. The inter-vessel area also showed moderate inflammatory cell infiltration and severe fibrosis. In the periadventitial area, moderate infiltration with lymphocytes and macrophages and angiogenesis were noted. Blood vessels without polymer depicted characteristic features and the cerebral parenchyma did not show any abnormality. Chaloupka et al. (1994) also noticed a similar kind of observation in the swine endovascular embolization model using ethylene vinyl alcohol copolymer.

5. SUMMARY AND CONCLUSIONS

In this thesis, development and evaluation of a new intrinsically radiopaque ethylene vinyl alcohol copolymer (EV) suitable for embolizing AVM was described. Intrinsically radiopaque EV co-polymers were generated by covalently linking iodine-containing compounds onto EV. Three iodo compounds were synthesized and two of them were covalently linked to EV copolymer. One compound was linked through an ether linkage and another through an ester linkage. Liquid embolic formulations were prepared from these radiopaque polymers and the suitability of these materials as a liquid embolic agent was investigated.

For the purpose of generating radiopaque EV, tetraiodo compounds having different functional groups were synthesized. The parent compound selected for iodination was BHP, which had four sterically free sites for iodination. Initially, BHP was iodinated to make tetra iodocompound having carboxyl functionality, i.e., IBHP. After that the carboxyl functionality of IBHP was reduced to hydroxyl functionality for the preparation of IBHOH. The hydroxyl functionality in IBHOH was again converted to haloalkane functionality (HR) for the attachment of iodocompound to EV through ether linkage.

After the preparation of iodocompounds, IBHR and IBHP were covalently linked to EV through ether and ester linkage, respectively. Studies revealed that by incorporating HR, EV having iodine content of about 45 wt% can be produced (EV27-g-HR-48h). Apart from radiopacity these EV exhibited excellent thermal stability, cytocompatibility and retained crystallinity comparable to the parent polymer. To make EV radiopaque, IBHP

was directly linked to EV through ester linkage (EV27-g-IBHP-120h). The polymer derived showed lesser thermal stability than EV27-g-HR-48h but had excellent cytocompatibility. Its iodine content was as high as 63.7 wt.%. The results obtained indicate that increasing the chain length decreases the grafting efficiency of the tetraiodo compound onto EV.

Liquid embolic formulations were prepared from both radiopaque polymers and they were evaluated for their properties. Results showed that EV27-g-IBHP-120h-35.5% had all the suitable characteristics to serve as a liquid embolic agent for arteriovenous malformation. It showed excellent radiopacity, low viscosity, and characteristic precipitation behavior in an aqueous medium. EV27-g-HR-48h-20% also showed characteristic precipitation behavior but its viscosity was relatively high and was not suitable for embolization of arteriovenous malformation. The radiopacity of EV27-g-HR-48h-20% was also not adequate for brain applications.

The selected liquid embolic formulation was successfully implanted in swine rete mirabile. The implantation of the material was followed by angiography and fluoroscopy. The tissue interactions towards the implanted material were analyzed by histopathology and RT-PCR. The material showed good biocompatibility, excellent visibility under X-ray, easy flow through the catheter and complete occlusion in the blood vessel.

To conclude, a promising liquid embolic formulation suitable for embolization of arteriovenous malformation was developed and evaluated successfully.

REFERENCES

Aamodt, A., Kvistad, K.A., Andersen, E., Lund-Larsen, J., Eine, J., Benum, P. and Husby, O.S., 1999.Determination of the Hounsfield value for CT-based design of custom femoral stems. The Journal of Bone and Joint Surgery.British volume, 81(1), pp.143-147.

Agusti, G., Jordan, O., Andersen, G., Doelker, É. and Chevalier, Y., 2015. Radiopaque iodinated ethers of poly (vinyl iodobenzyl ether) s: Synthesis and evaluation for endovascular embolization. Journal of Applied Polymer Science, 132(14).

Akpinar, S. and Yilmaz, G., 2016.Autologous blood clot embolization in posttraumatic high-flow priapism.Scottish Medical Journal, 61(4), pp.197-199.

Arakawa, H., Murayama, Y., Davis, C.R., Howard, D.L., Baumgardner, W.L., Marks, M.P. and Do, H.M., 2007. Endovascular embolization of the swine rete mirabile with Eudragit-E 100 polymer.American Journal of Neuroradiology, 28(6), pp.1191-1196.

Arano, Y., Wakisaka, K., Mukai, T., Uezono, T., Motonari, H., Akizawa, H., Kairiyama, C., Ohmomo, Y., Tanaka, C., Ishiyama, M. and Sakahara, H., 1996.Stability of a metabolizable ester bond in radioimmunoconjugates.Nuclear medicine and biology, 23(2), pp.129-136.

Ashour, R. and Ali Aziz-Sultan, M., 2014.Onyx® HD-500 for embolization of cerebral aneurysms. Neurological research, 36(4), pp.363-367.

Avery, R.K., Albadawi, H., Akbari, M., Zhang, Y.S., Duggan, M.J., Sahani, D.V., Olsen, B.D., Khademhosseini, A. and Oklu, R., 2016.An injectable shear-thinning biomaterial for endovascular embolization.Science translational medicine, 8(365), pp.365ra156-365ra156.

Ayx, I., Müller-Wille, R., Wohlgemuth, W.A., Pfeifer, M., Lepiorz, M., Hubauer, H., Goessmann, H., Stroszczynski, C. and Zorger, N., 2017. Treatment of acute hemoptysis by bronchial artery embolization with the liquid embolic agent ethylene vinyl alcohol copolymer.Journal of Vascular and Interventional Radiology, 28(6), pp.825-831.

Baba, Y., Higashi, M. and Awai, K., 2018. A new embolic liquid agent comprised of amino acid. Minimally Invasive Therapy & Allied Technologies, 27(1), pp.17-21.

Balegamire, J., Vandamme, M., Chereul, E., Si-Mohamed, S., Maache, S.A., Almouazen, E., Ettouati, L., Fessi, H., Boussel, L., Douek, P. and Chevalier, Y.,

2020. Iodinated polymer nanoparticles as contrast agent for spectral photon counting computed tomography. Biomaterials Science, 8(20), pp.5715-5728.

Barnett, B.P., Hughes, A.H., Lin, S., Arepally, A. and Gailloud, P.H., 2009.In vitro assessment of EmboGel and UltraGel radiopaque hydrogels for the endovascular treatment of aneurysms.Journal of Vascular and Interventional Radiology, 20(4), pp.507-512.

Becker, T.A., Preul, M.C., Bichard, W.D., Kipke, D.R. and McDougall, C.G., 2007. Preliminary investigation of calcium alginate gel as a biocompatible material for endovascular aneurysm embolization in vivo.Neurosurgery, 60(6), pp.1119-1128.

Bird, M.L. and Ingold, C.K., 1938. 176. Influence of directing groups on nuclear reactivity in oriented aromatic substitutions. Part IV. Nitration of the halogenobenzenes.Journal of the Chemical Society (Resumed), pp.918-929.

Björklund, S. and Kocherbitov, V., 2017. Alcohols react with MCM-41 at room temperature and chemically modify mesoporous silica. Scientific reports, 7(1), pp.1-11.

Brennecka, C.R., Preul, M.C., Bichard, W.D. and Vernon, B.L., 2012. In vivo experimental aneurysm embolization in a swine model with a liquid-to-solid gelling polymer system: initial biocompatibility and delivery strategy analysis. World neurosurgery, 78(5), pp.469-480.

Cabasso, I., Smid, J. and Sahni, S.K., 1989. Radiopaque miscible systems composed of poly (methyl methacrylate) and transition and nontransition metal salts: Spectroscopic, thermal, and radiographic characterization. *Journal of applied polymer science*, *38*(9), pp.1653-1666.

Cabasso, I., Smid, J. and Sahni, S.K., 1990. Radiopaque polymers based on acrylated phosphonate esters derived from polyols. Journal of applied polymer science, 41(11-12), pp.3025-3042.

Cankaya, N. and Temüz, M.M., 2014. Monomer reactivity ratios of cellulose grafted with N-cyclohexylacrylamide and methyl methacrylate by atom transfer radical polymerization. Cellulose Chemistry and Technology, 48(3-4), pp.209-215.

Cappello, J., Crissman, J.W., Crissman, M., Ferrari, F.A., Textor, G., Wallis, O., Whitledge, J.R., Zhou, X., Burman, D., Aukerman, L. and Stedronsky, E.R., 1998.In-situ self-assembling protein polymer gel systems for administration, delivery, and release of drugs.Journal of Controlled Release, 53(1-3), pp.105-117.

Chaloupka, J.C., Vinuela, F., Vinters, H.V. and Robert, J., 1994.Technical feasibility and histopathologic studies of ethylene vinyl copolymer (EVAL) using a swine endovascular embolization model.American Journal of Neuroradiology, 15(6), pp.1107-1115.

Chaloupka, J.C., Huddle, D.C., Alderman, J., Fink, S., Hammond, R. and Vinters, H.V., 1999. A reexamination of the angiotoxicity of superselective injection of DMSO in the swine rete embolization model.American Journal of Neuroradiology, 20(3), pp.401-410.

Chatterjee, G., Cabasso, I. and Smid, J., 1995. Radiopaque epoxy resins. Journal of applied polymer science, 55(6), pp.851-856.

Chauhan, A. and Chauhan, P., 2015. Usage of powder XRD technique for material characterization and analysis of Portland cement. J. Anal. Bioanal.Tech., 6(6), pp.1-3.

Chhour P, Cheheltani R, Naha PC, Litt HI, Ferrari VA, Cormode DP (2017) Nanoparticles for Cardiovascular Imaging with CT. In: Bulte JW, Modo MM (eds). Design and Applications of Nanoparticles in Biomedical Imaging. Springer International Publishing, Switzerland, pp. 357–384.

Cloft, H.J., Joseph, G.J. and Dion, J.E., 1999. Risk of cerebral angiography in patients with subarachnoid hemorrhage, cerebral aneurysm, and arteriovenous malformation: a meta-analysis. Stroke, 30(2), pp.317-320.

Combe, E.C., 1971, Studies on development of radiopaque denture materials. in journal of dental research, 50, p. 668.

Combe, E.C., 1972. Further studies on radio-opaque denture-base materials.Journal of dentistry, 1(2), pp.93-97.

Corkill, R.A., Mitsos, A.P. and Molyneux, A.J., 2007. Embolization of spinal intramedullary arteriovenous malformations using the liquid embolic agent, Onyx®: a single-center experience in a series of 17 patients. Journal of Neurosurgery: Spine, 7(5), pp.478-485.

Cormier, A.R., Pang, X., Zimmerman, M.I., Zhou, H.X. and Paravastu, A.K., 2013.Molecular structure of RADA16-I designer self-assembling peptide nanofibers.ACS nano, 7(9), pp.7562-7572.

Dalyai, R.T., Randazzo, C., Ghobrial, G., Gonzalez, L.F., Tjoumakaris, S.I., Dumont, A.S., Rosenwasser, R.H. and Jabbour, P., 2012. Redefining Onyx® HD 500 in the flow diversion era. International Journal of Vascular Medicine, 2012.

Daniela, G., Bauer, J. and Schoenberger, J., 2009. Blockade of neoangiogenesis, a new and promising technique to control the growth of malignant tumors and their metastases.Current vascular pharmacology, 7(3), pp.347-357.

Davy, K.W. and Causton, B.E., 1982. Radio-opaque denture base: a new acrylic co-polymer. Journal of dentistry, 10(3), pp.254-264.

Dawlee, S. and Jayabalan, M., 2011.Development of segmented polyurethane elastomers with low iodine content exhibiting radiopacity and blood compatibility.Biomedical Materials, 6(5), p.055002.

Dawlee, S., Jayakrishnan, A. and Jayabalan, M., 2009. Studies on novel radiopaque methyl methacrylate: glycidyl methacrylate based polymer for biomedical applications. Journal of Materials Science: Materials in Medicine, 20(1), pp.243-250.

de Roos, A.M., Rekker, R.F. and Nauta, W., 1967. Investigation into the stability of the ether bond in a series of benzhydryl ethers. IV. The influence of the basic chain on the rate of hydrolysis. Pharmaceutisch Weekblad, 102(29), pp.691-696.

Delaviz, Y., Cabasso, I. and Smid, J., 1990. X-ray contrast miscible blends of polyacrylates and bismuth trihalides: glass transition temperatures and radiopacities. Polymer, 31(11), pp.2083-2088.

Delaviz, Y., Zhang, Z.X., Cabasso, I. and Smid, J., 1990. Homogeneous radiopaque polymers with organobismuth compounds.*Journal of applied polymer science*, *40*(5-6), pp.835-843.

Dudeck, O., Jordan, O., Hoffmann, K.T., Okuducu, A.F., Husmann, I., Kreuzer-Nagy, T., Tesmer, K., Podrabsky, P., Bruhn, H., Hilborn, J. and Rüfenacht, D.A., 2006.Embolization of experimental wide-necked aneurysms with iodine-containing polyvinyl alcohol solubilized in a low-angiotoxicity solvent.American journal of neuroradiology, 27(9), pp.1849-1855.

Eliyas, J.K., Niekrasz, M., Wardrip, C. and Lee, S.K., 2016.Focused post mortem dissection technique for harvest of rete mirabile in domestic swine (Sus scrofa).Journal of NeuroInterventional Surgery, 8(9), pp.973-976.

Farrokhi, M., Abdollahi, M. and Alizadeh, A., 2019.An efficient method for straightforward phosphorylation of ethylene/vinyl alcohol copolymers using trialkyl phosphite/iodine.Polymer, 169, pp.215-224.

Flickinger, J.C., Pollock, B.E., Kondziolka, D. and Lunsford, L.D., 1996. A dose-response analysis of arteriovenous malformation obliteration after

radiosurgery.International Journal of Radiation Oncology* Biology* Physics, 36(4), pp.873-879.

Galperin, A., Margel, D., Baniel, J., Dank, G., Biton, H. and Margel, S., 2007. Radiopaque iodinated polymeric nanoparticles for X-ray imaging applications.Biomaterials, 28(30), pp.4461-4468.

Ganguli, S., Lareau, R., Jarrett, T. and Soulen, M.C., 2021. A Water-Based Liquid Embolic: Evaluation of its Safety and Efficacy in a Rabbit Kidney Model. Journal of Vascular and Interventional Radiology, 32(6), pp.813-818.

Ghodke, V.M. and Punekar, N.S., 2022.Environmental role of aromatic carboxylesterases.Environmental Microbiology, 24(6), pp.2657-2668.

Goh, S.H. and Lee, S.Y., 1990. Effect of iodination on the thermal properties of polystyrene.Thermochimica acta, 161(1), pp.119-123.

Gruber, A., Mazal, P.R., Bavinzski, G., Killer, M., Budka, H. and Richling, B., 1996. Repermeation of partially embolized cerebral arteriovenous malformations: a clinical, radiologic, and histologic study. American journal of neuroradiology, 17(7), pp.1323-1331.

Hainfeld JF (2021) Iodine based particles. US 10918742.

Hardas NR (1990) Hydrogen bond studies in simple alcohols. M.Sc. thesis.University of Texas.

He, J., Söderling, E., Lassila, L.V. and Vallittu, P.K., 2012.Incorporation of an antibacterial and radiopaque monomer in to dental resin system.Dental Materials, 28(8), pp.e110-e117.

Helmy, A. and Shaida, N., 2017. Treatment of type II endoleaks with a novel agent: precipitating hydrophobic injectable liquid (PHIL®). Cardiovascular and interventional radiology, 40(7), pp.1094-1098.

Herman JM, Spetzler RF, Bederson JB, Kurbat JM & Zabramaki JM. (1995). Genesis of a dural arteriovenous malformation in a rat model. J Neurosurg 83, 539-545.

Hermanto, Y., Takagi, Y., Yoshida, K., Ishii, A., Kikuchi, T., Funaki, T., Mineharu, Y. and Miyamoto, S., 2016. Histopathological features of brain arteriovenous malformations in Japanese patients. Neurologia medico-chirurgica, 56(6), pp.340-344.

Hill, H., Chick, J.F.B., Hage, A. and Srinivasa, R.N., 2018. N-butyl cyanoacrylate embolotherapy: techniques, complications, and management. Diagnostic and Interventional Radiology, 24(2), p.98.

Hsing, C.H. and Wang, J.J., 2015. Clinical implication of perioperative inflammatory cytokine alteration.Acta Anaesthesiologica Taiwanica, 53(1), pp.23-28.

Horak, D., Metalova, M., Švec, F., Drobnik, J., Kalal, J., Borovička, M., Adamyan, A.A., Voronkova, O.S. and Gumargalieva, K.Z., 1987.Hydrogels in endovascular embolization. III. Radiopaque spherical particles, their preparation and properties. Biomaterials, 8(2), pp.142-145.

Houston, K.R., Brosnan, S.M., Burk, L.M., Lee, Y.Z., Luft, J.C. and Ashby, V.S., 2017. Iodinated polyesters as a versatile platform for radiopaque biomaterials. Journal of Polymer Science Part A: Polymer Chemistry, 55(13), pp.2171-2177.

Huang, L., Shen, M., Li, R., Zhang, X., Sun, Y., Gao, P., Fu, H., Liu, H., He, Y., Du, Y. and Cao, J., 2016. Thermo-sensitive composite hydrogels based on poloxamer 407 and alginate and their therapeutic effect in embolization in rabbit VX2 liver tumors. Oncotarget, 7(45), p.73280.

Huckleberry, A., Merritt, W., Cotter, T., Settanni, C., Preul, M.C., Ducruet, A.F. and Becker, T.A., 2021.Application of a rabbit-elastase aneurysm model for preliminary histology assessment of the PPODA-QT liquid embolic.Surgical Neurology International, 12.

ISO 10993-3:2014, Biological evaluation of Medical devices- part 3: Tests for genotoxicity, carcinogenicity and reproductive toxicity.

ISO 10993-4:2017, Biological evaluation of medical devices- part 4: Selection of tests for interactions with blood.

ISO 10993-5:2009, Biological evaluation of medical devices- part 5: Tests for in vitro cytotoxicity.

ISO 10993-12:2012, Biological evalution of medical devices-part 12: sample preparation and reference materials

Izaaryene, J., Kilani, M.S., Rolland, P.H., Gaubert, J.Y., Jacquier, A., Bartoli, J.M. and Vidal, V., 2016.Preclinical study on an animal model of a new non-adhesive cyanoacrylate (Purefill®) for arterial embolization.Diagnostic and interventional imaging, 97(11), pp.1109-1116.

Jain, M.S., Do, H.M., Wintermark, M. and Massoud, T.F., 2019.Large-scale ensemble simulations of biomathematical brain arteriovenous malformation models using graphics processing unit computation.Computers in biology and medicine, 113, p.103416.

James, N.R., Philip, J. and Jayakrishnan, A., 2006. Polyurethanes with radiopaque properties.Biomaterials, 27(2), pp.160-166.

Jayakrishnan, A., Thanoo, B.C., Rathinam, K. and Mohanty, M., 1990. Preparation and evaluation of radiopaque hydrogel microspheres based on PHEMA/iothalamic acid and PHEMA/iopanoic acid as particulate emboli. Journal of biomedical materials research, 24(8), pp.993-1004.

Jayakrishnan, A. and Thanoo, B.C., 1992. Synthesis and polymerization of some iodine-containing monomers for biomedical applications.Journal of applied polymer science, 44(4), pp.743-748.

Jia, J.B., Green, C.S., Cohen, A.J. and Helmy, M., 2015.CT and radiographic appearance of extracranial Onyx® embolization.Clinical radiology, 70(3), pp.326-332.

Johnson, B.Z., Stevenson, A.W., Prêle, C.M., Fear, M.W. and Wood, F.M., 2020. The role of IL-6 in skin fibrosis and cutaneous wound healing.Biomedicines, 8(5), p.101.

Kannath, S.K. and Rajan, J.E., 2017. Percutaneous embolization of scalp arteriovenous malformation using new liquid embolic agent, SQUIDTM: a technical report. Journal of Clinical Interventional Radiology ISVIR, 1(03), pp.171-174.

Karakida, S., Sasaki, T., Kai, K., Harada, K., Yoshimura, S., Kono, M. and Narahara, H., 2013. Vaginal cesarean section for second-trimester therapeutic abortion.Taiwanese Journal of Obstetrics and Gynecology, 52(4), pp.564-567.

Kiran, S., James, N.R., Joseph, R. and Jayakrishnan, A., 2009.Synthesis and characterization of iodinated polyurethane with inherent radiopacity.Biomaterials, 30(29), pp.5552-5559.

Kiran, S., James, N.R., Jayakrishnan, A. and Joseph, R., 2012.Polyurethane thermoplastic elastomers with inherent radiopacity for biomedical applications.Journal of Biomedical Materials Research Part A, 100(12), pp.3472-3479.

Kirby, J.M., Kachura, J.R., Rajan, D.K., Sniderman, K.W., Simons, M.E., Windrim, R.C. and Kingdom, J.C., 2009. Arterial embolization for primary postpartum hemorrhage.Journal of Vascular and Interventional Radiology, 20(8), pp.1036-1045.

Kishimoto, T., 1989.The biology of interleukin-6.Blood, 74(1), pp.1-10.

Koubský, T., Fojtíková, J. and Kalvoda, L., 2017. Radical degradation stability of ether linkage in N, N, N′, N′-tetraoctyldiglycolamide and related organic extractants: A density functional study. Progress in Nuclear Energy, 94, pp.208-215.

Kramers, H.A., 1923. XCIII. On the theory of X-ray absorption and of the continuous X-ray spectrum. The London, Edinburgh, and Dublin Philosophical Magazine and Journal of Science, 46(275), pp.836-871.

Krueger, P.J. and Jan, J., 1970. Infrared spectra and the molecular conformations of some aliphatic amines.Canadian Journal of Chemistry, 48(20), pp.3229-3235.

Kumar, S. Spectroscopy of Organic Compounds. 2021. http://www.uobabylon.edu.iq/eprints/publication_11_8282_250.pdf.

Kurata, A., Suzuki, S., Ozawa, H., Yuzawa, I., Yamda, M., Fujii, K., Kan, S., Kitahara, T., Ohmomo, T. and Miyasaka, Y., 2005. Application of the liquid coil as an embolic material for arteriovenous malformations.Interventional Neuroradiology, 11(3), pp.287-295.

La Grutta, L., Galia, M., Gentile, G., Lo Re, G., Grassedonio, E., Coppolino, F., Maffei, E., Maresi, E., Lo Casto, A., Cademartiri, F. and Midiri, M., 2013. Comparison of iodinated contrast media for the assessment of atherosclerotic plaque attenuation values by CT coronary angiography: observations in an ex vivo model. The British Journal of Radiology, 86(1021), pp.20120238-20120238.

Lagaron, J.M., Catalá, R. and Gavara, R., 2004. Structural characteristics defining high barrier properties in polymeric materials.Materials science and technology, 20(1), pp.1-7.

Lamin, S., Chew, H.S., Chavda, S., Thomas, A., Piano, M., Quilici, L., Pero, G., Holtmannspolter, M., Cronqvist, M.E., Casasco, A. and Guimaraens, L., 2017. Embolization of intracranial dural arteriovenous fistulas using PHIL® liquid embolic agent in 26 patients: a multicenter study. American Journal of Neuroradiology, 38(1), pp.127-131.

Lan, B., Zhang, L., Yang, L., Wu, J., Li, N., Pan, C., Wang, X., Zeng, L., Yan, L., Yang, C. and Ren, M., 2021. Sustained delivery of MMP-9 siRNA via

thermosensitive hydrogel accelerates diabetic wound healing. Journal of nanobiotechnology, 19(1), pp.1-17.

Leati, G., Di Bartolomeo, F., Maffi, G., Boccalon, L., Diaco, D., Segalini, E. and Spinazzola, A., 2023. Translumbar type II endoleak embolization with a new liquid iodinated polyvinyl alcohol polymer: Case series and review of current literature. Frontiers in Radiology, 3, p.1145164.

Lee, D.H., Wriedt, C.H., Kaufmann, J.C., Pelz, D.M., Fox, A.J. and Vinuela, F., 1989.Evaluation of three embolic agents in pig rete.American journal of neuroradiology, 10(4), pp.773-776.

Lex, T.R., Brummel, B.R., Attia, M.F., Giambalvo, L.N., Lee, K.G., Van Horn, B.A., Whitehead, D.C. and Alexis, F., 2020. Iodinated polyesters with enhanced X-ray contrast properties for biomedical imaging. Scientific reports, 10(1), pp.1-9.

Li, W., Liang, S., Zhang, W., Zhao, X., Zhang, H. and Lv, X., 2020. Liquid embolic agent Fe3O4-EVOH for endovascular arteriovenous malformation embolisation: Preliminary evaluation in an in vivo swine rete mirabile model. The neuroradiology journal, 33(4), pp.306-310.

Li, Z.J., Wang, Z.Z., Zheng, Y.Z., Xu, B., Yang, R.C., Scadden, D.T. and Han, Z.C., 2005. Kinetic expression of platelet endothelial cell adhesion molecule-1 (PECAM-1/CD31) during embryonic stem cell differentiation.Journal of cellular biochemistry, 95(3), pp.559-570.

Lin, Z.Q., Kondo, T., Ishida, Y., Takayasu, T. and Mukaida, N., 2003.Essential involvement of IL-6 in the skin wound-healing process as evidenced by delayed wound healing in IL-6-deficient mice.Journal of leukocyte biology, 73(6), pp.713-721.

Lopera, J.E., 2010, March. Embolization in trauma: principles and techniques. In Seminars in interventional radiology (Vol. 27, No. 01, pp. 014-028).© Thieme Medical Publishers.

Lord, J., Britton, H., Spain, S.G. and Lewis, A.L., 2020. Advancements in the development on new liquid embolic agents for use in therapeutic embolisation.Journal of Materials Chemistry B, 8(36), pp.8207-8218.

Lusic, H. and Grinstaff, M.W., 2013. X-ray-computed tomography contrast agents. Chemical reviews, 113(3), pp.1641-1666.

Mason, J.R., Dodge, C. and Benndorf, G., 2018. Quantification of tantalum sedimentation rates in liquid embolic agents. Interventional Neuroradiology, 24(5), pp.574-579.

Massoud TF, Ji C, Vinuela F, Guglielmi G, Robert J, Duckwiler GR & Gobin YP. (1994). An experimental arteriovenous malformation model in swine: anatomic basis and construction technique. AJNR Am J Neuroradiol 15, 1537-1545.

Massoud TF, Ji C, Guglielmi G & Vinuela F. (1996). Endovascular treatment of arteriovenous malformations with selective intranidal occlusion by detachable platinum electrodes: technical feasibility in a swine model. AJNR Am J Neuroradiol 17, 1459-1466.

Massoud TF, Vinters HV, Chao KH, Vinuela F & Jahan R. (2000). Histopathologic characteristics of a chronic arteriovenous malformation in a swine model: preliminary study. AJNR Am J Neuroradiol 21, 1268- 1276.

Mathis, J.M., Evans, A.J., DeNardo, A.J., Kennett, K., Crandall, J.R., Jensen, M.E. and Dion, J.E., 1997. Hydrophilic coatings diminish adhesion of glue to catheter: an in vitro simulation of NBCA embolization. American journal of neuroradiology, 18(6), pp.1087-1091.

Mattamal, G.J., 2008. US FDA perspective on the regulations of medical-grade polymers: cyanoacrylate polymer medical device tissue adhesives. Expert Review of Medical Devices, 5(1), pp.41-49.

Moftakhar, P., Hauptman, J.S., Malkasian, D. and Martin, N.A., 2009. Cerebral arteriovenous malformations. Part 1: cellular and molecular biology. Neurosurgical focus, 26(5), p.E10.

Moszner, N., Salz, U., Klester, A.M. and Rheinberger, V., 1995.Synthesis and polymerization of hydrophobic iodine-containing methacrylates.Die Angewandte Makromolekulare Chemie, 224(1), pp.115-123.

Moszner, N. and Salz, U., 2001. New developments of polymeric dental composites.Progress in polymer science, 26(4), pp.535-576.

Mottu, F., Rüfenacht, D.A., Laurent, A. and Doelker, E., 2002. Iodine-containing cellulose mixed esters as radiopaque polymers for direct embolization of cerebral aneurysms and arteriovenous malformations. Biomaterials, 23(1), pp.121-131.

Moulay, S., 2013.Molecular iodine/polymer complexes.Journal of Polymer Engineering, 33(5), pp.389-443.

Murayama, Y., Viñuela, F., Ulhoa, A., Akiba, Y., Duckwiler, G.R., Gobin, Y.P., Vinters, H.V. and Greff, R.J., 1998. Nonadhesive liquid embolic agent for cerebral arteriovenous malformations: preliminary histopathological studies in swine rete mirabile. Neurosurgery, 43(5), pp.1164-1172.

Natarajan, S.K., Born, D., Ghodke, B., Britz, G.W. and Sekhar, L.N., 2009. Histopathological changes in brain arteriovenous malformations after embolization using Onyx® or N-butyl cyanoacrylate. Journal of neurosurgery, 111(1), pp.105-113.

Ning, X., Zhao, C., Pang, J., Ding, Z., Wang, Y., Xu, K., Chen, H., Li, B. and Luo, Q.I., 2015.Experimental study of temperature-sensitive chitosan/β-glycerophosphate embolic material in embolizing the basicranial rete mirabile in swines.Experimental and therapeutic medicine, 10(1), pp.316-322.

OECD Guidelines for the testing of chemicals-section 4: Test No.471, Bacterial reverse mutation test.

Ozdol, C., Turk, C.C., Hazer, D.B., Yildirim, A.E., Arat, A., Atilla, P., Muftuoglu, S. and Oruckaptan, H., 2015. Comparison of the Toxicities of Ethylene Vinyl Alcohol Copolymer Preparations, Dimethyl Sulphoxide and N-butyl 2-Cyanoacrylate on Cerebral Parenchyma in an Experimental rabbit Model.

Pakyari, M., Farrokhi, A., Maharlooei, M.K. and Ghahary, A., 2013. Critical role of transforming growth factor beta in different phases of wound healing. Advances in wound care, 2(5), pp.215-224.

Papagiannaki, C., Clarençon, F., Ponsonnard, S., Couquet, C., Maizeroi-Eugène, F., Bresson, D., Yardin, C. and Mounayer, C., 2017.Development of an angiogenesis animal model featuring brain arteriovenous malformation histological characteristics.Journal of neurointerventional surgery, 9(2), pp.204-210.

Pierot, L., Cognard, C., Herbreteau, D., Fransen, H., Van Rooij, W.J., Boccardi, E., Beltramello, A., Sourour, N., Kupcs, K., Biondi, A. and Bonafé, A., 2013. Endovascular treatment of brain arteriovenous malformations using a liquid embolic agent: results of a prospective, multicentre study (BRAVO). European radiology, 23(10), pp.2838-2845.

Pop, R., Mertz, L., Ilyes, A., Mihoc, D., Richter, J.S., Manisor, M., Kremer, S. and Beaujeux, R., 2019. Beam hardening artifacts of liquid embolic agents: comparison between Squid and Onyx. Journal of NeuroInterventional Surgery, 11(7), pp.706-709.

Pouchert, C. J. The Aldrich Library of NMR Spectra, 2nd ed.; Aldrich Chemical Co.: Milwaukee, 1983; Vol. 1.

Poursaid, A., Price, R., Tiede, A., Olson, E., Huo, E., McGill, L., Ghandehari, H. and Cappello, J., 2015. In situ gelling silk-elastinlike protein polymer for transarterial chemoembolization.Biomaterials, 57, pp.142-152.

Qian Z, Climent S, Maynar M, Uson-Garallo J, Lima-Rodriguez MAV, Calles C, Robertson H & Castaneda-Zuniga WR. (1999). A simplified arteriovenous malformation model in sheep: feasibility study. AJNR Am J Neuroradiol 20, 765-770.

Qu, W., Xia, W., Feng, C., Tuo, X. and Qiu, T., 2011.Synthesis and characterization of radiopaque poly (ether urethane) with iodine-Containing diol as chain extender. Journal of Polymer Science Part A: Polymer Chemistry, 49(10), pp.2191-2198.

Quinn, M.T. and Schepetkin, I.A., 2009. Role of NADPH oxidase in formation and function of multinucleated giant cells.Journal of innate immunity, 1(6), pp.509-526.

Rangel-Castilla, L., Russin, J.J., Martinez-del-Campo, E., Soriano-Baron, H., Spetzler, R.F. and Nakaji, P., 2014. Molecular and cellular biology of cerebral arteriovenous malformations: a review of current concepts and future trends in treatment. Neurosurgical focus, 37(3), p.E1.

Riederer, I., Bar-Ness, D., Kimm, M.A., Si-Mohamed, S., Noël, P.B., Rummeny, E.J., Douek, P. and Pfeiffer, D., 2019.Liquid embolic agents in spectral X-ray photon-counting computed tomography using tantalum K-edge imaging.Scientific Reports, 9(1), p.5268.

Roberts PA, Williams JR (2020) Farr's Physics for Medical Imaging (2020) Elseiver, New York.

Sadato, A., Wakhloo, A.K. and Hopkins, L.N., 2000. Effects of a mixture of a low concentration of n-butylcyanoacrylate and ethiodol on tissue reactions and the permanence of arterial occlusion after embolization.Neurosurgery, 47(5), pp.1197-1205.

Siekmann, R., 2005. Basics and principles in the application of Onyx® LD liquid embolic system in the endovascular treatment of cerebral arteriovenous malformations.Interventional Neuroradiology, 11(1_suppl), pp.131-140.

Schmitt, N., Floca, R.O., Paech, D., El Shafie, R.A., Neuberger, U., Bendszus, M., Möhlenbruch, M.A. and Vollherbst, D.F., 2021.Imaging artifacts of nonadhesive liquid embolic agents in conventional and cone-beam CT in a novel in vitro AVM model.Clinical Neuroradiology, pp.1-8.

Schumacher M & Schellhammer F. (1999).Experimental pseudo arteriovenous malformation.A model for training and research. Interv Neuroradiol 5, 213-217.

Schweitzer, J.S., Chang, B.S., Madsen, P., Vinuela, F., Martin, N.A., Marroquin, C.E. and Vinters, H.V., 1993.The pathology of arteriovenous malformations of the brain treated by embolotherapy.Neuroradiology, 35(6), pp.468-474.

Shah, T.M., 2000.Radiopaque Polymer Formulations for Medical Devices.Medical Device and Diagnostic Industry, 22(3), pp.102-111.

Sharma, K.V., Dreher, M.R., Tang, Y., Pritchard, W., Chiesa, O.A., Karanian, J., Peregoy, J., Orandi, B., Woods, D., Donahue, D. and Esparza, J., 2010. Development of "imageable" beads for transcatheter embolotherapy.Journal of Vascular and Interventional Radiology, 21(6), pp.865-876.

Shiralizadeh, S., Nasr-Isfahani, H., Keivanloo, A. and Bakherad, M., 2016.Mono-and triiodophenyl isocyanate as radiopacifying agents for methacrylate-based copolymers; biocompatibility and non-toxicity. RSC advances, 6(111), pp.110400-110408.

Sirakov, S., Sirakov, A., Minkin, K., Hristov, H., Ninov, K., Penkov, M., Karakostov, V., Orlov, K., Gorbatykh, A., Kislitsin, D. and Raychev, R., 2019.Initial experience with precipitating hydrophobic injectable liquid in cerebral arteriovenous malformations.Interventional Neuroradiology, 25(1), pp.58-65.

Smid, J., Cabasso, I., Rawls, H.R., Obligin, A., Delaviz, Y., Sahni, S.K. and Zhang, Z.X., 1987.Novel homogeneous polymer–heavy metal salt complexes for X-ray imaging. Die Makromolekulare Chemie, Rapid Communications, 8(11), pp.543-547.

Spetzler, R.F. and Martin, N.A., 1986. A proposed grading system for arteriovenous malformations.Journal of neurosurgery, 65(4), pp.476-483.

Srivastava, G.K., Alonso-Alonso, M.L., Fernandez-Bueno, I., Garcia-Gutierrez, M.T., Rull, F., Medina, J., Coco, R.M. and Pastor, J.C., 2018.Comparison between direct contact and extract exposure methods for PFO cytotoxicity evaluation.Scientific Reports, 8(1), pp.1-9.

Stedman T. Stedman's medical dictionary. 27. Philadelphia: Lippincott Williams & Wilkins; 2000.

Stewart, R.J., Wang, C.S., Song, I.T. and Jones, J.P., 2017. The role of coacervation and phase transitions in the sandcastle worm adhesive system. Advances in colloid and interface science, 239, pp.88-96.

Takayasu, K., Shima, Y., Muramatsu, Y., Moriyama, N., Yamada, T., Makuuchi, M., Hasegawa, H. and Hirohashi, S., 1987. Hepatocellular carcinoma: treatment with

intraarterial iodized oil with and without chemotherapeutic agents. Radiology, 163(2), pp.345-351.

Taki, W., Yonekawa, Y., Iwata, H., Uno, A., Yamashita, K. and Amemiya, H., 1990.A new liquid material for embolization of arteriovenous malformations.American Journal of Neuroradiology, 11(1), pp.163-168.

Tamura, G., Kato, N., Yamazaki, T., Akutsu, Y., Hosoo, H., Kasuya, H. and Sonobe, M., 2015.Endovascular Embolization of Brain Arteriovenous Malformations with Eudragit-E.Neurologia medico-chirurgica, pp.oa-2014.

Teli, M. and Jadhav, A., 2017.Effect of mercerization on the properties of pandanus odorifer lignocellulosic fibre.IOSR Journal of Polymer and Textile Engineering, 4(1), pp.7-15.

Terada, T., Nakamura, Y., Nakai, K., Tsuura, M., Nishiguchi, T., Hayashi, S., Kido, T., Taki, W., Iwata, H. and Komai, N., 1991. Embolization of arteriovenous malformations with peripheral aneurysms using ethylene vinyl alcohol copolymer: report of three cases. Journal of neurosurgery, 75(4), pp.655-660.

Thanoo, B.C. and Jayakrishnan, A., 1990. Barium sulphate-loaded p (HEMA) microspheres as artificial emboli: preparation and properties. Biomaterials, 11(7), pp.477-481.

Thanoo, B.C., Sunny, M.C. and Jayakrishnan, A., 1991. Preparation and properties of barium sulphate and methyl iothalamate loaded poly (vinyl alcohol) microspheres as radiopaque particulate emboli. Journal of Applied Biomaterials, 2(2), pp.67-72.

Thanoo, B.C., Sunny, M.C. and Jayakrisnnan, A., 1991. Tantalum-loaded polyurethane microspheres for particulate embolization: preparation and properties. Biomaterials, 12(5), pp.525-528.

Tokunaga, K., Kinugasa, K., Kawacla, S., Nakashima, H., Tamiya, T., Hirotsune, N., Mandai, S. and Ohmoto, T., 1999. Embolization of cerebral arteriovenous malformations with cellulose acetate polymer: a clinical, radiological, and histological study. Neurosurgery, 44(5), pp.981-989.

Tu, J., Karunanayaka, A., Windsor, A. and Stoodley, M.A., 2010. Comparison of an animal model of arteriovenous malformation with human arteriovenous malformation.Journal of Clinical Neuroscience, 17(1), pp.96-102.

Ungar, T.J.S.M., 2004. Microstructural parameters from X-ray diffraction peak broadening.Scripta Materialia, 51(8), pp.777-781.

Vaidya, S., Tozer, K.R. and Chen, J., 2008, September.An overview of embolic agents.In Seminars in interventional radiology (Vol. 25, No. 03, pp. 204-215). © by Thieme Medical Publishers.

Van Rooij, W.J., Sluzewski, M. and Beute, G., 2007.Brain AVM embolization with Onyx®.American Journal of Neuroradiology, 28(1), pp.172-177.

Varadharajan, S., Ramalingaiah, A.H., Saini, J., Gupta, A.K., Devi, B.I. and Acharya, U.V., 2017.Precipitating hydrophobic injectable liquid embolization of intracranial vascular shunts: initial experience and technical note.Journal of Neurosurgery, 129(5), pp.1217-1222.

Vasanthan, N., Kotek, R., Jung, D.W., Shin, D., Tonelli, A.E. and Salem, D.R., 2004. Lewis acid–base complexation of polyamide 66 to control hydrogen bonding, extensibility and crystallinity.Polymer, 45(12), pp.4077-4085.

Vollherbst, D.F., Sommer, C.M., Ulfert, C., Pfaff, J., Bendszus, M. and Möhlenbruch, M.A., 2017. Liquid embolic agents for endovascular embolization: evaluation of an established (Onyx®) and a novel (PHIL®) embolic agent in an in vitro AVM model. American Journal of Neuroradiology, 38(7), pp.1377-1382.

Vollherbst, D.F., Otto, R., Von Deimling, A., Pfaff, J., Ulfert, C., Kauczor, H.U., Bendszus, M., Sommer, C.M. and Möhlenbruch, M.A., 2018. Evaluation of a novel liquid embolic agent (precipitating hydrophobic injectable liquid (PHIL®)) in an animal endovascular embolization model. Journal of neurointerventional surgery, 10(3), pp.268-274.

Vollherbst, D.F., Otto, R., Hantz, M., Ulfert, C., Kauczor, H.U., Bendszus, M., Sommer, C.M. and Möhlenbruch, M.A., 2018.Investigation of a new version of the liquid embolic agent PHIL® with extra-low-viscosity in an endovascular embolization model.American Journal of Neuroradiology, 39(9), pp.1696-1702.

Vollherbst, D.F., Chapot, R., Bendszus, M. and Möhlenbruch, M.A., 2021.Glue, Onyx®, SquidTm or PHIL® Liquid embolic agents for the embolization of cerebral arteriovenous malformations and dural arteriovenous fistulas.Clinical Neuroradiology, pp.1-14.

Wakhloo, A.K., Lieber, B.B., Siekmann, R., Eber, D.J. and Gounis, M.J., 2005. Acute and chronic swine rete arteriovenous malformation models: hemodynamics and vascular remodeling. American Journal of Neuroradiology, 26(7), pp.1702-1706.

Wang, X., Geng, X., Ye, L., Zhang, A.Y. and Feng, Z.G., 2010. Synthesis and characterization of radiopaque iodine-containing methacrylate-based polymers via

reversible addition-fragmentation chain transfer (RAFT) polymerization. Frontiers of Materials Science in China, 4(4), pp.366-375.

Wang, Y., Xu, N., Luo, Q., Li, Y., Sun, L., Wang, H., Xu, K., Wang, B. and Zhen, Y., 2011. In vivo assessment of chitosan/β-glycerophosphate as a new liquid embolic agent.Interventional Neuroradiology, 17(1), pp.87-92.

Wang, W., Li, H., Tam, M.D., Zhou, D., Wang, D.X. and Spain, J., 2012. The amplatzer vascular plug: a review of the device and its clinical applications. Cardiovascular and interventional radiology, 35(4), pp.725-740.

Wang, Y., Shi, Y., Shao, W., Ren, Y., Dong, W., Zhang, F. and Liu, L.Z., 2020.Crystallization, structures, and properties of different polyolefins with similar grafting degree of maleic anhydride.Polymers, 12(3), p.675.

Wilgus, T.A., Roy, S. and McDaniel, J.C., 2013. Neutrophils and wound repair: positive actions and negative reactions. Advances in wound care, 2(7), pp.379-388.

Willinsky, R., Goyal, M., Terbrugge, K., Montanera, W., Wallace, M.C. and Tymianski, M., 2001. Embolisation of small (< 3 cm) brain arteriovenous malformations: correlation of angiographic results to a proposed angioarchitecture grading system. Interventional Neuroradiology, 7(1), pp.19-27.

Worzakowska, M., 2016.Thermal behavior, decomposition mechanism and some physicochemical properties of starch-g-poly (benzyl acrylate) copolymers.Journal of Thermal Analysis and Calorimetry, 126(2), pp.531-540.

Xu, P., Wu, Y., Zhou, L., Yang, Z., Zhang, X., Hu, X., Yang, J., Wang, M., Wang, B., Luo, G. and He, W., 2020. Platelet-rich plasma accelerates skin wound healing by promoting re-epithelialization. Burns & trauma, 8.

Yoon, N.M., Pak, C.S., Brown Herbert, C., Krishnamurthy, S. and Stocky, T.P., 1973.Selective reductions. XIX. Rapid reaction of carboxylic acids with borane-tetrahydrofuran. Remarkably convenient procedure for the selective conversion of carboxylic acids to the corresponding alcohols in the presence of other functional groups.The Journal of Organic Chemistry, 38(16), pp.2786-2792.

Young WL, Gao E, Hedemenos GJ & Massoud TF. (2007). Use of modeling for the study of cerebral arteriovenous malformations. In Stieg PE, Batjer HH, Samson D (Eds): Intracranial arteriovenous malformations (49-71). New York: Informa Health Care.

Zhang, M., Lu, S., Xu, E., He, M. and Yu, J., 2015.A new method for preparation of low melting point polyamide-6 (LPA6) and properties of compatibilized blends of

LPA6/glass beads/styrene and maleic anhydride copolymer.Science and Engineering of Composite Materials, 22(6), pp.599-606.

Zhang, C., Chau, N. and Ho, H., 2020. Patient-Specific Blood Flow Analysis for Cerebral Arteriovenous Malformation Based on Digital Subtraction Angiography Images. Frontiers in bioengineering and biotechnology, 8, p.775.

Zhao, H., Zheng, C., Feng, G., Zhao, Y., Liang, H., Wu, H., Zhou, G., Liang, B., Wang, Y. and Xia, X., 2013. Temperature-sensitive poly (N-isopropylacrylamide-co-butyl methylacrylate) nanogel as an embolic agent: distribution, durability of vascular occlusion, and inflammatory reactions in the renal artery of rabbits. American Journal of Neuroradiology, 34(1), pp.169-176.

LIST OF PUBLICATIONS

- Gopika V. Gopan, K. Kezia Susan, E. R. Jayadevan, Roy Joseph, 'Organic compound with potential for X-ray imaging applications', *ACS Omega*,2021,**6**, 24826-24833. https://doi.org/10.1021/acsomega.1c03671.

MANUSCRIPTS UNDER PREPARATION

1. Gopika V. Gopan, Aleesha Vahab, Reshmi Govindan, Eliza Divya Srishty Minz, Arvind Kumar Prajapati, Rahul Radhakrishnan, Sachin J. Shenoy, Jayadevan E.R., Sabareeswaran A., Roy Joseph, 'Evaluation of a tetraiodo compound grafted radiopaque ethylene vinyl alcohol co-polymer system for embolization in swine'.
2. Gopika V. Gopan, Kuriachan Kezia Susan, Aleesha Vahab, Reshmi Govindan, Enakshy Rajan Jayadevan, Roy Joseph, 'Imparting radiopacity to ethylene vinyl alcohol copolymer: Effect of vinyl alcohol content on the grafting efficiency, radiopacity and thermal stability'
3. Gopika V. Gopan, Sabareeswaran A., Remya N.S., Roy Joseph, 'Tissue response to the intramuscular implantation of a new radiopaque, tetraiodocompound based Ethylene vinyl Alcohol co-polymer'

LIST OF INDIAN PATENTS GRANTED

1. Roy Joseph, E.R. Jayadevan &Gopika V. Gopan: "A radiopaque polymeric liquid embolic system" Patent No. 415206, Date of Grant: 22/12/2022.
2. Roy Joseph, Gopika V. Gopan: "A non-cytotoxic diphenolic tetraiodo compound and method of preparation thereof" Patent No. 398081, Date of Grant: 30/05/2022.

INTERNATIONAL PATENT GRANTED

Roy Joseph, Jayadevan E.R. & Gopika V. Gopan: "A Radiopaque Polymeric Liquid Embolic System." EP3873547A4, Date of Grant: 03/08/2022.

AWARDS/ HONOURS RECEIVED

1. Best Poster Award at the National Conference on Material Science and Technology (NCMST) held at IIST, Thiruvananthapuram from 18-20th December 2019 for the poster entitled, 'Fabrication of inherently radiopaque biocompatible polymer for vascular embolization' (Authors: Gopika V. Gopan, Kezia Susan K., Aleesha Vahab, Reshmi Govindan, Enakshy Rajan Jayadevan and Roy Joseph).
2. Shared the 11th National Petrochemical award, June 2022 for the work entitled "Metal free radiopaque polymeric material for the embolization of arteriovenous malformation of brain" under the category of "Polymers in medical and pharmaceuticals applications" with Dr. Roy Joseph and Dr. E.R. Jayadevan.
3. Certificate of Excellence in National Science day and Institute day celebrations , Feb. 28, 2023.

CURRICULUM VITAE

Personal

Name	: Gopika V. Gopan
Date of Birth & Age	: 06th April 1992, 30 years
Address	: Sreevalsam, T.C. 92/492, AGRA-10A, Anayara P.O, Trivandrum-695029, Kerala, India
Phone No	: 8281514951
Email id	: gopikagopan123@gmail.com
Marital status	: Married
Gender	: Female
Nationality	: Indian

Education

Jan. 2018- Sep. 2023 : **Doctor of Philosophy**
Sree Chitra Tirunal Institute for Medical Sciences and Technology,Trivandrum, Kerala
Topic: Radiopaque Iodinated Compound Grafted Polymer: Synthesis and Evaluation for Embolotherapy
Area of Research: Organic chemistry, Biomaterials, Polymers

Sep. 2014- Apr. 2016: **Bachelor of Education (B.Ed.)** (Passed with Distinction)
Govt. College of Teacher Education, Thycaud, University of Kerala, Trivandrum
Specialization: Physical Science

July 2012 - July 2014: **Master of Science (M.Sc.)** (Passed with 8th Rank)
Department of Chemistry, Kariavattom campus University of Kerala, Trivandrum
Specialization: Chemistry
Relevant Courses: Analytical and Environmental Chemistry, Environmental Education and Sustainable Development, Environmental Biotechnology, Enzymology, Internet Techniques, Advanced physical chemistry, Instrumental Methods
Thesis: Synthesis and characterization of gold nanocluster-gold nanorod quenched System for the detection of trinitrotoluene (TNT)

June 2009 - June2012: Bachelor **of Science (B.Sc.)** (Passed with Distinction and college first)
All Saints' College,University of Kerala, Trivandrum
Specialization: Chemistry

July 2007- Apr. 2009: **Plus Two** (Passed with Distinction)
Govt. Girls H.S.S. Cottonhill, Trivandrum
Board of Higher Secondary Examination, Kerala
Specialization: Biology Science (Physics, Chemistry, Maths, Biology)

June 2006- Mar. 2007: **S.S.L.C** (Passed with all A^{+})
Fort Girls Mission H.S., Trivandrum
Board of Public Examination, Kerala
Specialization: All subjects

Professional Appointments

Aug. 2016 – Dec. 2017: Project Scientist
Sree Chitra Tirunal Institute of Medical Sciences and Technology
Synthesis and characterization of radiopaque compounds and polymers
Analysis of compounds by different instrumentation techniques
Report writing

Nov. 2023 – Apr. 2024: Technical Assistant (Instruments)
Sree Chitra Tirunal Institute of Medical Sciences and Technology
Testing, maintenance and test report preparation of various instruments such as Universal testing machine, Dynamic mechanical analyzer, Parylene coating machine, microviscometer etc

Research Experience

Jan. 2018 - Feb. 2020: Junior Research Fellow

Sree Chitra Tirunal Institute for Medical Sciences and Technology

Synthesis and evaluation of radiopaque iodinated compound grafted polymer for embolotherapy.

Feb. 2020 – Sep. 2023: Senior Research Fellow

Sree Chitra Tirunal Institute for Medical Sciences and Technology

Synthesis and evaluation of radiopaque iodinated compound grafted polymer for embolotherapy.

Publication Details

- **PhD Programme**

  Gopika V. Gopan, K. Kezia Susan, E. R. Jayadevan, Roy Joseph, 'Organic compound with potential for X-ray imaging applications', *ACS Omega*,2021,**6**, 24826-24833. https://doi.org/10.1021/acsomega.1c03671.

- **Collaboration with other lab during PhD**

  1. Adarsh RK, Das EC, **Gopan GV**, Rajan KK, Komath M. Quarternised chitosan compositeswith in situ precipitated nano calcium phosphate for making bioactive and degradable tissue engineering scaffolds. *Journal of Polymer Research*. 2022; 29(7):1-9.
  2. R K. Adarsh, Eva C. Das, **Gopika V. Gopan**, Shivaram Selvam, Manoj Komath. Functionally graded bioactive composites based on poly(vinyl alcohol) made through thiol-ene click reaction. ACS Omega. 2022; 7(33): 29246-29255.

Achievements

1. List of indian patents granted

1. Roy Joseph, E.R. Jayadevan &Gopika V. Gopan: "A radiopaque polymeric liquid embolic system" Patent No. 415206, Date of Grant: 22/12/2022.
2. Roy Joseph, Gopika V. Gopan: "A non-cytotoxic diphenolic tetraiodo compound and method of preparation thereof" Patent No. 398081, Date of Grant: 30/05/2022.

2. International patent granted

Roy Joseph, Jayadevan E.R. & Gopika V. Gopan: "A Radiopaque Polymeric Liquid Embolic System." EP3873547A4, Date of Grant: 03/08/2022.

3. Awards and Honors

Feb. 2023 Certificate of Excellence in National Science day and Institute day celebrations of SCTIMST.

June 2022 Shared the11th National Petrochemical award for the work entitled "Metal free radiopaque polymeric material for the embolization of arteriovenous malformation of brain" under the category of "Polymers in medical and pharmaceuticals applications" with Dr. Roy Joseph and Dr. E.R. Jayadevan.

Dec. 2019 Best Poster award for the poster entitled "Fabrication of inherently radiopaque biocompatible polymer for vascular embolization" presented in the National Conference on Recent trends in Materials Science and Technology (NCMST-2019).

Aug. 2015 State Eligibility Test (SET) in Chemistry.

Mar. 2015 Graduate Aptitude Test in Engineering (GATE) in chemistry

Conference presentations

1. Gopika V. Gopan, Kezia Susan K. and Roy Joseph. Radiopaque Iodocompound for Imparting Radiopacity in Polymers: Synthesis and Characterization, International Conference on Advanced Functional Materials (ICAFM), December 9-10, 2019.
2. Gopika V. Gopan, Kezia Susan K., Aleesha Vahab, Reshmi Govindan, Enakshy Rajan Jayadevan and Roy Joseph. Fabrication of inherently radiopaque biocompatible polymer for vascular embolization, NationalConference on Material Science and Technology (NCMST), December 18-20, 2019.

3. Gopika V. Gopan, K. Kezia Susan, Aleesha Vahab, Reshmi Govindan, Enakshy Rajan Jayadevan, Arvind Kumar Prajapati, Rahul Radhakrishnan and Roy Joseph. *In Vitro* Functional Evaluation of a Radiopaque Polymer for Vascular Embolization, International Conference on Polymeric Materials in Medicine (ICPMM), February 25-26, 2022.